TARGETING THE PHOSPHOINOSITIDE-DEPENDENT PROTEIN KINASE-2 FOR ANTICANCER DRUG DISCOVERY

DISSERTATION

Presented in Partial Fulfillment of the Requirements for the Degree Doctor of Philosophy in the Graduate School of The Ohio State University

By

SU-LIN LEE M.S.

Graduate Program in Pharmaceutical Sciences

The Ohio State University

2012

Dissertation Committee:

Professor Ching-Shih Chen, Advisor

Professor Pui-Kai Li

Professor Karl Werbovetz

Professor Matthew D. Ringel

Copyright by

Su-Lin Lee

2012

Abstract

The phosphatidylinositol 3-kinase (PI3K)/Akt signaling axis plays a pivotal role in regulating multiple cellular events including cell growth, survival, metabolism, and motility through the modulation of a plethora of downstream effectors. Two important kinases, phosphoinositide-dependent protein kinase-1 and 2 (PDK1 and PDK2) are required for the activation of Akt by phosphorylating the Akt at Thr-308 and Ser-473, respectively. The role and identity of PDK1 is well studied while the PDK2 remains unclear. Herein, we focused on developing a selective PKD2 inhibitor, which we further identified the molecular target as integrin-linked kinase (ILK).

In this study, we used AR-12 (formerly OSU-03012), a novel PDK1 inhibitor, as a lead to design and synthesize a series of derivatives to generate a small kinase inhibitor library. After initial *in vitro* screening, a potent PDK2 inhibitor, designated T315, has been identified to efficiently inhibit the phosphorylation of Akt at Ser-473 without altering the Thr-308 site. T315 consistently inhibited cell proliferation against a panel of cancer cell lines at IC_{50} values ranging from 1.0 to 2.5 μM, while normal epithelial cells were unaffected. Through western blot analysis, T315 facilitated the dephosphorylation of two other ILK targets, including glycogen synthase kinase-3β (GSK3β) and myosin light chain (MLC). Moreover, T315 suppressed the expression of the transcription/translation factor YB-1 and its targets: human epidermal growth factor

receptor 2 (HER2) and epidermal growth factor receptors (EGFR) in PC-3 cells, which could be rescued by the stable expression of constitutively active ILK. Evidence indicates that T315 induced autophagy and apoptosis, both of which were integral to its antiproliferative activity. Together, this broad spectrum of mechanisms underlies the therapeutic potential of T315 in cancer treatment, which is manifested by its *in vivo* efficacy as a single oral agent in suppressing PC-3 xenograft tumor growth.

As a follow-up to our work, in the process of screening T315 in a panel of prostate and breast cancer cell lines, we discovered that T315 alone has no significant PDK2 inhibitory activity in LNCaP cells, which was opposite to other cell lines tested. This phenomenon gives us the notion that there might be a kinase other than ILK that act as the PDK2 in LNCaP cells. To date, the phosphorylation of Akt at its PDK2 site has been attributed to at least nine candidate kinases, in which we believe that the mTOR complex 2 (mTORC2), and ILK are the major PDK2s in most of the cancer cell lines. Pursue to this aspect, by using pharmacological and molecular biological approaches, we identified ILK and mTORC2 as the major PDK2s in PC-3 and LNCaP cells, respectively. This information is important for future development of PDK2-targeted therapies.

Dedication

This document is dedicated to my parents and my dearest wife.

Acknowledgments

I would like to thank my advisor, Dr. Ching-Shih Chen, for letting me enter the drug discovery track from the very beginning of my graduate research training. He encouraged me to expose myself to broaden my expertise in computer modeling, organic synthesis, and biological assays. I wouldn't have the chance to learn so many things without his support and guidance. He is my role model in terms of his work ethic and passion to science research.

I would also like to express my sincere appreciation to my advisory committee members: Dr. Pui-Kai Li, Dr. Karl Werbovetz, and Dr. Matthew Ringel, for all their help and advice in my research dissertation.

I am grateful for Dr. Samuel Kulp for the support of tumor xenograft studies and the critical review for my manuscripts; and Dr. Dasheng Wang and Dr. Kapuriya Naval for the help and guidance in organic synthetic methods.

I appreciate Hsiao-Ching (Jessie) Chuang, Chih-Chien (Adam) Chou, Eni-Chi (Andrew) Hsu, Po-Chen (Lewis) Chu, Kuen-Haur Lee and I-Ru Lai for spending there time to teach me through various biological assays. I also thank all of the former and current members of Chen's lab for you company and the wonderful times together.

At last I would like to thank my dearest wife, Shanshan He, for always on my side sharing the love and joy with me.

Vita

Sep. 21, 1979	Born - Taipei, Taiwan
2002	B.S. Chemistry National Chung-Cheng University, Taiwan
2004	M.S. Pharmacy National Taiwan University, Taiwan
2005 - 2007	Research Associate Drug Research Center National Taiwan University, Taiwan
2007 - present	Graduate Research Associate College of Pharmacy The Ohio State University

Publications

1. **Lee, S.-L.**, Hsu, E.-C., Chou, C.-C., Chuang, H.-C., Bai, L.-Y., Kulp, S. K., and Chen, C.-S. (2011) Identification and characterization of a novel integrin-linked kinase inhibitor. *Journal of Medicinal Chemistry. 54,* 6364-6374.
2. Guh, J.-H., Chang, W.-L., Yang, J., **Lee, S.-L.**, Wei, S., Wang, D., Kulp, S. K., and Chen, C.-S. (2010) Development of novel adenosine monophosphate-

activated protein kinase activators. *Journal of Medicinal Chemistry*. *53,* 2552-2561.

3. Wei, S., Yang, J., **Lee, S.-L.**, Kulp, S. K., and Chen, C.-S. (2009) PPAR gamma-independent antitumor effects of thiazolidinediones. *The Cancer Letter*. *276,* 119-124.

4. Lin, C.-J., Chen, C.-H., Liu, F.-W., Kang, J.-J., Chen, C.-K., **Lee, S.-L.**, and Lee, S.-S. (2006) Inhibition of intestinal glucose uptake by aporphines and secoaporphines. *Life Science. 79:* 144-153.

5. **Lee, S.-L.**, Huang, W.-J., Lin, W.-W., Lee, S.-S., and Chen, C.-H. (2005) Preparation and anti-inflammatory activities of diarylheptanoid and diarylheptylamine analogs. *Bioorganic & Medicinal Chemistry. 13,* 6175-6181.

6. Huang, W.-J., Chen, C.-H., Singh, O. V., **Lee, S.-L.**, Lee, S.-S. (2002) A facile method for the synthesis of glaucine and norglaucine from boldine. *Synthetic Communication*. *32,* 3681-3686.

Fields of Study

Major Field: Pharmaceutical Sciences

Table of Contents

Abstract ii

Dedication iv

Acknowledgments v

Publications vi

Table of Contents viii

List of Tables xiv

List of Figures xv

List of Schemes xviii

Chapter 1 Introduction 1

1.1. Molecular targeted therapy for cancer 1

1.2. PI3K/Akt pathway 1

1.3. Inhibitors for the PI3K/Akt pathway 3

1.3.1. Inhibitors targeting pathways upstream of PI3K/Akt 4

1.3.1.1. Humanized antibodies 4

1.3.1.2. Small molecule tyrosine kinase inhibitors 5

1.3.2. Inhibitors targeting PI3K 5

1.3.3. Inhibitors targeting the downstream pathways of PI3K/Akt 6

1.4. Targeting PDK1/PDK2 for inhibiting the Akt activation 8

1.5. ILK as a PDK2 candidate 9

1.5.1 ILK structure and functions 9

1.5.2 The ILK signaling pathway and inhibitor 12

1.6. mTORC2 as a PDK2 candidate 15

1.6.1 The mTOR complexes: mTORC1 and mTORC2 15

1.6.2 The mTORC2 signaling pathway 16

1.6.3 The second generation mTORC1/C2 inhibitors 16

1.7 Research rationale 19

Chapter 2 Design, synthesis, and target validation of a novel integrein-linked kinase inhibitor 20

2.1. Design and synthesis of a kinase inhibitor library 20

2.1.1. AR-12 as a potent PDK1 inhibitor 21

2.1.2. Use AR-12 as a lead to design a kinase inhibitor library 22

2.1.3. Synthesis of pyrazole ring-based compounds: **5**, **14**-**23**, and **53**-**55**. 25

2.1.3.1 Optimizing reaction condition 30

2.1.3.1.1. Preparing intermediate **iVa** 30

2.1.3.1.2. Preparing intermediate **Va** 31

2.2. Screening for potent PDK1/PDK2 inhibitors 35

2.3 Target validation of T315 36

2.3.1. Cell viability and selectivity of T315 between cancer and normal epithelial cells 37

2.3.2. Western blot analysis of T315 in ILK and mTORC2 pathways..... 38

2.3.3. Evidence of ILK is the target of T315 40

2.3.3.1 *In vitro* activity of T315..... 40

2.3.3.2 Protective effect against T315 with the overexpression of ILK in PC-3 cells 41

2.3.3.3. T315 suppressed the expression of YB-1 and its targets HER2 and EGFR via an ILK-dependent mechanism 42

2.3.4. Specificity of T315 in kinase inhibition..... 45

2.3.5. T315 causes cell death through autophagy and apoptosis 49

2.3.6. Suppressive effect of T315 in xenograft tumor growth..... 51

2.4. Structure-activity relationship studies of T315 53

2.4.1. *In vitro* activities of T315 derivatives 53

2.4.2. Molecular docking experiment of T315 against ILK kinase domain 56

2.5. Discussion 60

2.6 Conclusion 63

Chapter 3 Identification of the multiple identities of PDK2 in prostate cancer cells 64

3.1 The effects of T315 in different cell lines 64

3.2 Profiling the endogenous expression of ILK and mTORC2 in a panel of cancer cell lines 67

3.3 Identification of the major PDK2 in LNCaP and PC-3 cells through pharmacological and molecular biological approaches 69

3.3.1 Antiproliferative effects of PDK2 inhibitors in prostate and breast cancer cell lines 69

3.3.2 Western blot analysis of PDK2 inhibitors in prostate and breast cancer cell lines 71

3.3.3 Confirmation of pharmacological inhibitor findings using a molecular biological approach 75

3.4 Conclusion 78

Chapter 4 80

4.1 Reagents and antibodies 80

4.2 Cell culture 81

4.3 Cell viability assay 82

4.4 Immunoblotting 82

4.5 Transfection and generation of stable sublines. 83

4.6 RNA extraction and RT-PCR 84

4.7 Radiometric ILK kinase assay 84

4.8 Cell cycle analysis 85

4.9 Annexin V-PI staining 86

4.10 Animal studies 86

4.11 Statistical analysis 87

4.12 Molecular docking 87

4.13 Chemistry 88

4.13.1Chemistry general information 88

4.13.2 Synthetic procedures 89

4.13.2.1 General procedure for synthesis of **iia-c**: Step a. 89

4.13.2.2 Synthesis of (*Z*)-ethyl 2-hydroxy-4-oxo-4-(4'-(trifluoromethyl)-[1,1'-biphenyl]-4-yl)but-2-enoate **(iii)**: Step b. 91

4.13.2.3 General procedure for synthesis of **iVa-e**: Step c. 91

4.13.2.4 General procedures for synthesis of **Va-e** (n = 2): Step d. 94

4.13.2.5 Synthesis of ethyl 1-(4-nitrophenyl)-5-(4'-(trifluoromethyl)-[1,1'-biphenyl]-4-yl)-1*H*-pyrazole-3-carboxylate (**Vf**) (n = 0)..... 97

4.13.2.6 General procedure for synthesis of **Via-f"**: Step e..... 98

4.13.2.7 General procedure for synthesis of **Viia-f"**: Step f. 104

4.13.2.8 General procedure for synthesis of **15-20**: Step g..... 109

4.13.2.9 General procedure for synthesis of **5**, **14**, **21-23**, **54-55**: Step h. 113

4.13.2.10 Synthesis of *N*-methyl-3-(1-(4-morpholinophenyl)-5-(4'-(trifluoromethyl)-[1,1'-biphenyl]-4-yl)-1*H*-pyrazol-3-yl)propanamide (**53**): Step i. 119

Bibliography 121

List of Tables

Table 1. Structures of compound **5**, **14**-**23**, and **54**-**55**..... 29

Table 2. Reaction conditions for optimizing the yield of the intermediate **Va**..... 34

Table 3. Remaining activities of kinase (%) after treatment with T315 at 5 μM. 47

Table 4. *In vitro* activities of T315 derivatives..... 56

Table 5. Effects of T315 on cell viability in prostate and breast cancer cell lines. 65

List of Figures

Figure 1. The activation mechanism of the PI3K/Akt pathway..... 3

Figure 2. Small molecule inhibitors that target the PI3K/Akt pathway related molecules. 8

Figure 3. Schematic of ILK primary structure and domains. 12

Figure 4. The multi-protein ILK complex and its signaling pathways. 14

Figure 5. The PI3K/Akt/mTORC1/mTORC2 pathway. 18

Figure 6. Structure of the second generation mTOR inhibitors. 19

Figure 7. The structures of celecoxib (COX-2) and AR-12 (PDK1 inhibitor). 22

Figure 8. Design strategies of the pyrazole ring-based kinase inhibitor library. 24

Figure 9. Chemical structures of **1**-**55** in the kinase inhbitor library used for the bioactivity screening. 27

Figure 10. Identification of putative PDK2 inhibitors by screening of an in-house focused compound library. 36

Figure 11. Selectivity of T315 between cancer and normal epithelial cell lines. 38

Figure 12. The suppressive effects of shRNA-mediated knockdown of ILK and T315 on the phosphorylation of Akt at Ser-473 and Thr-308 and the downstream targets of ILK (GSK3β and MLC) versus those of mTORC2 (SGK and PKCα) in PC-3 and/or MDA-MB-231 cells. 39

Figure 13. Evidence that T315 is an ILK inhibitor. 43

Figure 14. Dose-dependent effects of T315 on the protein (left panel) and mRNA (right panel) expression of YB-1 and its targets HER2 and EGFR. 44

Figure 15. Specificity of T315 in kinase inhibition. 48

Figure 16. Evidence that T315 induces cell death through both apoptosis and autophagy. 50

Figure 17. *In vivo* antitumor efficacy of T315. 52

Figure 18. Design of T315 derivatives. 55

Figure 19. Molecular docking results of T315 (balls and stick) binding to the ATP-binding site of ILK kinase domain. 59

Figure 20. Further structure optimization strategies of T315 against ILK kinase domain. 60

Figure 21. Western blot analysis of the effect of T315 on ILK downstream targets in five cancer cell lines. 66

Figure 22. Endogenous expression levels of the ILK, mTORC2 members (mTOR and rictor) and phosphorylated Akt in prostate (PC-3, LNCaP) and breast (MCF7, MDA-MB-231, MDA-MB-468, and SKBR3) cancer cell lines. 68

Figure 23. Structure of PDK2 inhibitors: T315 and KU-0063794. 70

Figure 24. Cell viability assay of T315 versus KU-0063794. 70

Figure 25. Western blotting analysis of the suppressive effects of T315 and KU-0063794 on ILK and mTORC1/2 pathways in prostate and breast cancer cells. 73

Figure 26. Western blotting analysis of the combination treatment of T315 and KU-0063794 in (A) LNCaP and (B) PC-3 cells. 74

Figure 27. Western blot analysis of p-Ser-473-Akt and p-Ser-9-GSK3β expression after shRNA-mediated knockdown of rictor, ILK, and/or mTOR with or without co-treatment with T315 or KU0063794 in (A) LNCaP and (B) PC-3 cells. 77

Figure 28. Western blot analysis of p-Ser-473-Akt and p-Ser-9-GSK3β expression in LNCaP cells overexpressing CA-ILK. 78

List of Schemes

Scheme 1. General synthetic procedures of compound **5**, **14-23**, **53-55**. 28

Scheme 2. Preparation methods of intermediate **iVa**..... 31

Scheme 3. Reaction routes and conditions for preparing **Va** and its isomer. 33

Chapter 1

Introduction

1.1. Molecular targeted therapy for cancer

Cancer is a leading cause of human death worldwide with no effective systematic therapeutic treatment. Traditionally, treatments for cancer include surgery removal of tumor tissues, radiotherapy and chemotherapy. However, these methods are not specific and selective, and have severe adverse effects to normal cells. An advance anticancer treatment for drugs that directly target the abnormal proteins in cancer cells is called targeted therapy. For the past few decades, the increase understanding of the protein signaling pathways has provided insightful information for researchers to identify potential targets that lead to certain cellular behaviors, including cell proliferation, survival, grow, metabolism and metastasis. Small molecules or monoclonal antibodies are designed to selectively block or interrupt specific pathways, proteins or genes that are critical to cancer cells, and minimize the toxicity to normal cells (Ross et al., 2004; Tsuruo et al., 2003). Based on this strategy, several successful drugs have entered the drug market and provided promising therapeutic values, such as trastuzumab (Herceptin) and imatinib (Gleevec) (Vivanco and Sawyers, 2002).

1.2. PI3K/Akt pathway

The serine/threonine kinase Akt, also known as protein kinase B (PKB), play as an central node in several signal pathways (Manning and Cantley, 2007). By activating the Akt kinase, will trigger the phosphorylation of its downstream targets, in addition to activate or inhibit its downstream cascades. The abnormal loss or overexpress of Akt activation will lead to disrupting a series of signaling transduction events and cause to diseases, like type-2 diabetes and cancer. In the past two decades, the Akt has been reported to be overexpressed in various cancer types and the development of inhibiting the Akt pathway has gathered substantial interests (Vivanco and Sawyers, 2002).

The activation mechanism of Akt is directly regulated by phosphorylate/activate phosphatidylinositol 3-kinase (PI3K), in which together were called the PI3K/Akt pathway. As illustrated in Figure 1 (Vivanco and Sawyers, 2002), the activation of the PI3K/Akt pathway starts from the tyrosine receptor kinase, which will be stimulated by the binding of its ligands and further activate the tyrosine phosphorylation of scaffolding adaptors (IRS) by auto-phosphorylation. The activated IRS will then further phosphorylate/activate PI3K. The main function of PI3K, an intracellular signal transducer enzyme, is to convert a minor cell membrane component: phosphatidylinositol-4,5-bisphosphate [$PI(4,5)P_2$] into phosphatidylinositol-3,4,5-trisphosphate [$PI(3,4,5)P_3$]. This conversion can also be negatively regulated by PIP_3 phosphatases, phosphatase and tensin homologue deleted on chromosome ten (PTEN) and Src homology 2 domain-containing inositol phosphatase (SHIP) (Fresno Vara et al., 2004). The PIP_3 will then act as an anchor to recruit proteins that have the pleckstrin homology (PH) domains (such as Akt) to the cellular membrane. After the Akt was

localized to the cellular membrane, two other kinases: phosphoinositide-dependent protein kinase-1 (PDK1) and by phosphoinositide-dependent protein kinase-2 (PDK2) will phosphorylate the Akt at Thr-308 and Ser-473, respectively. Once the two sites of Akt have been phosphorylated, the Akt kinase will be fully activated and initiate its downstream target activation.

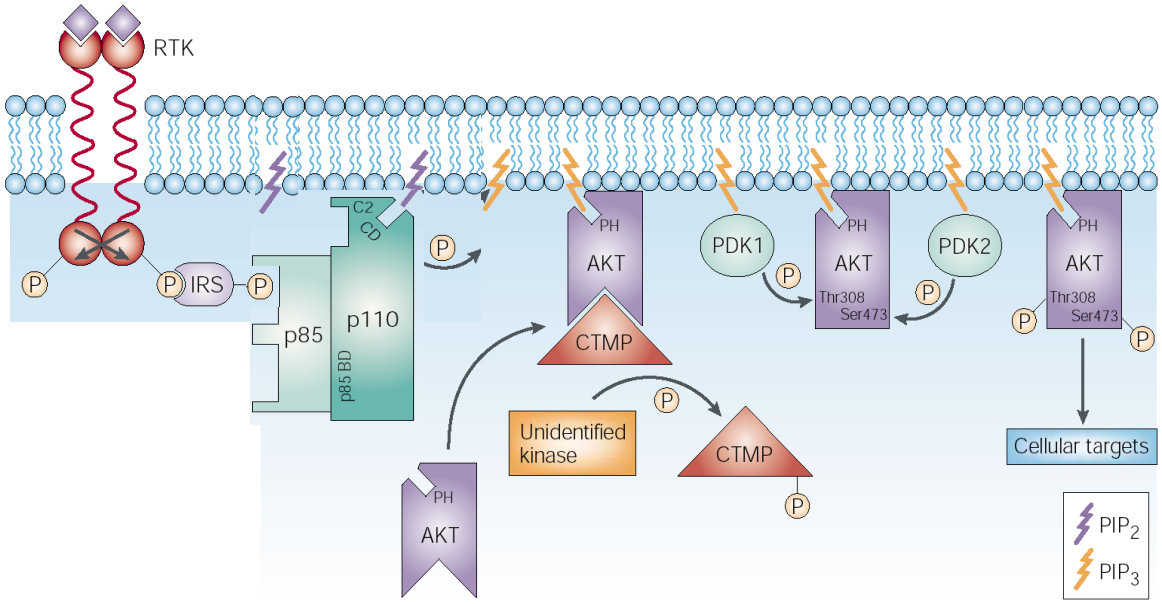

Figure 1. The activation mechanism of the PI3K/Akt pathway.

Reprint with permission form Macmillan Publishers Ltd: [Nature Review Cancer] (Vivanco and Sawyers, 2002), copyright (2002).

1.3. Inhibitors for the PI3K/Akt pathway

Since, the major players of the PI3K/Akt pathway have been defined, and the importance of this pathway in human cancers is determined. This pathway has become an attractive target for anticancer drug development. During the past two decades, several selective inhibitors designated for the members in the PI3K/Akt activation mechanism have been developed, and some have now entered clinical trials. These include inhibitors that target the upstream regulators of PI3K/Akt, such as epidermal growth factor receptors (EGFR); PI3K; and downstream effectors, such as mammalian target of rapamycin (mTOR) (Fresno Vara et al., 2004).

1.3.1. Inhibitors targeting pathways upstream of PI3K/Akt

The PI3K/Akt pathway is not always mutationally activated in tumors cells. This pathway is normally stimulated by aberrant activation of its upstream signaling pathways. The upstream regulators for PI3K/Akt are the growth factor receptor tyrosine kinases, in particular, the EGFR and human epidermal growth factor receptor 2 (HER2/neu, or erbB2). Hence, a lot of efforts have been made to target this kinase family through two major approaches: small molecule tyrosine kinase inhibitors and humanized antibodies that targets the receptor extracellular domains (Fresno Vara et al., 2004).

1.3.1.1. Humanized antibodies

Trastuzumab (Herceptin; Genentech) (Hudis, 2007), a humanized monoclonal

antibody against HER2, has been proved to be effective against overexpressed HER2 breast tumors. The antibodies will inactivate HER2 by binding to its extracellular domain and inhibit the original ligand binding, which further cause the internalization and down regulation of the receptor. Trastuzumab has been approved by FDA as a single agent for treating metastatic breast cancer with HER2 overexpression in 2008.

1.3.1.2. Small molecule tyrosine kinase inhibitors

ZD1839 (gefitinib, Iressa; AstraZeneca) (Herbst, 2002) and OSI-774 (erlotinib,Tarceva; OSI Pharmaceuticals) (Hidalgo et al., 2001) are ATP competitive inhibitors of EGFR. ZD1839 has been through several Phase I and II trials, which showed promising antitumor activity in advanced head and neck cancer and prostate carcinoma (NSCLC). OSI-774 is structurally similar to ZD1839 and share the same pharmacophores, but it is ten folds more active in EGFR *in vitro* kinase assay. Other same class EGFR inhibitors that are in early stage trials include EKB-569 (Genetics Institute/Wyeth–Ayerst), CI-1033 (Pfizer), PKI116 (Novartis), and GW2016 (GlaxoSmithKline) (Figure 2) (Fresno Vara et al., 2004).

1.3.2. Inhibitors targeting PI3K

Wortmannin is a fungal metabolite and a potent non-competitive, irreversible inhibitor of type I PI3K (Figure 2). Wortmannin has demonstrated significant *in vitro*

activity with the IC_{50} value of 2~4 nM in PI3K kinase assay (Powis et al., 1994). With this potent *in vitro* activity, *in vivo* studies in animal models have been conducted to test the efficacy of wortmannin in inhibiting tumor growth (Powis et al., 1994). Despite the high potency of using wortmannin to block the PI3K/Akt pathway for anticancer treatment, one disadvantage of wortmannin is its poor solubility in aqueous solution. Wortmannin is highly hydrophobic, which limit its use in clinical trials. To overcome this issue, water-soluble wortmannin pro-drugs are being developed. Other combination treatment of wortmannin with radiation or traditional chemotherapeutic drugs has also been studied, which shows further enhancement of the antitumor effect (Sarkaria et al., 1998; Kim et al., 2000).

LY294002, a flavonoid derivative, is an ATP competitive and reversible inhibitor of PI3K (Figure 2). The *in vitro* IC_{50} value against PI3K is around 1.4 μM, which is less potent than wortmannin. However, several *in vitro* studies have shown that LY294002 has antiproliferative and proapoptotic activities (Casagrande, 1998). LY294002 has also showed significant inhibition of tumor growth at 100 mg/kg and induced apoptosis in human cancer xenografts studies (Hu et al., 2000). The combination of LY294002 with various cytotoxic drugs or radiation will also enhance the effectiveness of caner treatments, which highlights the therapeutic potential of targeting the PI3K.

1.3.3. Inhibitors targeting the downstream pathways of PI3K/Akt

One of the major downstream targets of the PI3KAkt pathway is mTOR. The

rapamycin (sirolimus, Rapamune; Wyeth), a macrolide isolated from bacteria, and its derivatives CCI-779 (temsiroliumus, Torisel; Wyeth) and RAD001 (everolimus, Zortress; Novartis) are inhibitors for mTOR (Figure 2). The mode of action for this class of inhibitors to inhibit mTOR, is to first bind to a member of the ubiquitous immunophilin family, FK-506-binding proteins (FKBP) and form a complex. This complex will then further interacts with mTOR and inhibit the kinase activation, and subsequently downregulate its downstream targets. All three rapamycin derivatives have demonstrated antiproliferative activity in a variety of hematological and solid tumor systems (Eng et al., 1984; Douros and Suffness, 1981; Muthukkumar et al., 1995). CCI-779 is an ester form of rapamycin and RAD001 is the 40-*O*-(2-hydroxyethyl) derivative of rapamycin. These two derivatives both have similar *in vitro* and *in vivo* active as rapamycin, but with improved pharmaceutical property.

In summary, many new developed targeted-therapy anticancer drugs are based on the inhibition of the PI3K/Akt pathway, and many of the effects of the new-targeted anticancer drugs have mechanistic connections with the PI3K/Akt pathway. The further understanding of the relationship of the PI3K/Akt pathway and cancer can help to develop more potent and selective new drugs.

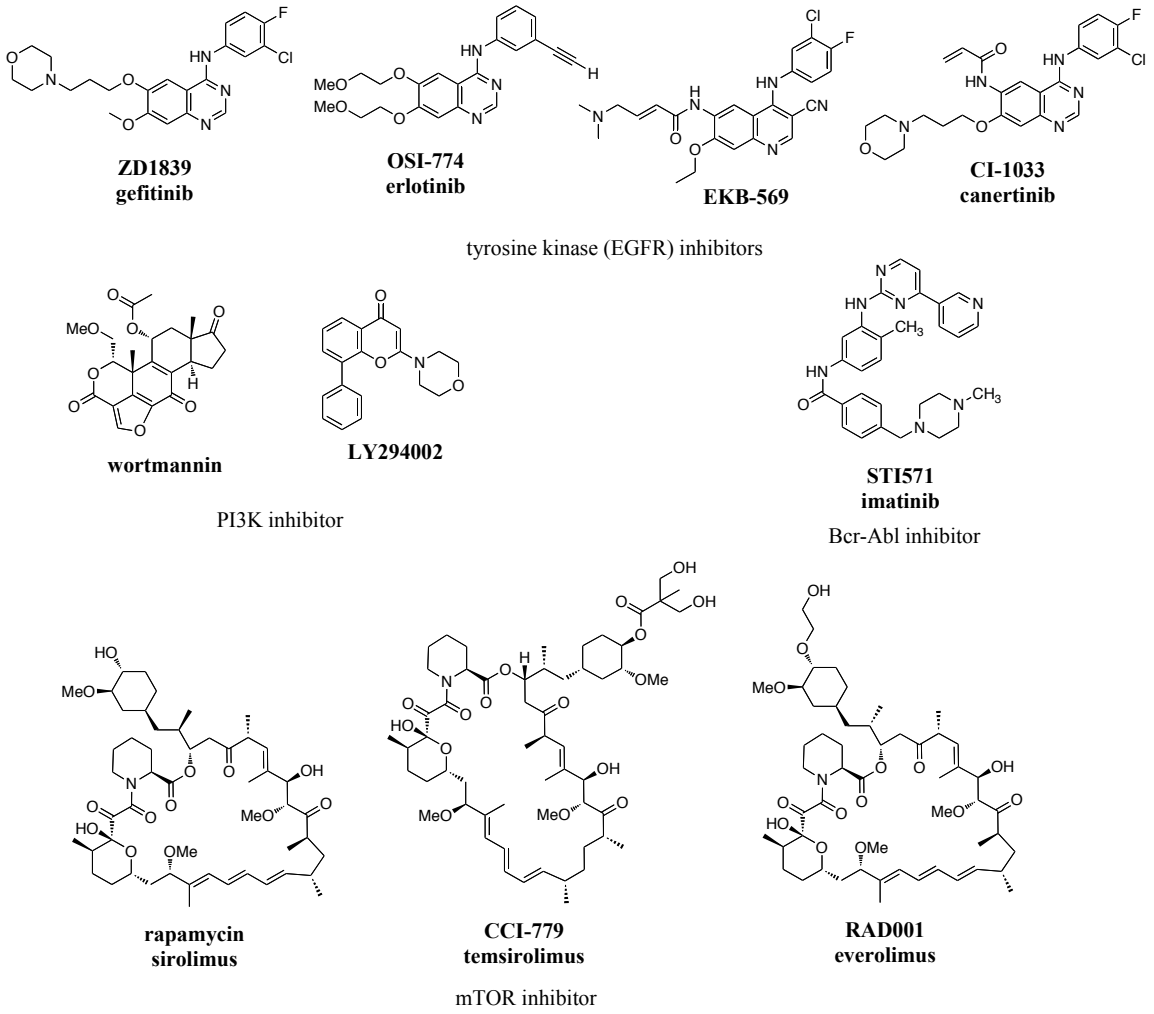

Figure 2. Small molecule inhibitors that target the PI3K/Akt pathway related molecules.

1.4. Targeting PDK1/PDK2 for inhibiting the Akt activation

Another target that is suitable for inhibiting the PI3K/Akt pathway is the direct activator of Akt: PDK1, which will phosphorylate the Thr-308 in the activation loop; PDK2, which phosphorylate the Ser-473 in a hydrophobic motif (HM) near the COOH terminus. The structure and sequence of PDK1 has been identified and several specific

inhibitors had been developed (Alessi et al., 1997; Sato et al., 2002). However, the kinase(s) that phosphorylate the Akt at the Ser-473 remains uncharacterized. So far, there are at least ten kinases that have been suggested to act as PDK2, including mitogen-activated protein (MAP) kinase-activated protein kinase-2 (MK2), integrin-linked kinase (ILK), p38 MAP kinase, protein kinase C α (PKCα), PKCβ, the NIMA-related kinase-6 (NEK6), the mTOR complex 2 (mTORC2), the doublestranded DNA-dependent protein kinase (DNK-PK), and the ataxia telangiectasia mutated (ATM) gene product, p21 protein-activated kinase 1/2 (PAK1/2) (Dong and Liu, 2005). However, not all of these kinases have sufficient evidence that act as a specific PDK2. Equally important, there is the possibility of multiple PDK2 systems acting simultaneously in cells to regulate the phosphorylation of Akt at Ser-473. In addition, the phosphorylation level of the Akt at Ser-473 could be cell type and signaling pathway specific. The development of specific PKD2 inhibitors and the identification and characterization of the broad spectrum of PDK2 kinase(s) in different cancer cell line systems will be essential to verify these hypotheses.

1.5. ILK as a PDK2 candidate

1.5.1 ILK structure and functions

Among all the PDK2 candidates, the integrin-linked kinase is one of most interesting target that we are focused on. ILK was originally identified as a binding partner of the cytoplasmic tail of integrin β1 through a yeast two-hybrid screening

(Hannigan et al., 1996) and has been characterized as an unique intracellular adaptor that links the cell-adhesion receptors, integrins and growth factors to the actin cytoskeleton. The ILK is also a kinase with a range of its unique signaling pathways (Hannigan et al., 2005). ILK is associated in the regulation of several cellular event, including cell growth and survival, cell cycle progression (Leung-Hagesteijn et al., 2005; Wu and Dedhar, 2001), epithelial-mesenchymal transition (EMT), invasion and migration (Oloumi et al., 2004), and tumor angiogenesis (Tan et al., 2004; Kaneko et al., 2004). Moreover, ILK overexpression has been associated with the oncogenesis and tumor progression of many types of malignancies, including those of prostate (Graff et al., 2001), ovary (Ahmed et al., 2003), breast (Pontier et al., 2010), colon (Bravou et al., 2006), pancreas (Schaeffer et al., 2010), stomach (Ito et al., 2003), and liver (Chan et al., 2011). ILK represents a relevant target for cancer therapy.

The ILK protein is 452 amino acids in length, and comprises three major domains, as showed in Figure 3 (Hannigan et al., 2005), namely the N-terminal ankyrin repeats, a central PH domain, and C-terminal kinase domain. Each of these domains plays a role in mediating ILK's biological functions through interaction with intracellular signaling proteins or PIP_3. For example, the ankyrin repeats domain of ILK will interact with the adaptor protein, PINCH and ILK-associated phosphatase (ILKAP), together with the binding of α-parvin and β-parvin to the ILK kinase domain, will form the ternary ILK/PINCH/parvin complex, which serves as a molecular scaffold that link integrins with the actin cytoskeleton (Figure 4A) (Legate et al., 2006; Hannigan et al., 2005). The catalytic domain of ILK contains two major regions, a integrin binding region that binds

with the actin-binding adaptor proteins (Figure 4A) (Yamaji et al., 2001; Tu et al., 2001; Hannigan et al., 2005); and a kinase catalytic region that contains the ATP binding site for the ILK kinase activity. It has been reported that the catalytic domain of ILK has high degree of sequence similarity with other kinases. However, through point mutational studies of the residues at the ATP binding site, have demonstrated that there are no residues thought to be necessary for the ILK catalytic activity. Since, there are arguments against ILK as a real kinase or a pseudo kinase (Wickstrom et al., 2010). Furthermore, by examining the secondary structure of the ILK kinase domain, the structure lacks the standard DFG glycine at the activation loop that allows the DFG motif to flip in (active) and out (inactive) as a gate to control the kinase active site (Fukuda et al., 2009). Comparing to other kinase domain (such as, AGC kinase family) the ILK kinase domain's structure is relatively rigid, and there is no significant change of conformation with or with out the Mg-ATP binding. All together, indicating that the ILK has its unique and sophisticated function/structure.

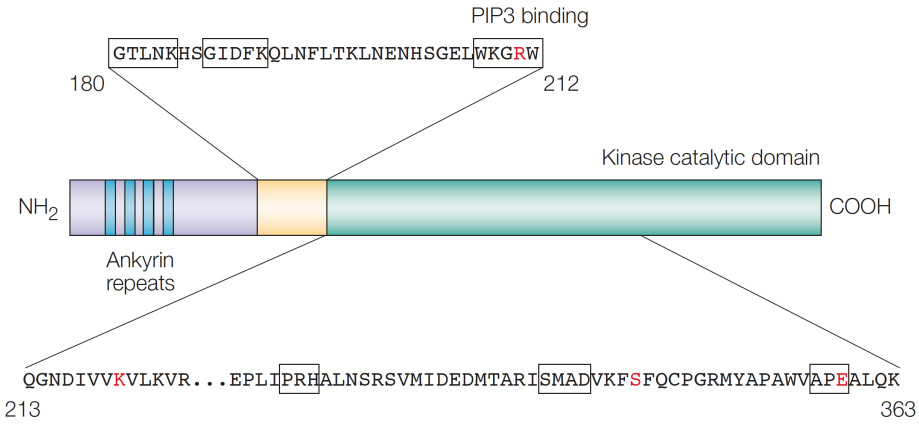

Figure 3. Schematic of ILK primary structure and domains.

Reprint with permission from Macmillan Publishers Ltd: [Nature Review Cancer] (Hannigan et al., 2005), copyright (2005).

1.5.2 The ILK signaling pathway and inhibitor

The ILK activity is regulated by the function of PI3K. Similar to the Akt activation mechanism, the ILK will be localized to the cellular membrane by the binding of its PH domain and PIP_3 (Figure 4A) (Hannigan et al., 2005). The ILK kinase activity was inhibited by inhibitors of PI3K, indicating that ILK activation was dependent on PI3K (Hannigan et al., 2005). Furthermore, same as Akt, the tumor suppressor PTEN phosphatase will negatively regulate the activation of ILK (Delcommenne et al., 1998).

Although whether ILK contains a functional kinase domain remains a contentious issue, ILK has been shown to mediate the phosphorylation of a unique set of signaling proteins (Figure 4B). By overexpressing the wild type ILK will increase the phosphorylation of AKT at Ser-473 and stimulate several signaling pathways that will lead to cell survival through the inhibition of caspase-3. ILK also stimulates the phosphorylation of glycogen synthase kinase (GSK3β) at Ser-9 (Delcommenne et al., 1998), leading to its inhibition that will relieve several negatively regulated signaling pathways that result in cell invasion and proliferation (Hannigan et al., 2005). Furthermore, ILK can phosphorylate the myosin light chain (MLC), resulting in myosin-mediated contractility and cell motility (Hannigan et al., 2005).

So far, there is only one ILK inhibitor that has been reported, the QLT-0267 (QLT

Inc., structure not available), which has been reported to suppress of the growth glioblastoma and breast cancer (Kalra et al., 2009; Eke et al., 2009). The *in vitro* IC_{50} value of QLT-0267 in cell-free assay is 26 nM; however, this compound has issue in terms of poor bioavailability. For this reason, there is great urgency to develop novel selective ILK inhibitors.

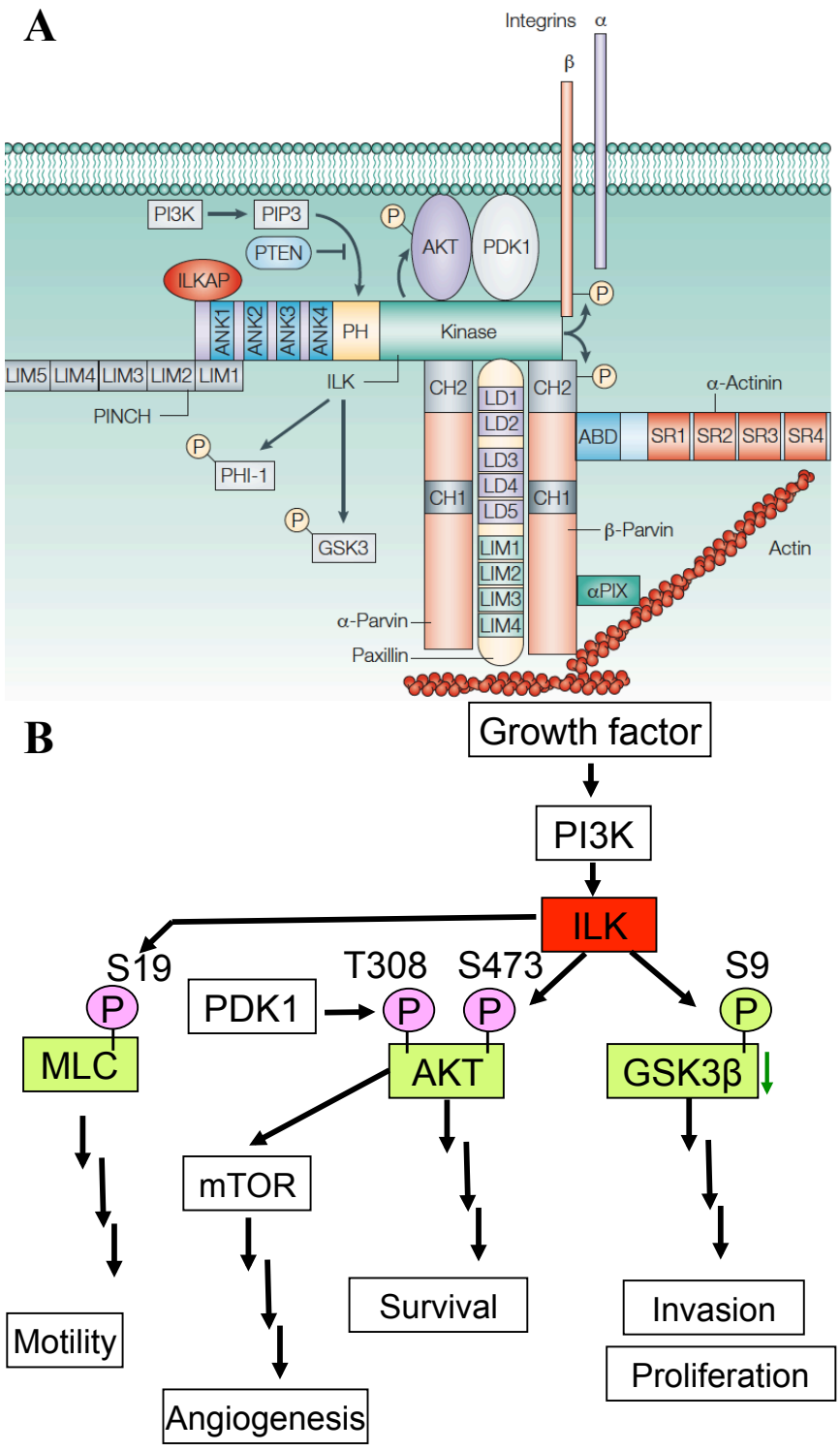

Figure 4. The multi-protein ILK complex and its signaling pathways.

(A) Illustration of the ILK/PINCH/parvin complex that links the scaffold of integrin and actin cytoskeleton. (B) The three major downstream targets of ILK and the related signaling pathways.

Reprint with permission from Macmillan Publishers Ltd: [Nature Review Cancer] (Hannigan et al., 2005), copyright (2005).

1.6. mTORC2 as a PDK2 candidate

1.6.1 The mTOR complexes: mTORC1 and mTORC2

For the last decade, the mTOR kinase is one the key targets for anticancer drug development (Huang and Houghton, 2003). The mTOR is a mammalian serine/threonine kinase of 289 kDa in size and play an important role in regulating cell growth, metabolism, and proliferation. The mTOR is activated through the downstream signaling of the PI3K/Akt pathway. Substantial research and clinical trial has been focused on developing the mTOR inhibitors: rapamycin and its analogs. However, although rapamycin have been shown promising response in some tumor with PTEN null/mutation, other cancers have shown resistance to this line of treatment. In these other cases resulted in clinical trial have been disappointing (Margolin et al., 2005; Chang et al., 2005). This portion resistance effect of rapamycin was due to the two kinds of complexes formed by mTOR. As shown in Figure 5, mTOR exists in two complexes: the mTOR complex 1 (mTORC1) is composed of mTOR, raptor, and mLST8 and is sensitive to the inhibition by rapamycin; the mTORC2, consists of mTOR, rictor, mLST8, and Sin1 and is generally

considered to be rapamycin-insensitive, which will decrease to effect of rapamycin treatment. By inhibiting the mTORC1 pathway will also form a negative feed back loop to activate the phosphorylation of IRS through p70S6K (Figure 5, right loop) (Fingar et al., 2002). The phosphorylation of p70S6K inactivates the IRS, which is essential for activating the PI3K. Hence, by inhibiting the mTORC1 with rapamycin will induce the IRS activity from the p70S6K inhibition.

1.6.2 The mTORC2 signaling pathway

Compare to mTORC1, which has extensive research over the last decade, the cellular functions of mTORC2 have just begun to be understood. The mTORC2 is exclusively growth factor responsive and Akt is its first recognized substrate protein. The mTORC2 have the ability to function as a PDK2, that regulates the Akt phosphorylation at Ser-473, which forms a feedback loop to promotes cell survival (Figure 5. left loop) (Malagu et al., 2009). Other reported mTORC2 substrates are serumand glucocorticoid-induced protein kinase-1 (SGK1) and protein kinase C-α (PKCα) (Figure 5) (Cybulski and Hall, 2009).

1.6.3 The second generation mTORC1/C2 inhibitors

As discribed in section 1.3.3. the rapamycin anologs will bind to the FKPB and further inhibit the mTOR kinase activity. Recent reports have indicated that the

rapamycin-FKPB complex is mTOCR1 specific, which limits the inhibition activity of the PI3K/Akt/mTOR pathway. Therefore it is proposed that the kinase domain targeted mTOR inhibitors will have the ability to target both mTORC1 and mTORC2 complexes, and such compounds should have a better scope of pharmacological propertiy (Vilar et al., 2011). Hence, a second generation mTORC1/C2 dual inhibitors have been develoed, including AZD-8055 (AstraZeneca) (Chresta et al., 2010), INK-128 (Intellikine, structure not available) (Vilar et al., 2011) and OSI-027 (OSI Pharmaceuticals) (Figure 6) (Bhagwat et al., 2011). All of these compounds have shown potent *in vitro* activities by inhibiting the phosphorylation of p70S6K, 4E-BP1, and Akt at Ser-473. This class of compounds also demonstrated antiproliferative activities against multiple xenograft models and cells lines that are resistant to rapamycin. Currently, these three componds are under phase I clinical development.

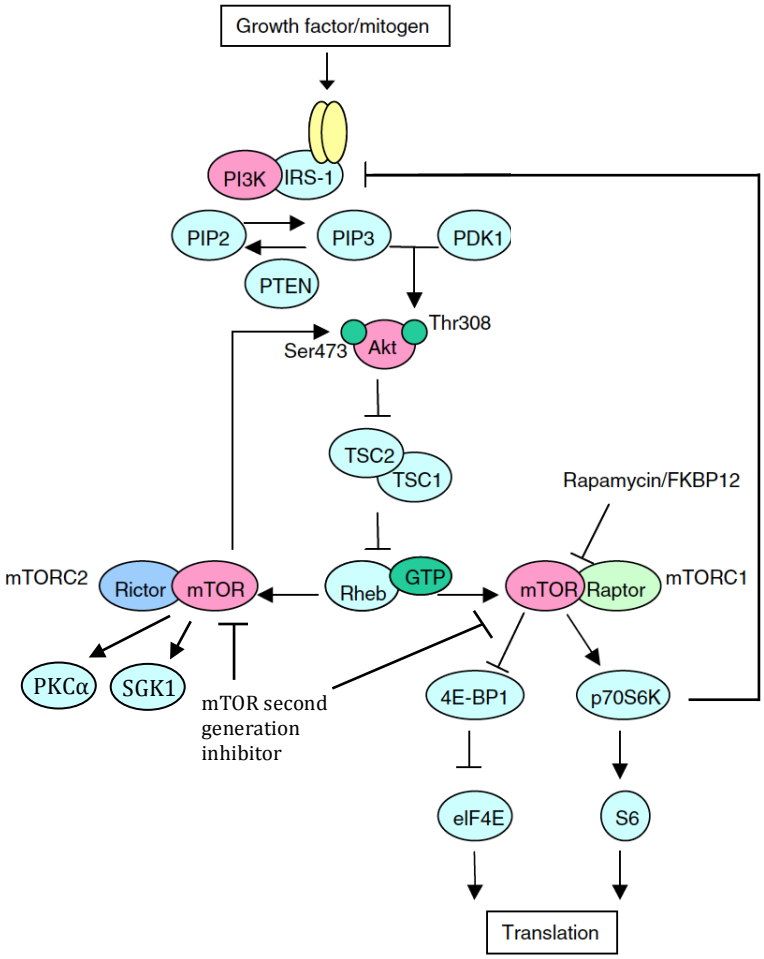

Figure 5. The PI3K/Akt/mTORC1/mTORC2 pathway.

Reprint from (Malagu et al., 2009), with permission from Elsevier.

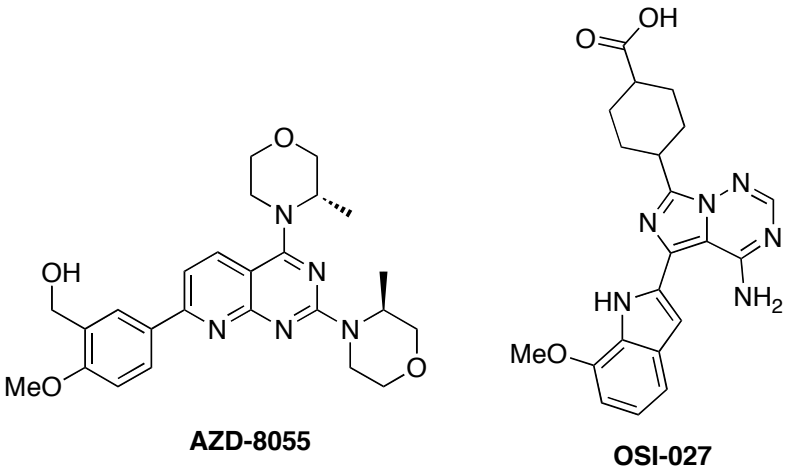

Figure 6. Structure of the second generation mTOR inhibitors.

1.7 Research rationale

The importance and mechanism of the PI3K/Akt pathway and most of its key players have been well studied. However, the real identities and mechanism of PDK2 are still unclear, and the lack of selective PDK2 inhibitor is an issue. Hence, my research topic is divided into two parts. First, I was focused on developing a selective PDK2 inhibitor, by using an in house developed PDK1 inhibitor—AR12 as a lead. Secondly, I was focused on identifying the major kinase that function as a PDK2 in specific cell lines.

Chapter 2

Design, Synthesis, and Target Validation of a Novel Integrin-Linked Kinase Inhibitor

To shed light on the role of ILK in the PI3K/Akt pathway and its potential therapeutic applications in targeted cancer therapy, I focused on developing a selective ILK inhibitor. This agent has demonstrated strong *in vitro* activity for cancer cell antiproliferation, and *in vivo* efficacy for suppressing tumor growth.

2.1. Design and synthesis of a kinase inhibitor library

The first and most crucial step of this project is to generate a drug-like compound library for activity screening. Instead of randomly generate a huge compound library, the strategy we use is to took advantage of the "off target effect" (MacDonald et al., 2006) of an existing bioactive agent, and further transfer the original activity into its off target activity by structure modifications. Compounds like ATP-competitive kinase inhibitors all share the same target—the ATP-binding pocket. It is likely to switch selectivities between kinase inhibitors by minor change of structures. Herein, based on the structures of an in-house established PDK1 inhibitor—AR12, we started the design and synthesis of a kinase inhibitor library that targets the PI3K/Akt activation pathway. We are interested in the

PDK1 and PDK2 kinases, which play the essential roles in Akt activation.

2.1.1. AR-12 as a potent PDK1 inhibitor

The pyrazole ring based compound AR-12 (formerly OSU-03012) was developed in our lab as a PDK1 inhibitor (Figure 7). This compound was originally derived from the structure of an anti-inflammatory drug, celecoxib (Celebrex, Pfizer), a selective COX-2 inhibitor. It has been reported that celecoxib has minor off target activity as a PDK1 inhibitor with an IC_{50} value of 48 μM (Zhu et al., 2004; Arico et al., 2002). By picking up this off target effect, the compound AR-12 was then generated after a series of structural modification, with further improved IC_{50} value of 5μM against PDK1. Furthermore, AR-12 no longer possesses the COX-2 inhibition activities. AR-12 can dose-dependently dephosphorylate Akt at Thr-308, and cause cancer cell death through apoptosis (PC-3 cell, IC_{50}: 5μM) (Zhu et al., 2004). Recently, this agent has been licensed by Arno Therapeutics Inc. and entered phase I clinical trial for treatment of advanced or recurrent solid tumors or lymphoma at 2010 (study NCT00978523).

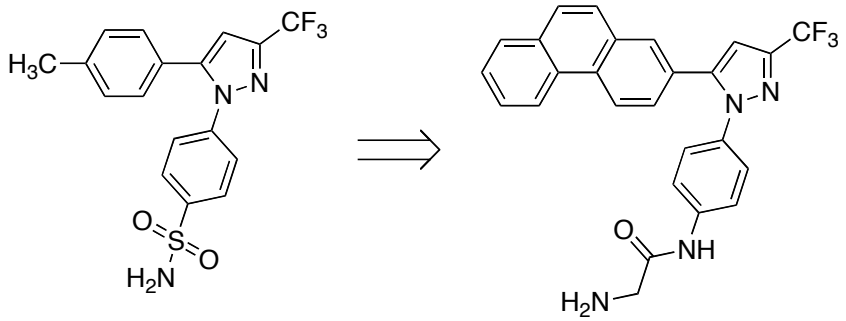

Figure 7. The structures of celecoxib (COX-2) and AR-12 (PDK1 inhibitor).

2.1.2. Use AR-12 as a lead to design a kinase inhibitor library

The development of AR-12 is a successful example of transferring the "off target effect" into the main activity. However, for further studies of AR-12 in three thyroid cancer cell lines have demonstrated that this compound also have the activity to inhibit the p21-activated kinase-1 (PAK1) in low micromolar concentration (Porchia et al., 2007) . Suggesting that AR-12 also has its own off target effect. Hence, to further extend the potential activities associated with AR-12, a second batch of derivatives were designed.

The structure of AR-12 can be divided into three segments (Figure 8): 1. The R_1 group is mostly aromatic ring systems. We are interested in the effect of changing the original flat and highly conjugated phenanthrene into a rotatable substituted biphenyl ring system; or introducing a heterocycle ring as dibenzo[b,d]furan; or changing the position

of 2-phenanthrene with 3-phenanthrene, which will provide a different geometry effect of the compound. 2. The substitution of trifluoromethyl group at the R_2 position was borrowed from the structure of celecoxib, which provides strong electronegativity effect. Here, we are interested in replacing the trifluoromethyl group with a polar amide moiety, which has the ability to form hydrogen bonds with the targeted receptor. Furthermore, preliminary molecular docking experiments indicated that prolonging the R_2 group should provide a chance to let this arm reach further deep inside the ATP-binding pocket (data not shown). 3. The glycine residue on the R_3 group can be exchanged with a variety of amino acids that provide different length of the free amine tail; the piperazine ring provides a fused ring structure with the same two carbons length and free amine as AR-12; other substitution at the 4-position of the piperazine can also enlarge the structural diversity.

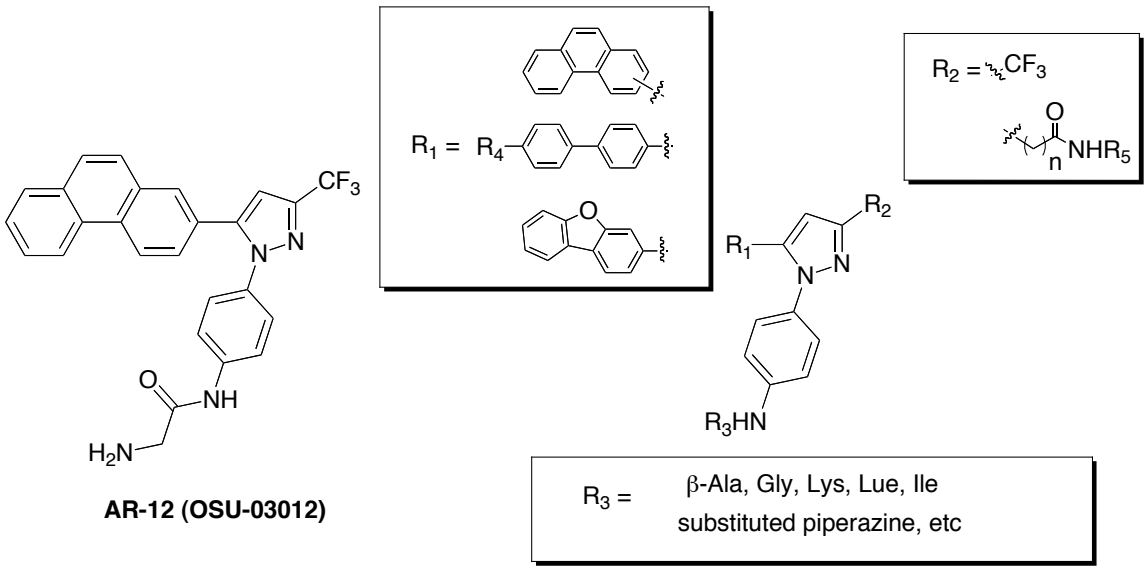

Figure 8. Design strategies of the pyrazole ring-based kinase inhibitor library.

Based on this design strategy, fourteen new compounds (**5**, **14-23,** and **53-55)** have been synthesized and by combining with previous prepared derivatives (Zhu et al., 2004), a total fifty-five member compound library was generated for further screening (Figure 9) (Lee et al., 2011). This pyrazole ring-based kinase inhibitor library has been divided into five series (series A-E). Series A-C are focusing on modifying the two other segments without altering the trifluoromethyl group. Series A: fixing the aromatic segment as 2-phenanthrene; series B: fixing the aromatic segment as a rotatable biphenyl ring system; series C: exchange the substitution of phenanthrene from 2 to 3, and change the center B ring of phenanthrene to furan as a dibenzo[b,d]furan moiety. By exchanging the trifluoromethyl group to alkyl amide group as R_2 in Figure 8, will add two hydrogen

bond donor/acceptor, which leads to a new class of compounds (series D and E). The following synthesis and discussion will be focusing on these two series of compounds.

2.1.3. Synthesis of pyrazole ring-based compounds: **5**, **14**-**23**, and **53**-**55**.

The general synthetic pathway of compounds in series D and E was carried out as outlined in Scheme 1. Each compound requires six reaction steps as described below.

The synthesis of compound **5**, **14**-**23**, and **53**-**55** were started with using 1-(4-bromophenyl)ethanone (**i**) to mix with either (4-(trifluoromethyl)phenyl)boronic acid, (4-cyanophenyl)boronic acid, or *p*-tolylboronic acid, and catalyzed by palladium (II) acetate to conduct the Suzuki coupling reaction and form the biphenyl ring intermediate **iia**-**c**. The following modifications on the ketone group went into two branched: one was condensed **iia** with diethyl oxalate to form the 1, 3-diketone intermediate **iii**; the other one was to condensed **iia**-**c** and two other commercially available intermediates (**iid** and **e**) with pre-prepared ethyl 4-(1*H*-benzo[*d*][1,2,3]triazol-1-yl)-4-oxobutanoate to form **iVa**-**e**, a series of 1, 3-diketone intermediates with two extra carbon in the middle. Together, the diketone moiety of **iii** and **iVa**-**e** were then concentrated with 4-nitrophenylhydrazine hydrochloride to generate the pyrazole derivatives **Va**-**f**. The ester groups were then converted to alkylamide **Via**-**f"** by refluxing **Va**-**f** with alkylamine ethanol solutions in seal tubes. **Via**-**f"** further underwent reduction through hydrogenation in the presence of Pd/C to afford **Viia**-**f"**. **Viia**-**a"** and **Viif**-**f"** were coupled with Boc-protected β-alanine, and directly followed with Boc-deprotection to compound **18**-**20** and **15**-**17** respectively.

Viia, **a'**, **b**, **c**, **d**, **e**, and **f** were mixed with bis(2-chloroethyl)amine hydrochloride under high temperature (170°C) to form the cyclized piperazine ring compound **22** (T315) , **23**, **5**, **54**, **55**, **14**, and **21** respectively; compound **53** can be obtained under the same reaction condition by changing bis(2-chloroethyl)amine hydrochloride into bis(2-iodoethyl)amine and perform the reaction with **Viia**. The structures of compound **5**, **14**-**23**, and **53**-**55** are listed in Table 1.

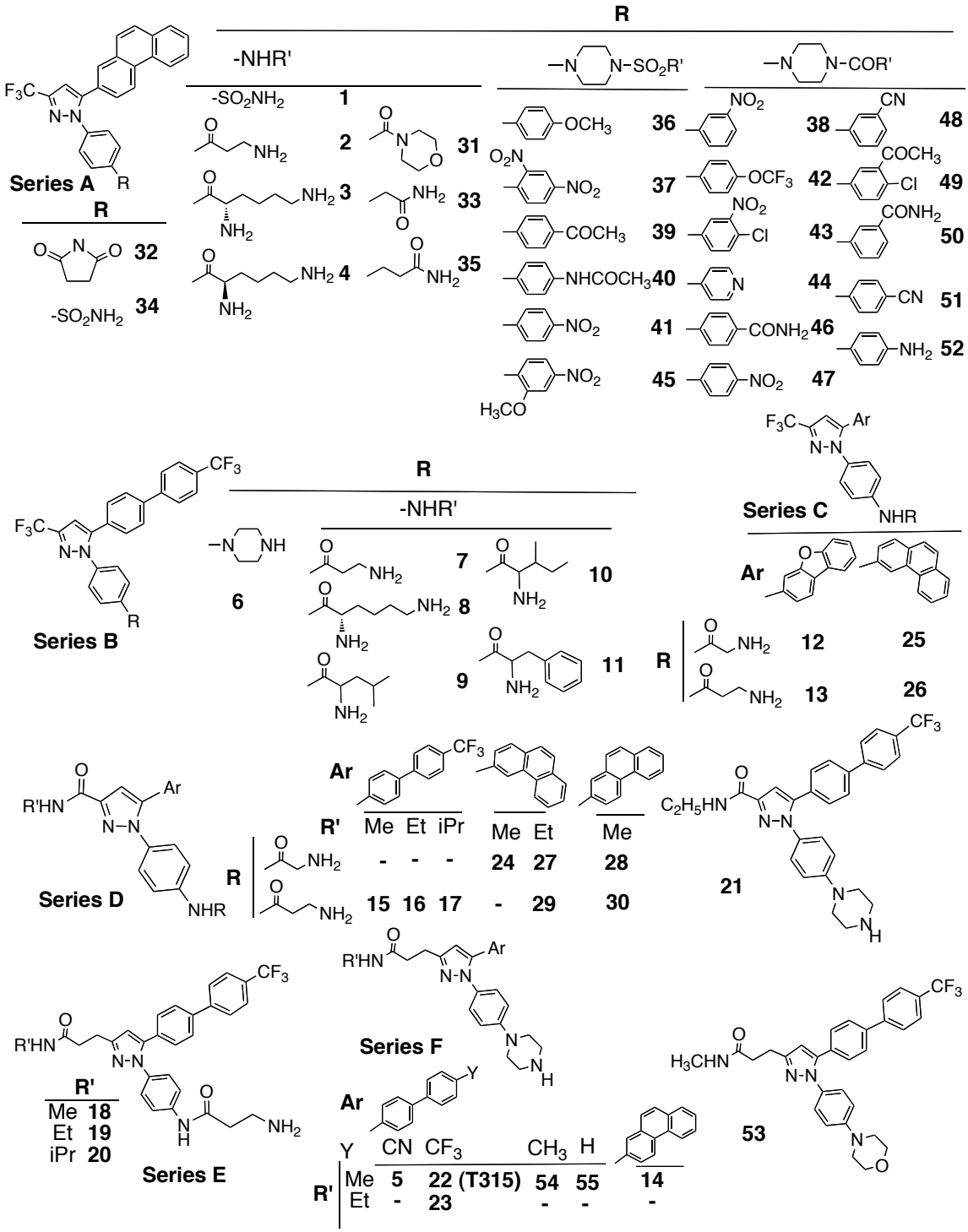

Figure 9. Chemical structures of **1**-**55** in the kinase inhbitor library used for the bioactivity screening.

Co-author and reprint (adapted) with permission from (Lee et al., 2011). Copyright (2012) American Chemical Society.

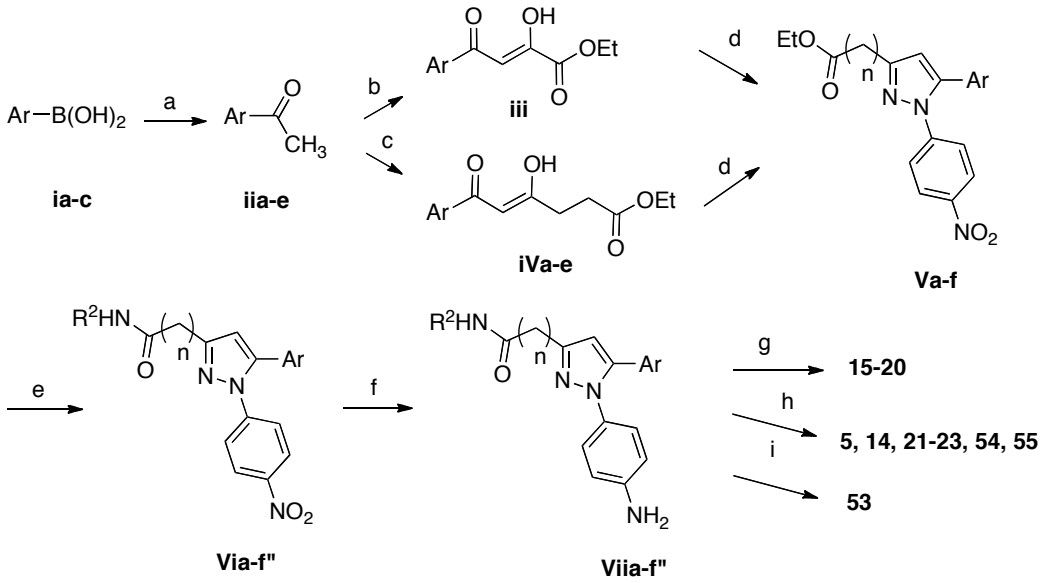

Reagents and conditions: (a) 1-(4-bromophenyl)ethanone, Bu_4NBr, K_2CO_3, $Pd(OAc)_2$ (cat.), H_2O, 60°C; (b) diethyl oxalate, NaH, THF, r.t.; (c) ethyl 4-(1*H*-benzo[*d*][1,2,3]triazol-1-yl)-4-oxobutanoate, $MgBr_2$, CH_2Cl_2, DIPEA, r.t.; (d) (4-nitrophenyl)hydrazine hydrochloride, TsOH, EtOH, microwave 130°C, 10 min; (e) NH_2R^2 in EtOH, 120°C; (f) $H_{2(g)}$ 70 psi, 10 % Pd/C, MeOH/EtOAc, r.t.; (g) (i) BocN-AlaOH, EDC, THF, r.t. (ii) 1HCl/MeOH, r.t.; (h) bis(2-chloroethyl)amine hydrochloride, xylene, 170°C; (i) 1-iodo-2-(2-iodoethoxy)ethane, xylene, 170°C.

Scheme 1. General synthetic procedures of compound **5**, **14**-**23**, **53**-**55**.

Co-author and reprint (adapted) with permission from (Lee et al., 2011). Copyright (2012) American Chemical Society.

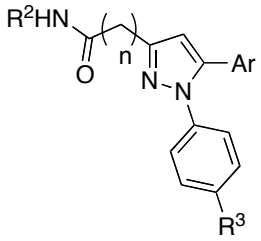

i-Vii	Ar	n	R^2	R^3	cpd
a	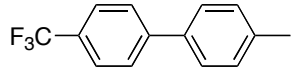	2	Me		**22** (T315)
				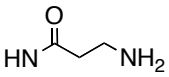	**18**
					53
a'		2	Et		**23**
				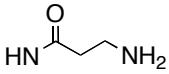	**19**
a"		2	*i*-Pr	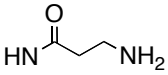	**20**
b	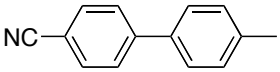	2	Me		**5**
c	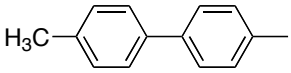	2	Me		**54**
d	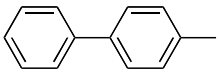	2	Me		**55**
e	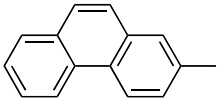	2	Me		**14**
f	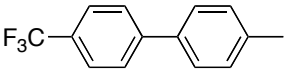	0	Me	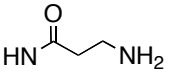	**15**
f'			Et		**21**
				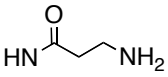	**16**
f"			*i*-Pr	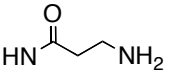	**17**

Table 1. Structures of compound **5**, **14**-**23**, and **54**-**55**.

2.1.3.1 Optimizing reaction condition

In the process of large-scale preparation of compound **22** (T315), several reaction conditions were optimized to improve the yields of the intermediates and products.

2.1.3.1.1. Preparing intermediate **iVa**

The diketone intermediate **iVa** is an important intermediate for the whole synthetic route. As outlined in Scheme 2, the traditional method to perform this condensation reaction between a β-ketone and acyl group is to use strong Lewis base to catalyze the reaction under low temperature condition. However, this reaction condition was limited by the poor solubility of the reactant and product in THF solution. Furthermore, the Lewis base reagent requires inert atmosphere reaction conditions, which is difficult to achieve in large-scale reactions. In the initial reaction trial, as outlined in Scheme 2A, the yield was only 22 % by using succinate anhydride as the acyl source, and the yield was increased to 44 % by switching to ethyl 4-chloro-4-oxobutanoate. However, this reaction yield is not applicable for gram-scale prepation and requires further optimization. This undesired low yield was further significantly improved by modification of reported procedures (Lim et al., 2007). The reaction was separated into two steps, by first connect the ethyl 4-chloro-4-oxobutanoate on benzotriazole to form a stable but good leaving group. This intermediate was then catalyzed by Lewis acid, magnesium bromide ethyl etherate, as a chelating agent to orientate the two ketone groups

together and the condensation reaction can be completed with 99 % yield in 30 gram-scale preparation (Scheme 2B).

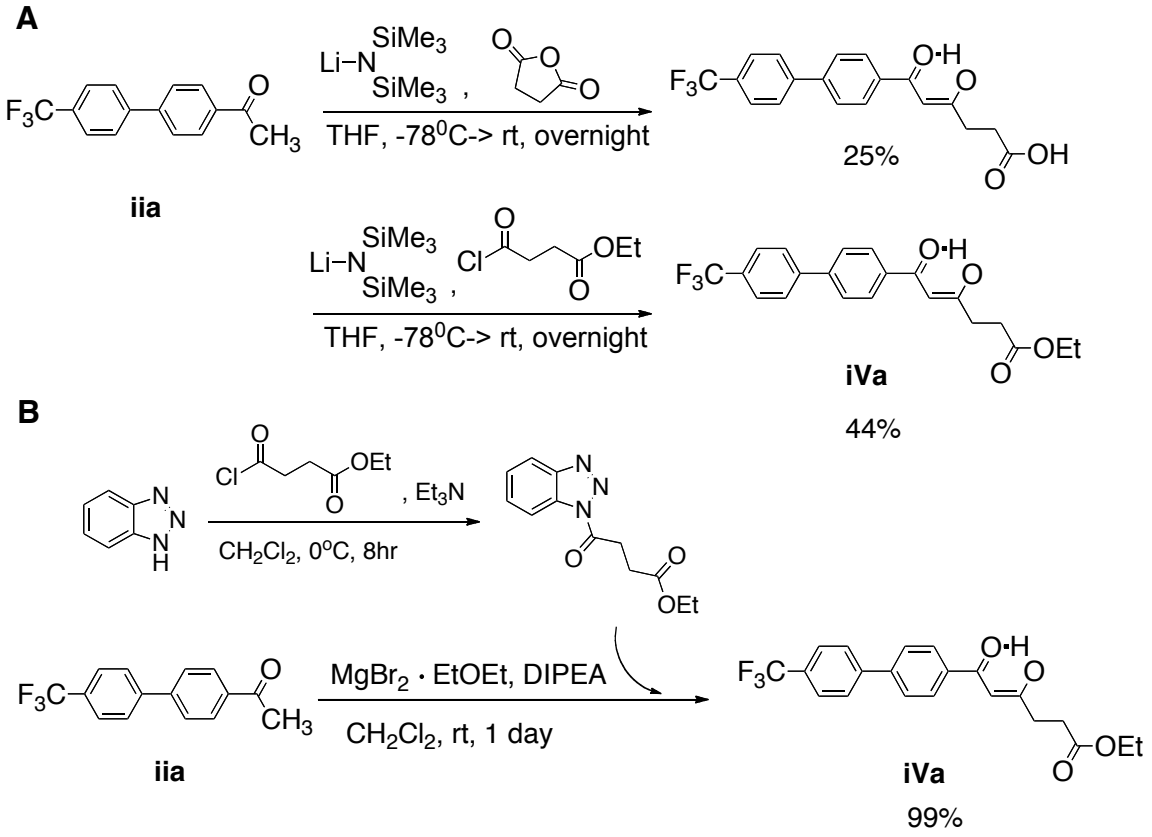

Scheme 2. Preparation methods of intermediate **iVa**.

(A) Low yield reaction condition by using Lewis base as catalyst. (B) Improved reaction condition by introducing a stable/good leaving group, which was then catalyzed by a chelating agent to prepare **iVa**.

2.1.3.1.2. Preparing intermediate **Va**

The step d in Scheme 1 that forms the pyrazole moiety, **Va**, was also critical for the preparation of the following product. By analyzing the reaction mechanism (Scheme 3), there are two routes for the reaction to process. By following route a: the hydrazine forms the Schiff base with the 3-ketone of **iVa** first, and the second amine group will cyclized with 1-ketone, to form the desire pyrazole ring structure **Va**. On the contrary, by following route b will form an undesired isomer. The intermediate **Va** and its isomer possess the same polarity under EtOAc/hexane, CH_2Cl_2/hexane, and toluene/hexane solvent systems, which is difficult for compound purification. The difference of the chemical shifts in ^{1}H-NMR spectrum is the only way to distinguish the two isomers. Under ^{1}H-NMR detection, the proton signal of the H-pyrazole is δ 6.68 for **Va**, and δ 6.45 for the isomer. By detecting the ratio of these two sets of signals can determine if the reaction is heading the correct path.

After several attempts of changing the reaction temperature, acid, solvent system, and heating methods (Table 2), the optimal reaction condition is to use microwave as the heating source with the presence of *p*-TsOH as catalyst. The yield after re-crystallization is 58% at 1 gram scale. The requirement of microwave energy also indicates that intermediate **Va** is the kinetically stable product, while its isomer is the thermodynamically stable product and requires no additional energy to achieve the stable state.

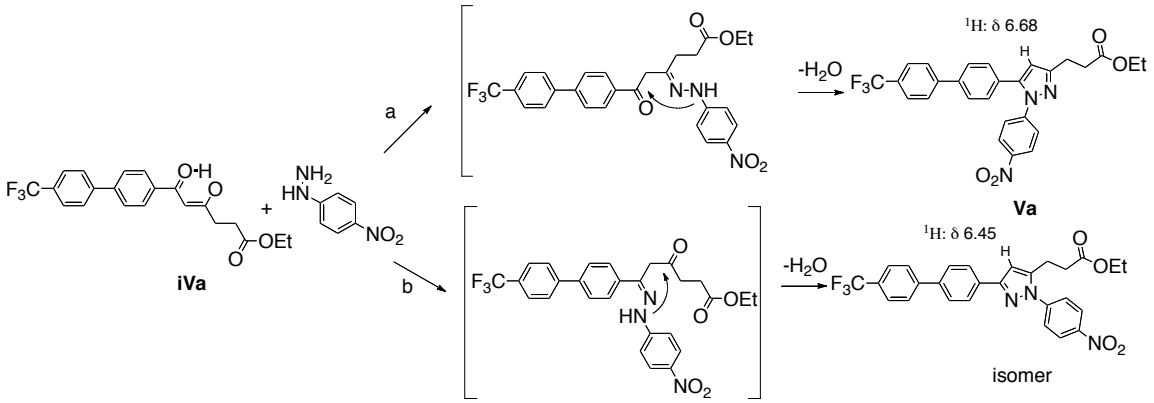

Scheme 3. Reaction routes and conditions for preparing **Va** and its isomer.

Both reaction route of (a) and (b) are catalyzed with HCl in EtOH. The proton chemical shifts for the H-pyrazoles are listed above the structures.

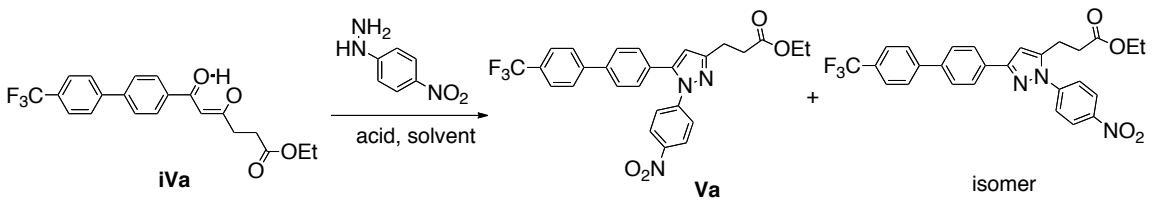

Entry	acid	solvent	Temp.	Reaction time	Yield (%), **Va**/isomer
1	HCl	EtOH	RT	2 days	33 %, 3/1
2	HCl	EtOH	80°C	2 days	80 %, 1/3
3	HCl	CH_2Cl_2/EtOH	RT	4 days	29 %, 3:2
4	*p*-TsOH	CH_2Cl_2/EtOH	RT	16 h	38 %, 3/1
5	*p*-TsOH	CH_2Cl_2/EtOH	RT	2 days	71%, 3/2
6	*p*-TsOH	EtOH	Microwave,130°C	5 min X 3	33 %, 1/0
7	*p*-TsOH	EtOH	Microwave,130°C	30 min x 3	45 %, 1/0
8	*p*-TsOH	EtOH	Microwave,130°C	10 min	58 %, 1/0

Table 2. Reaction conditions for optimizing the yield of the intermediate **Va**.

2.2. Screening for potent PDK1/PDK2 inhibitors

In order to directly access the inhibition activity against PDK1 and PDK2, the kinase inhibitor library was screened in PC-3 prostate cancer cells by using western blotting methods (Figure 10) (Lee et al., 2011). The concentration was fixed at 2.5 μM in 5% FBS RPMI-1640 medium for 24 h. The decrease level of the phosphorylation of Akt at either the Thr-308 or Ser-473 site, will point out possible PDK1 or PDK2 inhibitor, respectively.

From the screening result, out of 53 compounds (**54** and **55** not included), only two compounds: **22** and **23**, have shown significant dephosphorylation of Akt at Ser-473 without affecting that of Thr-308, while other agents have no effect on either sites, demonstrating that these two compounds are possible PDK2 inhibitors. And since the structures of these two compounds only have one methylene group difference, the following activity validation experiments are all focused on compound **22**, which we rename as T315 for the following report.

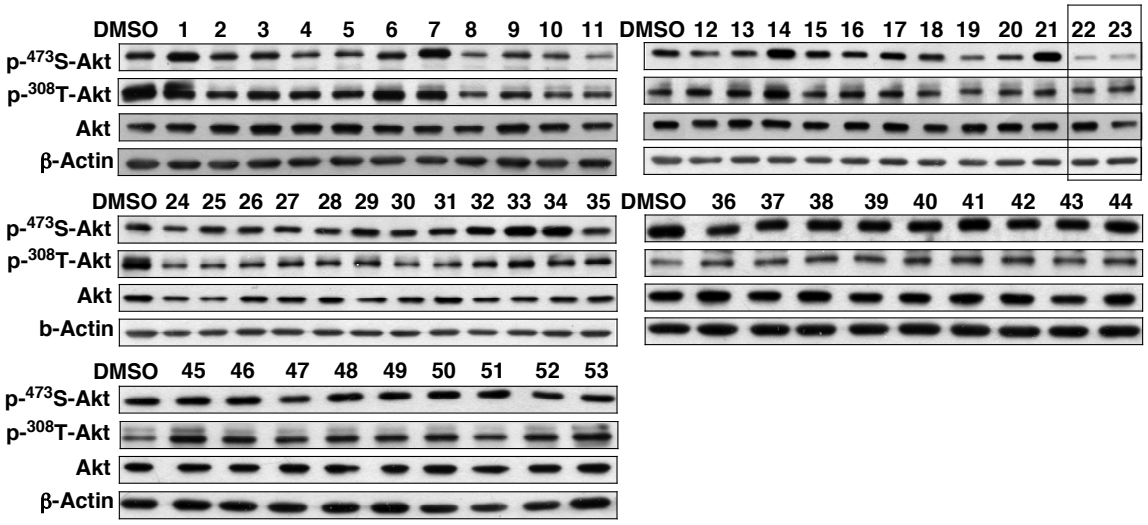

Figure 10. Identification of putative PDK2 inhibitors by screening of an in-house focused compound library.

Western blot analysis of the effects of **1-53** versus DMSO control on the phosphorylation of Akt on Ser-473 versus Thr-308 in PC-3 cells. Cells were exposed to individual test agents at 2.5 μM or DMSO vehicle in 5% FBS-supplemented RPMI 1640 medium for 24 h.

Co-author and reprint (adapted) with permission from (Lee et al., 2011). Copyright (2012) American Chemical Society.

2.3 Target validation of T315

With the discovery of T315 as a potential PDK2 inhibitor, we further pursue to identify the real identity of this PDK2. Through literature review, we hypothesize that the

two major possible targets are ILK and mTORC2. Herein, we use several lines of biological approaches to identify the target of T315.

2.3.1. Cell viability and selectivity of T315 between cancer and normal epithelial cells

In order to validate the anti-tumor effect of T315, a panel of prostate (PC-3 and LNCaP) and breast (MCF7, SKBR3, MDA-MB-231, and MDA-MB-468) cancer cell lines were treated with T315 in MTT assay for 24 h (Figure 11) (Lee et al., 2011). T315 effectively suppress the viabilities of cancer cell with the following IC_{50} value: LNCaP, 1.6 μM; PC-3, 2 μM; MDA-MB-231, 1 μM; MDA-MB-468, 1.5 μM; SKBR3, 1.8 μM; MCF-7, 2.5 μM. We further examine the cell viability of T315 against normal prostate epithelial cells (PrECs) and mammary epithelial cells (MEC) to determine the selectivity of T315 between cancer and normal cell lines. In contrast to cancer cells, normal cells show significant resistance to the anti-proliferative effect of T315 with the IC_{50} value > 5 μM, demonstrating that T315 is relatively safe for cancer treatment.

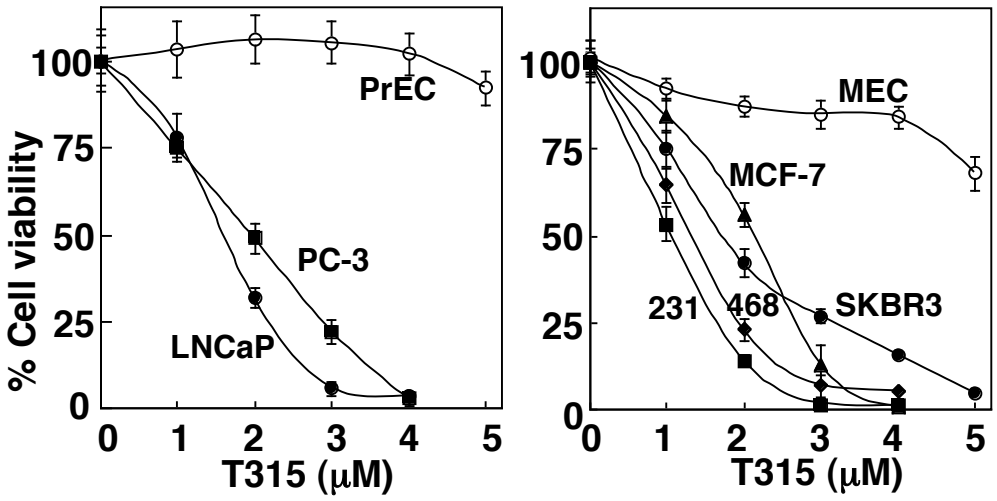

Figure 11. Selectivity of T315 between cancer and normal epithelial cell lines.

Dose-dependent suppressive effects of T315 on the viability of PC-3 and LNCaP prostate cancer cells versus PrECs (left panel), and of MDA-MB-231, MDA-MB-468, SKBR3, and MCF-7 breast cancer cells versus MECs (right panel) in 5% FBS supplemented medium after 24 h of treatment. Cell viability was determined by MTT assays. Points, means; bars, SD (n = 6).

Co-author and reprint (adapted) with permission from (Lee et al., 2011). Copyright (2012) American Chemical Society.

2.3.2. Western blot analysis of T315 in ILK and mTORC2 pathways

The PDK2 inhibitory activity of T315 was further confirmed in PC-3 and MDA-MB-231 cells in western blot analysis. T315 demonstrated dose-dependent effect of dephosphoylating the Akt at Ser-473 without affecting the Thr-308 site (Figure 12) (Lee et al., 2011). At the same time, two other ILK downstream effectors: GSK3β and MLC

also show parallel dephosphorylation at Ser-9 and Thr-18/Ser-19, respectively. On the other hand, two direct downstream targets of mTORC2: SGK1 and PKCα, shows no effect of their phosphorylation status. Furthermore, in ILK shRNA-mediated knockdown experiments in PC-3 cells, also show similar effects as in T315 treatments. Together, these evidence suggested that T315 might mediate the dephosphorylation of Akt at Ser-473 through the inhibition of ILK, instead of mTORC2.

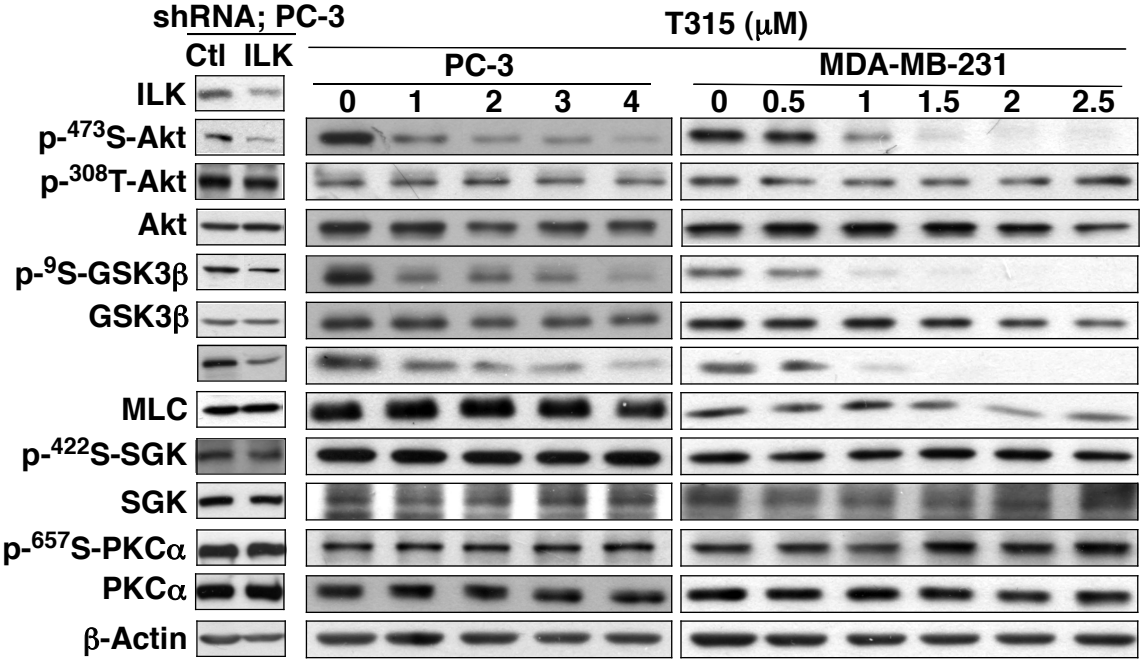

Figure 12. The suppressive effects of shRNA-mediated knockdown of ILK and T315 on the phosphorylation of Akt at Ser-473 and Thr-308 and the downstream targets of ILK (GSK3β and MLC) versus those of mTORC2 (SGK and PKCα) in PC-3 and/or MDA-MB-231 cells.

Cells were exposed to T315 at the indicated concentrations for 24 h in 5% FBS-supplemented medium. The immunoblots shown are representative of three independent experiments.

Co-author and reprint (adapted) with permission from (Lee et al., 2011). Copyright (2012) American Chemical Society.

2.3.3. Evidence of ILK is the target of T315

The western blot analysis data have demonstrated that T315 can inhibit the "function of the ILK pathway." However, that does not provide the evidence that T315 is directly or indirectly inhibiting ILK. Hence, three approaches, including ILK *in vitro* kinase assay, protection effect of ectopic expression of GFP-tagged CA-ILK in cells, and other ILK-dependent pathways, were conducted to provide evidence to support that T315 is a direct ILK inhibitor.

2.3.3.1 *In vitro* activity of T315

The ILK *in vitro* kinase assay is the most straightforward method to examine if T315 is an ILK inhibitor. However, ILK also has been reported to act as a pseudo kinase that can only phosphorylate its downstream targets as a ILK/PINCH/parvin complex, and there were debates of whether recombinant ILK protein itself has the kinase activity or not (Wickstrom et al., 2010). Furthermore, so far, there are no commercial available resources to provide the ILK kinase assay service or assay kit. Hence, a self-assembled

radiometric ILK kinase assay was developed by modifying reported procedures (Persad et al., 2000; Hannigan et al., 1996). The ILK protein was pulled down from EGF stimulated PC-3 cells by ILK antibody and binding with protein A/G beads. The assay was performed by incubating the ILK protein with the presence of a dose-range of T315, myelin basic protein (MBP) as substrate, and [γ-^{32}P] ATP as phosphate donor. Representative autoradiographic data from one of several experiments are shown in Figure 13A (Lee et al., 2011), of which the densitometric analysis indicates that the *in vitro* IC_{50} value of T315 against ILK is 0.6 μM.

2.3.3.2 Protective effect against T315 with the overexpression of ILK in PC-3 cells

If the cytotoxicity of T315 against cancer cell is mediated through the inhibition of ILK, then by increasing the expression of ILK in cancer cells should provide protection effect to the cell against T315. To prove this hypothesis, we transfected the GFP-tagged constitutively active (CA)-ILK plasmids in PC-3 cells to generate a CA-ILK stable clone. The expression level of ILK was validated through western blotting. As shown in Figure 13B (left panel) (Lee et al., 2011), the stable expression of GFP-tagged CA-ILK has increased the phosphorylation of Ser-473-Akt and Ser-9-GSK3β, while the levels of p-Thr-308-Akt, p-PKCα, and p-SGK1 remained unaltered. In addition, comparing with the GFP-PC-3 (control, IC_{50}: 2 μM), the CA-ILK-PC-3 demonstrates a increase of the IC_{50} value (4 μM) (Figure 13B, right panel) (Lee et al., 2011). Indicating that the cell killing effect of T315 is related to ILK.

2.3.3.3. T315 suppressed the expression of YB-1 and its targets HER2 and EGFR via an ILK-dependent mechanism

The expression level of transcriptional/translational regulator YB-1 has been reported to be regulated in an ILK-dependently pathway (Kalra et al., 2010; Stratford et al., 2007). By suppressing the activity of ILK through siRNA –mediated knockdown will reduce the expression of several growth factor receptors, including HER2 and EGFR through this pathway. Pursuant to these findings, we examined the ability of T315 to modulate the expression of these important signaling effectors in PC-3 and SKBR3 cells. Western blot and RT-PCR analyses indicate that T315 reduced the expression of YB-1, HER2, and EGFR, at both protein and transcript levels, in a dose-dependent manner in both cell lines (Figure 14A, PC-3; Figure 14B, SKBR3) (Lee et al., 2011). Equally important, overexpression of CA-ILK, through stable and transient transfection in PC-3 and SKBR3 cells, respectively, diminished the suppressive effect of T315 on these signaling effectors.

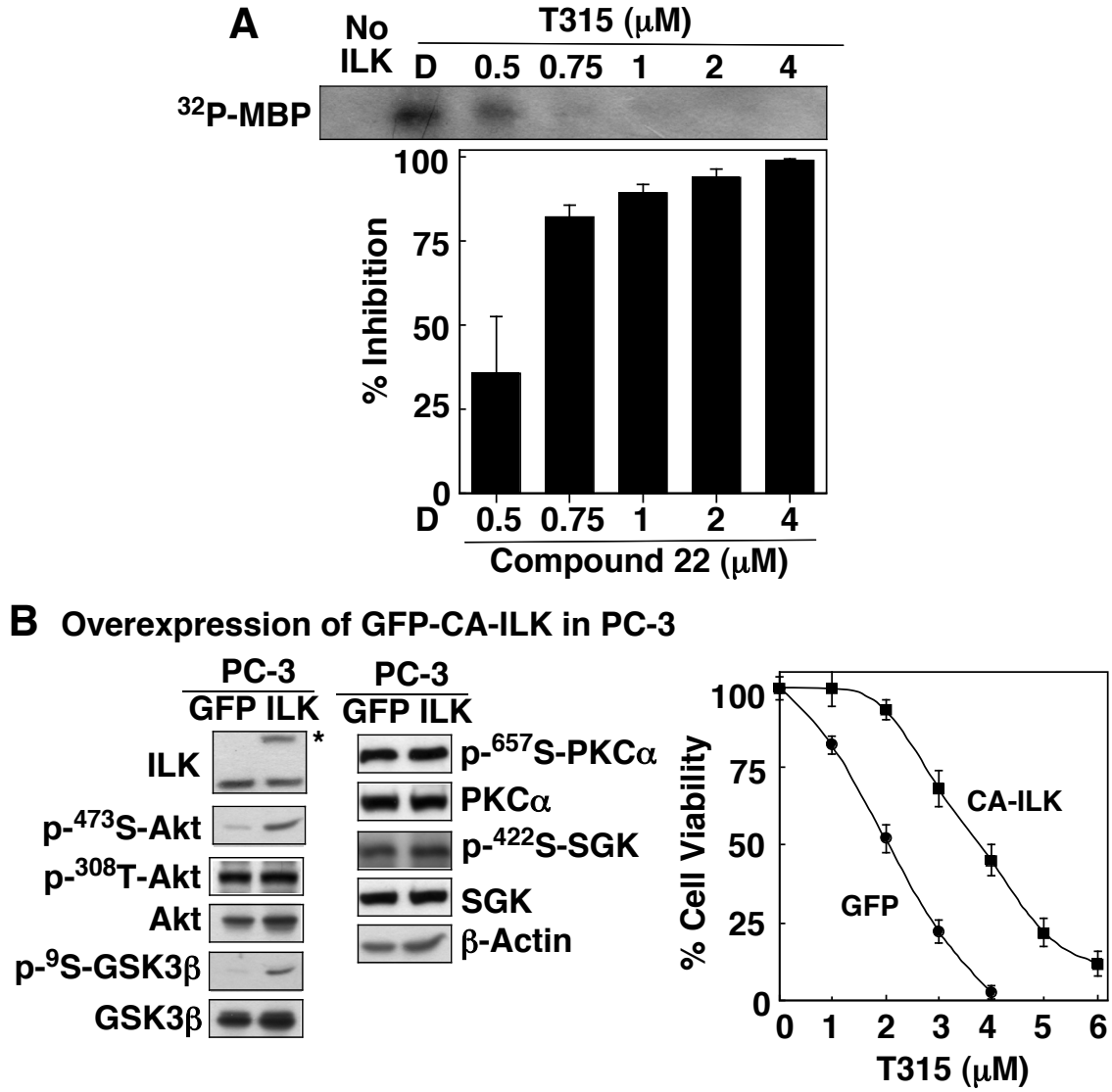

Figure 13. Evidence that T315 is an ILK inhibitor.

(A) Dose-dependent suppressive effect of T315 on the kinase activity of immunoprecipitated ILK. Kinase activity was determined in the presence of T315 at the indicated concentrations by measuring ^{32}P-phosphorylation of the ILK substrate MBP as described in the Experimental Section. Data are presented as means ± SD (n = 3). (B) Effects of ectopic expression of GFP-tagged CA-ILK versus GFP alone on the phosphorylation of Akt, GSK3β, PKCα, and SGK in stable PC-3 transfectants (left panel)

and on the viability of PC-3 cells after 24 h treatment with T315 at different concentrations in 5% FBS-supplemented medium (right panel). Blot on the left confirms the presence of the CA-ILK protein (*) in transfected PC-3 cells. The immunoblots shown are representative of three independent experiments. Points, means; bars, SD (n = 6).

Co-author and reprint (adapted) with permission from (Lee et al., 2011). Copyright (2012) American Chemical Society.

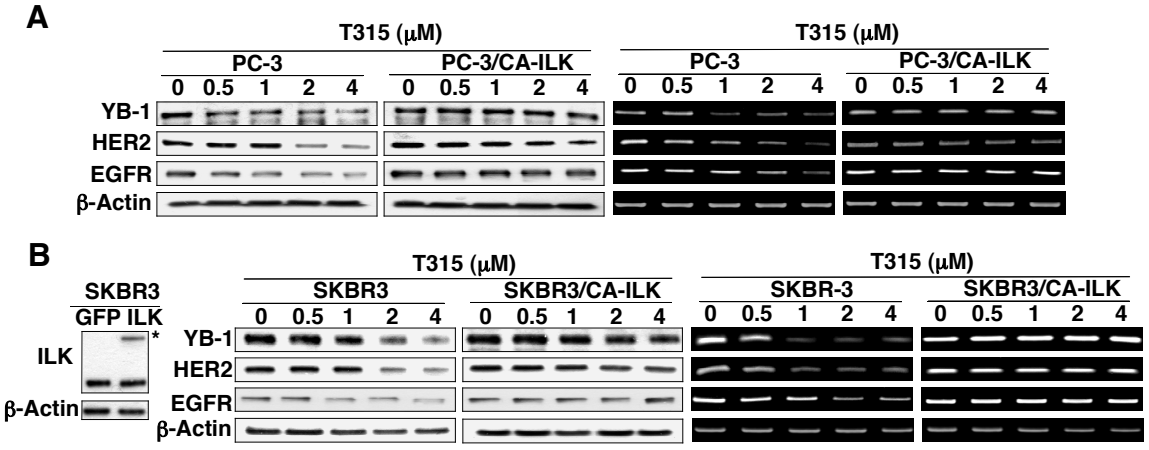

Figure 14. Dose-dependent effects of T315 on the protein (left panel) and mRNA (right panel) expression of YB-1 and its targets HER2 and EGFR.

(A) PC-3 cells versus stable PC-3 transfectants expressing CA-ILK (PC-3/CA-ILK), and (B) SKBR3 cells versus transient SKBR3 transfectants expressing ectopic CA/ILK (SKBR3/CA-ILK). Cells were treated with T315 at the indicated concentrations in 5% FBS-supplemented medium for 24 h. These data are representative of three independent experiments. Blot on the left confirms the presence of the CA-ILK protein (*) in

transfected SKBR3 cells.

Co-author and reprint (adapted) with permission from (Lee et al., 2011). Copyright (2012) American Chemical Society.

2.3.4. Specificity of T315 in kinase inhibition

Specificity is always a challenge in terms of developing selective ATP competitive kinase inhibitors, since all the kinase domains share the same substrate: ATP. The selectivity of a kinase inhibitor was based on the minor difference of the binding energy between the substrate (inhibitor) and the binding pockets of different kinases. The specificity of T315 was evaluated against a panel of 22 recombinant kinases by kinase-profiling assays performed by a commercial vendor (Millipore, Billerica, MA). The results as listed in Table 3 supported a high degree of specificity of T315 for ILK. Among the 22 recombinant kinases examined, the only exception was p70S6K, which exhibited greater than 50% inhibition by T315 (44% residual activity after treatment). This finding was confirmed by western blot analysis of the dose-dependent effects of T315 on the phosphorylation of p70S6K versus its target S6 in PC-3 cells (Figure 15A) (Lee et al., 2011). As shown, T315 exhibited a modest suppressive effect on phosphorylated S6 levels, without affecting the phosphorylation status of p70S6K, an mTOR substrate. Moreover, in contrast to the reported effects of the known ILK inhibitor QLT0267 (Kalra et al., 2009), T315 did not affect the auto-phosphorylation of focal adhesion kinase (FAK) at Tyr-397, a marker of FAK inhibition (Cary and Guan, 1999). In addition, as evidence suggests the intermediary role of ILK in mediating growth

factor/integrin-induced activation of ERKs (Huang et al., 2000; Su et al., 2010; White et al., 2001; Tabe et al., 2007) or p38 (Esfandiarei et al., 2010; Ishii et al., 2001; Leung-Hagesteijn et al., 2005a; Sawai et al., 2006) in various cell systems, we investigated the phosphorylation status of ERKs and p38 versus JNKs in T315-treated cells. As shown in Figure 15A (Lee et al., 2011), of the three MAP kinases evaluated, T315 showed dose-dependent suppressive effects on the levels of phospho-ERK1/2 and phospho-p38, while that of p-JNK remained unaltered. Equally important, stable expression of CA-ILK prevented T315-facilitated inhibition of ERK and p38 phosphorylation, supporting the functional role of ILK in regulating the activation of ERKs and p38 in PC-3 cells (Figure 15B) (Lee et al., 2011). In contrast, CA-ILK showed no protective effect on the downregulation of S6 phosphorylation, confirming that T315 cross-inhibited p70S6K.

Kinase	Kinase activity % T315 (5 μM)	Kinase	Kinase activity % T315 (5 μM)
Abl (h)	73	JAK2 (h)	114
CDK1/cyclinB (h)	98	JAK3 (h)	128
CDK5/p25(h)	99	Met (h)	110
CDK5/p35(h)	110	mTOR (h)	122
cKit(h)	100	P70S6K	44
cSRC(h)	91	PDK1 (h)	94
DAPK1 (h)	50	PKBα (h)	88
EGFR (h)	103	PKCα (h)	97
Flt3 (h)	66	Ros (h)	103
GSK3β (h)	142	Rsk1 (h)	65
IKKβ (h)	102	ZAP-70 (h)	104

Table 3. Remaining activities of kinase (%) after treatment with T315 at 5 μM.

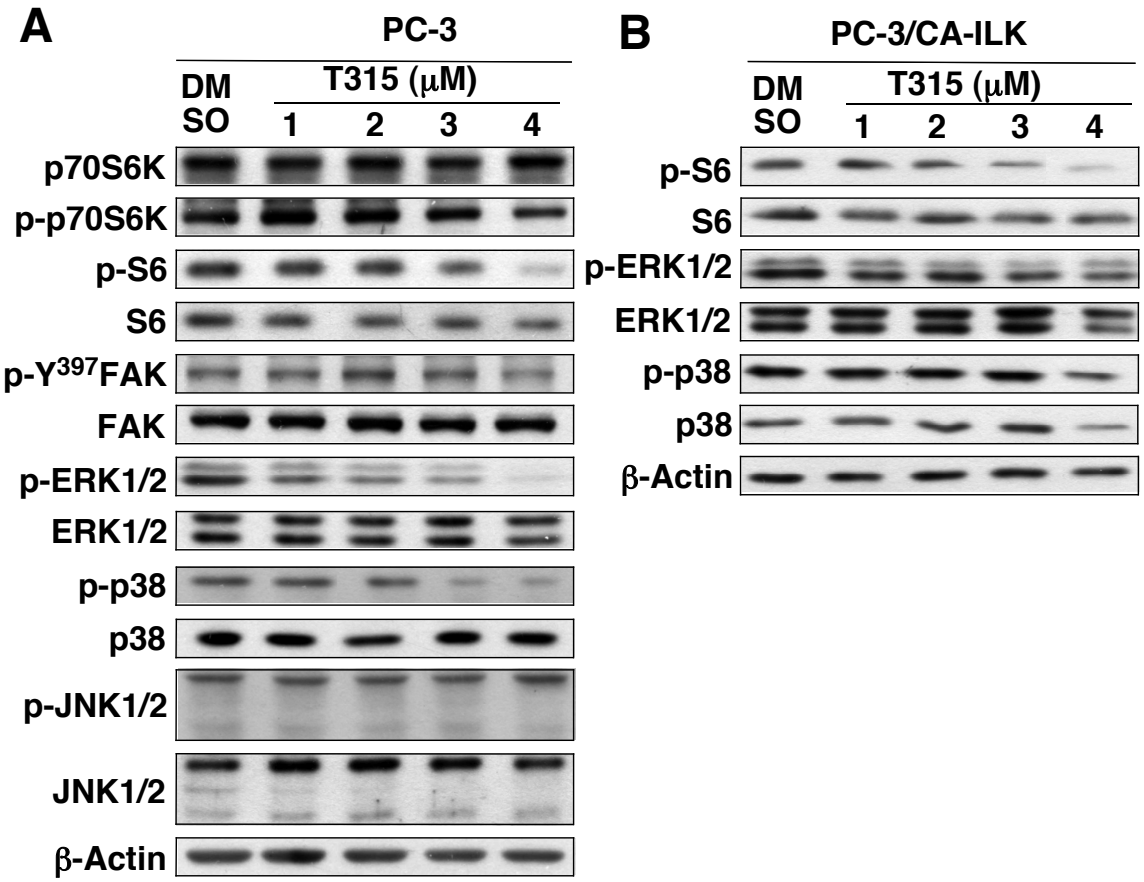

Figure 15. Specificity of T315 in kinase inhibition.

(A) Western blot analysis of the dose-dependent effect of T315 on the phosphorylation of p70S6K, S6, Tyr-397-FAK, ERKs, p38, and JNK in PC-3 cells. Cells were exposed to the indicated concentrations of T315 in 5% FBS-supplemented medium for 24 h. (B) Effects of the stable expression of CA-ILK, as depicted in Figure 13B, on T315-mediated dephosphorylation of S6, ERKs, and p38 in PC-3 cells . The immunoblots shown are representative of three independent experiments.

Co-author and reprint (adapted) with permission from (Lee et al., 2011). Copyright (2012)

American Chemical Society.

2.3.5. T315 causes cell death through autophagy and apoptosis

To further evaluate the mode of antiproliferation activity of T315 is through which programmed cell death pathway, we analyze its effects in PC-3 cells through flow cytometry and western blotting. Under flow cytometry, the cell cycle analysis and Annexin V staining demonstrates that T315 will not induce sub G1 phase accumulation and apoptosis effect before the concentration of T315 reaches 2 μM (Figure 16A,B) (Lee et al., 2011). Furthermore, T315 demonstrates a dose-dependent effect of PARP cleavage at ≥ 2 μM, while LC-3 conversion occurs at ≤ 1 μM, under western blot analysis (Figure 16C) (Lee et al., 2011). This indicates that T315 will initially induce autophagy at low concentration, followed by apoptosis effect at higher concentration. The effect of LC-3 conversion can also be blocked by the stable expression of CA-ILK, suggesting that T315-induced autophagy was attributable to ILK inhibition (Figure 16D) (Lee et al., 2011). Autophagy plays a dichotomous role in mediating cell fates, either protective or destructive, in response to metabolic stress or therapeutic agents (Codogno and Meijer, 2005). Hence, we further examined the effect of siRNA-mediated knockdown of autophagy-related 5 homologue (Atg5) on T315-mediated suppression of PC-3 cell viability. As shown, silencing of Atg5 disrupted T315-induced LC3-II processing and attenuated drug-induced cytotoxicity in PC-3 cells (Figure 16E) (Lee et al., 2011). This finding suggests that the induction of autophagy represents a mechanism by which T315 mediates its antiproliferative activity, especially at low concentrations.

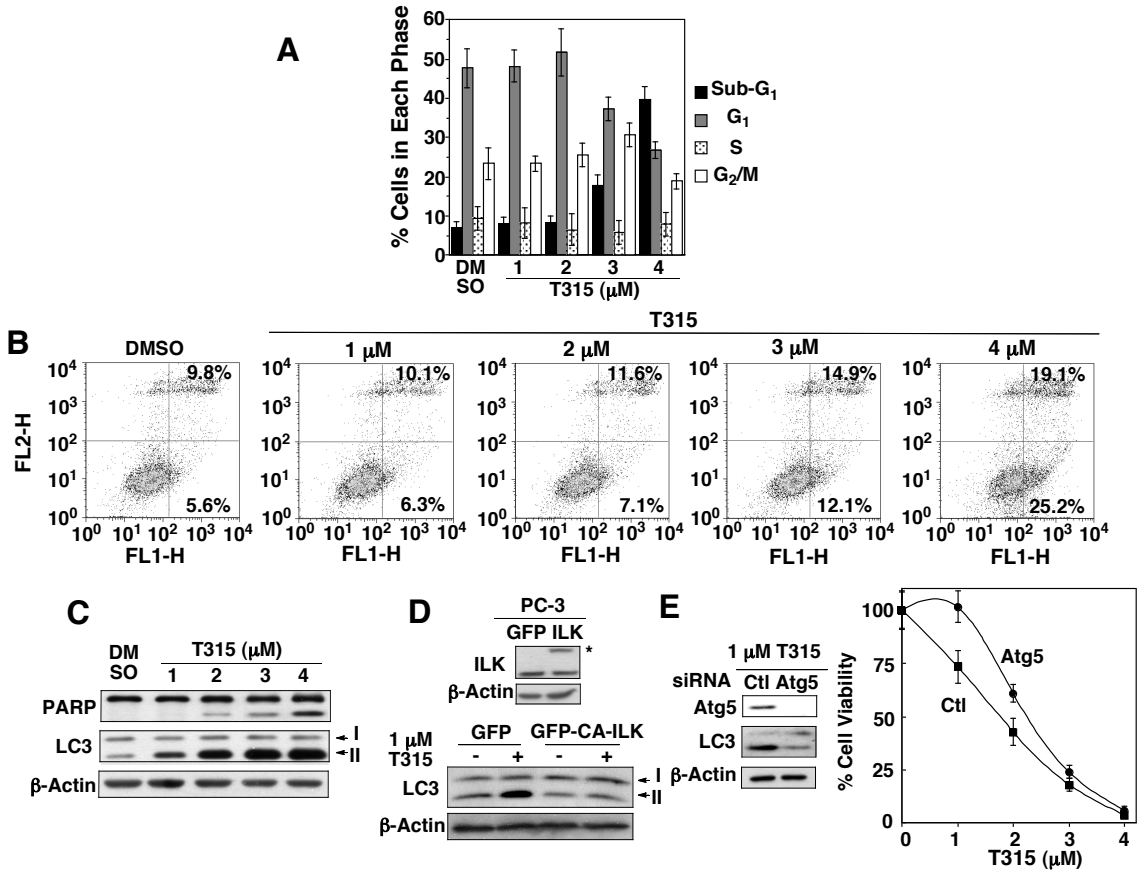

Figure 16. Evidence that T315 induces cell death through both apoptosis and autophagy. (A) Histograms depicting the percentages of PC-3 cells at various phases of the cell cycle after exposure to the indicated concentrations T315 in 5% FBS-supplemented medium for 24 h. Each data point represents the mean ± SD (n = 3). (B) Dose-dependent effect of T315 on the extent of apoptosis induction, as detected by annexin V/PI staining. The values in the right upper and lower quadrants denote the average of three independent experiments. (C) Dose-dependent effects of T315 on PARP cleavage and LC3-II conversion in PC-3 cells after 24 h of treatment. (D) Protective effect of the stable transfection of CA-ILK (*), as depicted in Fig. 12B, on the induction of LC3-II conversion by 1 μM T315 in PC-3 cells. (E) siRNA-mediated knockdown of Atg5

inhibited T315-induced autophagy (left panel) as determined by LC3-II conversion, and provided partial protection against T315-mediated suppression of PC-3 cell viability (right panel). Points, means; bars, SD (n = 6). All immunoblots shown are representative of three independent experiments.

Co-author and reprint (adapted) with permission from (Lee et al., 2011). Copyright (2012) American Chemical Society.

2.3.6. Suppressive effect of T315 in xenograft tumor growth

The *in vivo* antitumor efficacy of T315 was further evaluated in a PC-3 tumor xenograft model. The PC-3 subcutaneous xenograft tumors were established in athymic nude mice and start the administration of T315 orally, once daily for 35 days (mean starting tumor volume, 157.1 ± 29.1 mm^3). The volumes of the tumor size were measured once weekly. Comparing with the vehicle group, T315 demonstrated significant suppression of tumor growth under 25 and 50 mg/kg treatment (48% and 62%, respectively) (Figure 17A) (Lee et al., 2011). Furthermore, the western blot analysis of the tumor tissues that were extracted at the end of the 35 days treatment, show similar ILK signaling pathway downregulation pattern as in cellular level experiment (Figure 17B) (Lee et al., 2011). Indicating that T315 possess certain degree of oral bioavailability, and the suppression of tumor growth is mediated through ILK inhibition.

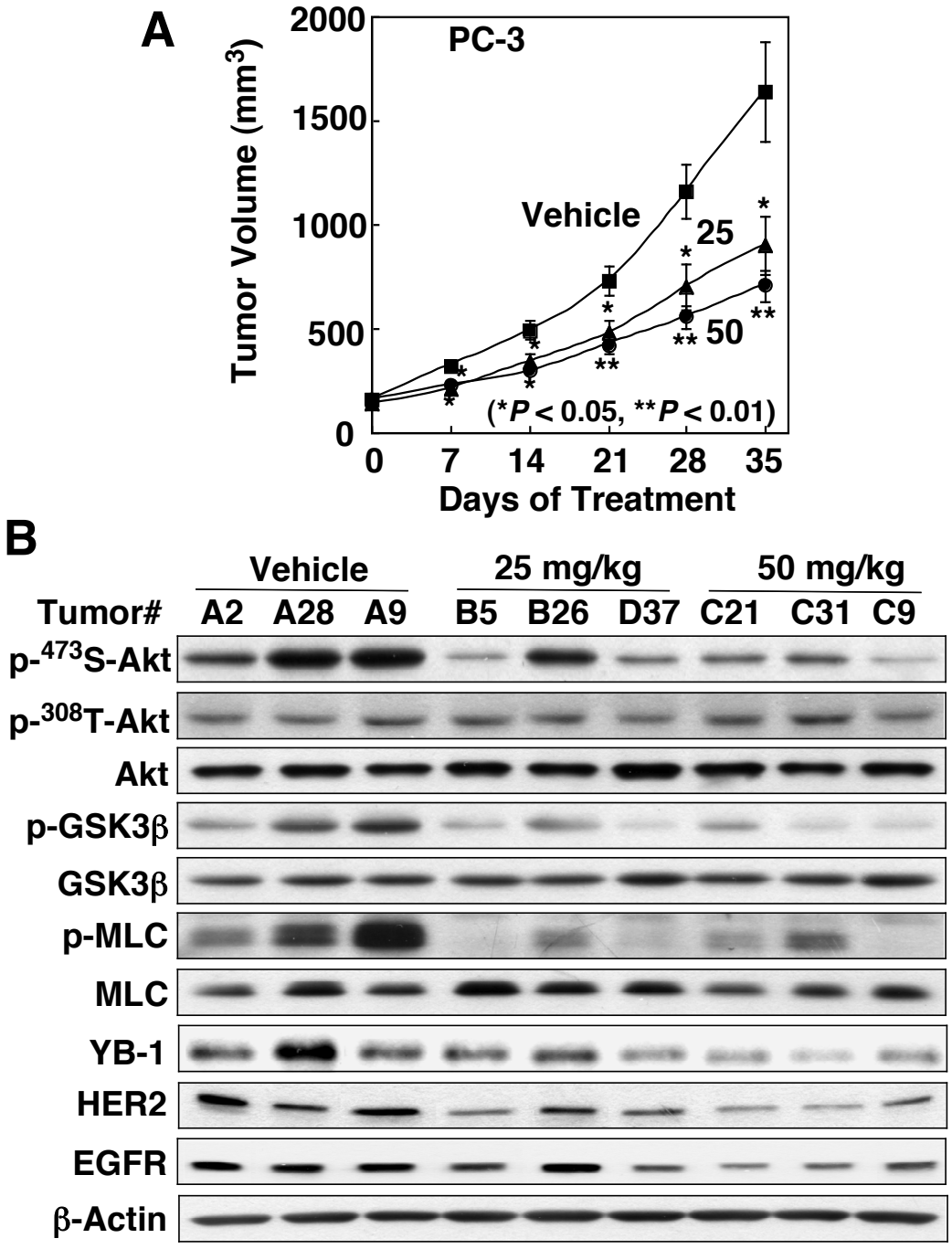

Figure 17. *In vivo* antitumor efficacy of T315.

(A) Effect of oral T315 on PC-3 xenograft tumor growth in athymic nude mice. Mice with established s.c. PC-3 xenograft tumors were treated orally once daily with T315 at

25 and 50 mg/kg or vehicle for 35 days and tumor growth was monitored as described in the Materials and Methods section. Points, mean; bars, SEM (n = 6). (B) Western blot analysis of intratumoral biomarkers of drug activity in three representative PC-3 tumors from each group of mice treated for 35 days as described above in (A).

Co-author and reprint (adapted) with permission from (Lee et al., 2011). Copyright (2012) American Chemical Society.

2.4. Structure-activity relationship studies of T315

2.4.1. *In vitro* activities of T315 derivatives

With strong *in* vitro/*in vivo* potency of inhibiting ILK, we further pursue to optimize the structure of T315, and determine its pharmacophore. The structure of T315 can be briefly divided into four structural motifs: a. aromatic ring moiety; b. hydrogen bond donor/acceptor arm; c. piperazine moiety; d. pyrazole ring core (Figure 18A). Base on this partition, eleven T315 derivatives were chosen from the compound library or newly synthesized as listed in Figure 18B. Compound **21**, **23**, and **6** were used to evaluate the importance of the length and substitution of the hydrogen bond donor/acceptor arm, and compound **53** was selected to evaluate the effects of the amine of the piperazine ring, by switching it into morpholine ring. The different substitution on the biphenyl moiety (**55**, **5**, and **54**) or phenanthrene ring system (**14**) can provide useful information of the optimal bulkiness for the aromatic ring region. Three other derivatives: **56-58** were further synthesized to provide the same motifs as T315, but with different geometry and

ring core, which can be used to determine the role of the angles between each motif.

The antiproliferation activities of these compounds were accessed by MTT assay in PC-3 cells for 24 h treatment. The ILK inhibition activities were determined by western blot analysis of the effects of compounds verses DMSO control on the dephosphorylation level of p-Ser-473-Akt at 2.5 and 5 μM in PC-3 cells (Table 4). Structure-activity relationship analysis revealed a stringent structural requirement for cytotoxicity and p-Ser-473-Akt dephosphorylating activity of T315. By changing of any motif of a-d (Figure 18A.) resulted in loss of ILK inhibitory activity, such as compound **53**. By changing the amino group to oxygen on the piperazine ring will completely diminish the activity of T315 in either cell killing or ILK inhibition. The only two compounds that demonstrated similar level of antiproliferation and ILK inhibition activities as T315 are compound **23** and **54**. However, by comparing the structures, **23** only has one extra methylene group at the amide substitution; and compound **54** was just simply transferring the trifluoromethyl group to one of its bioisostere: methyl group. Hence, the conclusion from this SAR study is: each motif of T315 is equally important, especially the length and appearance of hydrogen bond donor/acceptor group on motif b. T315 remains to be the most active ILK inhibitor in this study.

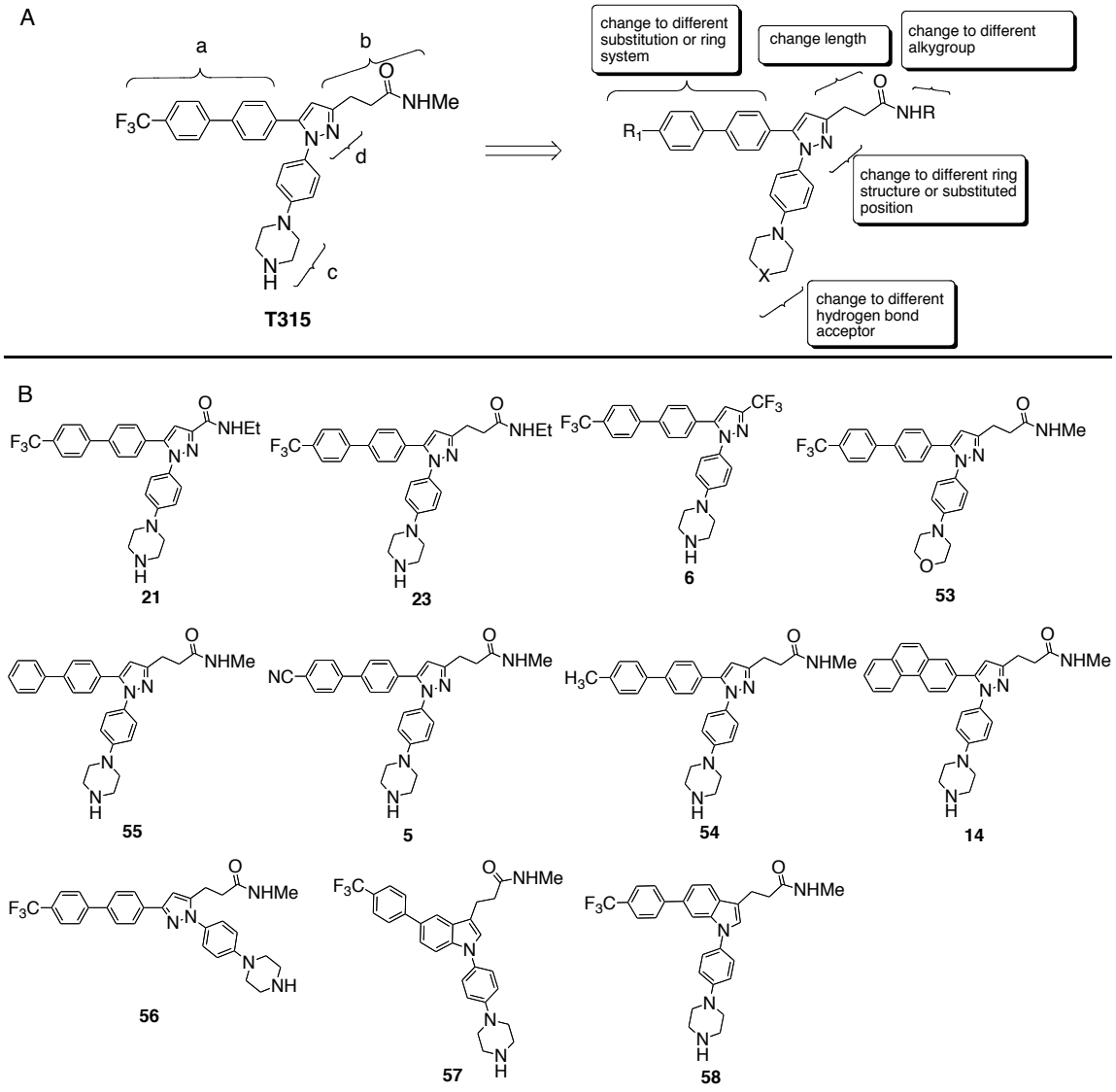

Figure 18. Design of T315 derivatives.

(A) Structural motif of T315 and related modification strategies. (B) Structures of T315 derivatives for SAR studies.

Compound	**T315**	**21**	**23**	**6**	**53**	**55**	**5**	**54**	**14**	**56**	**57**	**58**
PC-3 Cell viability IC_{50} (μM)	1.8	7.0	2.4	2.3	>10	4.3	8.0	1.8	2.8	3.4	3.4	3.8
ILK activity inhibition												
2.5 μM	**		**		N/A	**	*	**	*	*	**	**
5 μM	****	N/A	N/A	**	N/A	N/A	N/A	****	***	***	****	****

Table 4. *In vitro* activities of T315 derivatives.

The cell viabilities of each compound were evaluated in PC-3 cells after 24 h treatment in 5% FBS-supplemented medium. (n = 6). The ILK inhibition activity of each compounds were access by monitoring the dephosphorylation of p-Ser-437-Akt through western blotting under two concentration treatment (2.5 and 5 μM) for 24 h (*, 25%; **, 50%; ***, 75%; and ****, 100% inhibition).

2.4.2. Molecular docking experiment of T315 against ILK kinase domain

The X-ray crystal structure of ILK kinase domain was not solved until late 2009, which is the same time we hypothesized that ILK might serve as a promising target for T315. Hence, we further used molecular docking experiment to support our *in vitro*

experimental data. The molecular docking prediction can also provide detail information of how the inhibitors bind to the ATP-binding pocket of ILK. We extracted the ILK kinase domain from the X-ray crystal structure (PDB ID: 3KMW) (Fukuda et al., 2009), and performed the *in silico* screening of the ILK kinase domain with T315 derivatives. As shown in Figure 19A and B, T315 can dock inside the ATP-binding site of ILK kinase domain with the binding energy of -8.12 kcal/mol, and calculated inhibition constant of 1.12 μM. This result supports our theory of T315 as an ATP competitive kinase inhibitor. Moreover, T315 can form three hydrogen bonds with the residues inside the ATP-binding pocket. The methylamide arm of T315 will reach inside the pocket and form two hydrogen bonds with the backbone structure of the hinge region residues His-270 and Met-272, where it was the only surface area that has hydrophilic properties in that region. The free amine on the piperazine of T315 will form an extra hydrogen bond with Glu-283 at the edge of the ATP-binding pocket, where it has high population of hydrophilic properties (Figure 19C and D). These three hydrogen bonds can provide tight interactions between T315 and the ILK kinase domain. This binding mode of T315 can also explain why any minor change of the motifs of T315 will lose the ILK inhibition activity. For instance, the ethylamide arm of **21** is too short to reach to the hinge region of the ATP-binding pocket, the trifluoromethyl group of **6** has no ability to form the two important hydrogen bonds; and the morpholine ring of compound **53** cannot form the extra hydrogen binding with Glu-283.

The lipophilicty map of the ILK kinase domain and the binding mode of T315 also provide us two directions to further design the next generation of ILK inhibitors (Figure

20). 1. Although the three single bond length of the methylamide arm is essential, the free rotation of the three single bonds will generate extra free energy that will increase the original binding energy. Hence, introducing a double bond or a fused ring can provide rigidity to this motif and decrease the binding energy. 2. There is a large hydrophilic region around the binding environment of the trifluoromethyl biphenyl motif. Extra hydrophilic interactions should be achieved by introducing heterocycle rings, such as pyridine, to the aromatic motif.

Furthermore, by comparing the docking results of T315 and AR-12 with both PDK1 and ILK kinase domain (data not shown). T315 can only form 2 hydrogen bonds with the PDK1 kinase, where AR-12 has 4 hydrogen bond interactions and lower binding energy, which is vise versa when docking to ILK. This result also supports the target specificities of the two compounds.

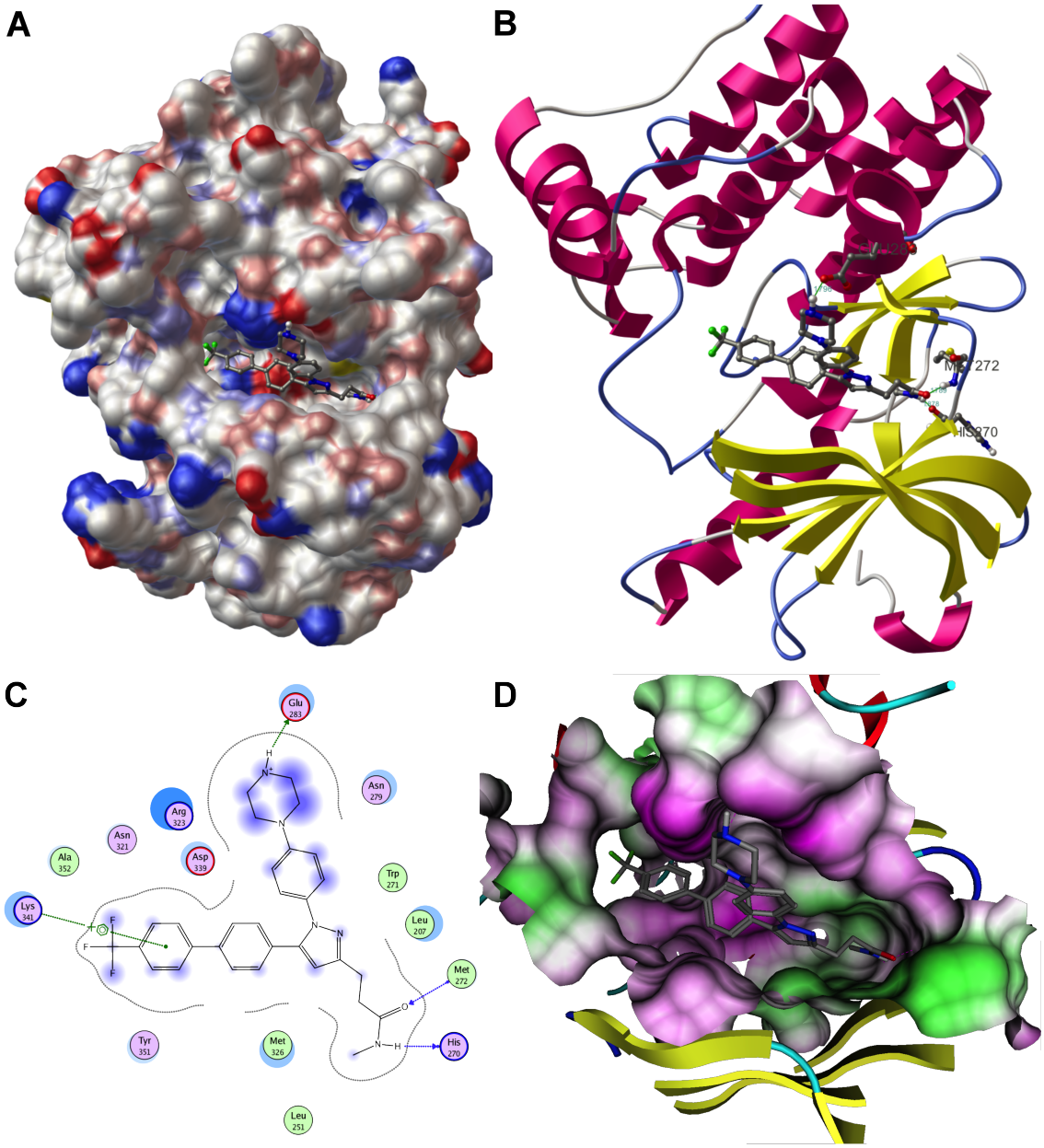

Figure 19. Molecular docking results of T315 (balls and stick) binding to the ATP-binding site of ILK kinase domain.

(A) Molecular surface mode of ILK kinase domain: red, oxygen; blue, nitrogen; white,

carbon. (B) Ribbon model of ILK kinase domain: magenta, α-helix; yellow, β-sheet. (C) Interaction map of T315 with the residues of ILK kinase domain. Three hydrogen bonds were formed from this binding mode. (D) Lipophilicity surface map of the ILK kinase domain: purple, hydrophilic; green, hydrophobic; white, neutral.

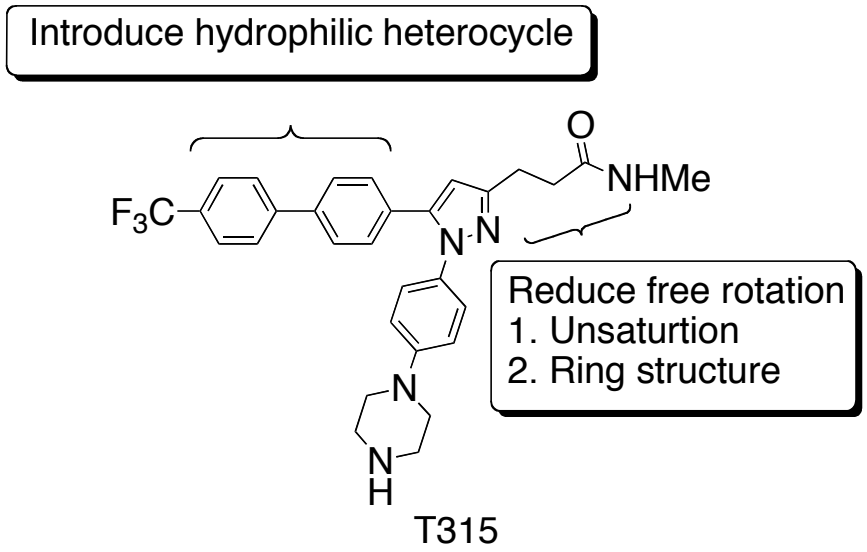

Figure 20. Further structure optimization strategies of T315 against ILK kinase domain.

2.5. Discussion

The ILK kinase plays a pivotal role in regulating cell proliferation, survival, and angiogenesis. It also serves as an adaptor protein to link the cellular signals from integrin to the actin cytoskeleton. Moreover, substantial evidence has indicated the important role

of ILK in tumor progression, and its abnormal overexpression in several types of cancer. So far, the QLT-0267 (QLT, Inc, Canada) is the only ILK inhibitor that has been reported (Fukuda et al., 2009), and the compound structure is currently under patent protection. Current research on this ILK inhibitor has provided evidence that the ILK activity is related to tumor progression. Targeting ILK can suppress cancer cell through the inhibition of its downstream targets, such as Akt, and YB-1 (Kalra et al., 2009; Eke et al., 2009). However, by using QLT-0267 as a single agent cannot achieve substantial *in vivo* activities (Stratford et al., 2007; Kalra et al., 2010; Troussard et al., 2006). Hence, there is an urgency to develop novel ILK inhibitors with higher potency and specificity.

The potency of T315 was first identified through the screening of an in-house kinase inhibitor library by western blotting of the phosphorylation of Akt at Ser-473 versus Thr-308. T315 demonstrated significant inhibition effect of PDK2 by dephosphorylating the p-Ser-473-Akt without altering the p-Thr-308-Akt at the concentration of 2.5 μM. The real identity of the inhibited PKD2 was considered as ILK, by judging the parallel dephosphorylation of two other downstream targets of ILK: GSK3β and MLC. This effect was consistent with the ILK silencing cell lines (Figure 12). Radiometric ILK kinase assay was then conducted to further prove that T315 is a direct ATP-competitive inhibitor for ILK. By using immunoprecipitated ILK from PC-3 cells, MBP as substrate, and [γ-^{32}P] ATP as phosphate donor; T315 demonstrated the ability to inhibit the ILK activity with the IC_{50} of 0.6 μM (Figure 13A). Equally important, T315 possess a high degree of specificity against a panel of 22 recombinant kinases, including PDK1, Akt, mTOR, GSK3β, FAK, cKit, EGFR, and FAK. Out of 22 kinase targets, only

two kinases (p70S6K and DAPK1) shown 50% activity inhibition under high concentration treatment of T315 (Table 3). An additional line of evidence for the ILK-targeted activity of T315 was its repressive effect on the mRNA and protein levels of the transcription/translation factor YB-1 and its representative targets HER2 and EGFR (Figure 14).

T315 has demonstrated consistent antiproliferation effect in a panel of six cancer cell lines under MTT assay with IC_{50} of 1.5~2.0 μM, where there is no significant cytotoxicity against normal epithelial cell at the concentration of ≤5 μM (Figure 11). The sensitivity of these cancer cells against T315 is highly related to the overexpression of ILK and its mediated oncogenic pathway. Further evidence suggests that T315 mediates its antiproliferative effect through the induction of both autophagy and apoptosis in PC-3 cells (Figure 16). Our data indicate that there is a threshold concentration of 2 μM for T315 to trigger the induction of apoptosis in PC-3 cells. T315 will mainly induce autophagy through ILK inhibition before 2 μM, and then further activate apoptosis when it reaches the threshold concentration. Moreover, by silencing Atg5 in PC-3 cells, will attenuate autophagy and suppress the effect of T315 on cell viability, especially at low concentrations (Figure 16E). These data also provide an unsolved link between ILK and autophagy. As a whole, these evidence have developed the foundation of T315 as an effective and selective antitumor agent. And at last, the *in vivo* efficacy of T315 in PC-3 tumor xenograft model (Figure 17) has outlined the potential value of this agent in cancer target therapy.

Based on the structure of T315 and the crystal structure of the ILK kinase domain,

a series of T315 derivatives were prepared, and the structure-activity relationship of T315 has been evaluated through *in vitro* and *in silico* studies. Through cell viability assay and western blot analysis, the pharmacophore of T315 has been identified as the *N*-methylpropanamide side chain, and the amine of the piperazine ring. By changing any one of these two motifs, will attenuate the ILK inhibition activity as well as the antitumor effect. The molecular docking results also support this stringent structural requirement. These two hydrophilic motifs of T315 play an important role in terms of forming three hydrogen bonds within the ILK kinase domain ATP-binding pocket. These three hydrogen bond interactions provide the foundation of T315's binding energy with ILK.

2.6 Conclusion

In conclusion, our data demonstrate that T315 is a novel, orally bioavailable ILK inhibitor with a distinct mode of action that inhibits tumor cell growth by modulating multiple signaling pathways associated with oncogenesis and tumor progression. So far, T315 still remains the most active structure and further optimizations are underway.

Chapter 3

Identification of the Multiple Identities of PDK2 in Prostate Cancer Cells

From the research foundation established in Chapter 2, we developed a potent ILK inhibitor that can effectively decrease the phosphorylation of Akt at Ser-473 in PC-3 cells. Moreover, our data also indicate that ILK plays a major role in PC-3 cells as the PDK2 regulating this site-specific phosphorylation of Akt. However, it was unclear whether the effect of T315 on Akt-Ser-473 phosphorylation and ILK's role as a PDK2 could be extended to other types of human cancer cells. Herein, we focused on identifying the multiple identities of PDK2 in different cell lines.

3.1 The effects of T315 in different cell lines

As a follow-up to our work described in Chapter 2, we broadened the scope of our evaluation of ILK inhibition by T315 to a panel of cancer cell lines. Previous results indicated that T315 consistently inhibited cell proliferation in six cancer cell lines at IC_{50} values ranging from 1.0 to 2.5 μM (Figure 11; Table 5). In light of the fact that T315's antiproliferative effect paralleled that on ILK inhibition, we evaluated the effect of T315 on ILK downstream targets by immunoblotting in five different cell lines, including PC-3, LNCaP, MDA-MB-231, MDA-MB-468, and SKBR3 cells. As shown in Figure 21, after

24 h treatment, ILK protein expression levels were unaffected by T315 in all five cell lines, while two downstream targets of ILK, Ser-9-GSK3 and Thr-18/Ser-19-MLC, exhibited dose-dependent reductions in phosphorylation levels, indicating the expected inhibition of ILK activity by T315. Among the 5 cell line examined, however, LNCaP cells were unique in that the phosphorylation of Akt at Ser-473 was not affected by T315. Furthermore, during the process of immunoblotting experiment, we found out that LNCaP cells possess extra-large amount of endogenous p-Ser-473-Akt. Together, these results suggest that, in LNCaP cells, a molecule other than ILK serves as the major functionally active PDK2. Hence, the following studies focused on identifying the major PDK2 in LNCaP cells using a variety of experimental approaches.

	Cell line	Cell viability IC_{50} (μM)
Prostate	PC-3	2.0
	LNCaP	1.8
Breast	MDA-MB-231	1.0
	MDA-MB-468	1.5
	SKBR3	1.8
	MCF7	2.2

Table 5. Effects of T315 on cell viability in prostate and breast cancer cell lines.

Cells were exposed with T315 in 5% FBS-supplemented medium for 24 h. Cell viability was determined by MTT assays.

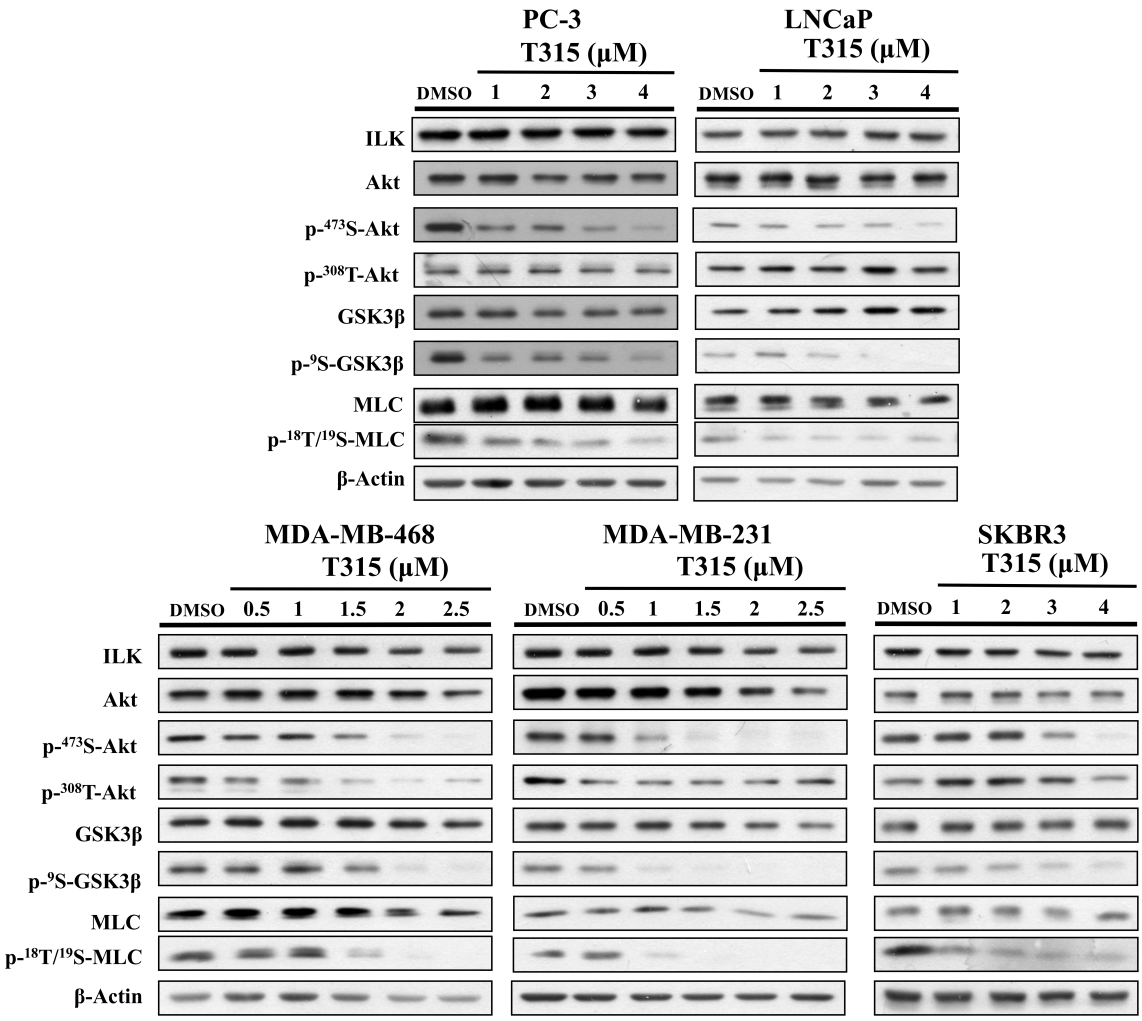

Figure 21. Western blot analysis of the effect of T315 on ILK downstream targets in five cancer cell lines.

The suppressive effects of T315 on the phosphorylation at Ser-473-Akt, Ser-9-GSK3β and Thr-18/Ser-19-MLC in prostate (upper panel: PC-3, LNCaP) and breast (lower panel:

MDA-MB-468, MDA-MB-231, and SKBR3) cancer cells. Cells were exposed to T315 at the indicated concentrations for 24 h in 5% FBS-supplemented medium. The immunoblots shown are representative of three independent experiments.

3.2 Profiling the endogenous expression of ILK and mTORC2 in a panel of cancer cell lines

A review of the literature revealed that, to date, at least ten kinases have been reported to have the ability to act as a PDK2 in phosphorylating Akt at Ser-473 (Dong and Liu, 2005). This information raises a number of issues, such as whether multiple PDK2s exist in a single cell, or whether the identity of a PDK2 is cell type-specific. Among the possible PDK2 candidates reported, ILK and mTORC2 are the most cited as PDK2s. Hence, we speculated that these two kinases are the major PDK2s in most of the cancer cell lines. Thus, we sought to determine the proportional distribution of these two PDK2s in individual cell lines.

To investigate this issue, we first used immunoblotting to evaluate the relative expression levels of ILK, members of mTORC2 (mTOR and rictor), and phosphorylated Akt in six prostate and breast cancer cell lines (Figure 22). As shown, expression levels of ILK and p-Ser-473-Akt vary among these cell lines. In PC-3 cells, the expression levels of ILK and p-Ser-473-Akt are moderate, while the level of mTOR (the major kinase component of mTORC2) is relatively low, consistent with our T315 treatment data indicating that ILK may be the major PDK2 in PC-3 cells. The triple-negative breast

cancer line, MDA-MB-468, shows a high degree of phosphorylation of Akt at Ser-473, which may reflect the strong expression level of ILK. However, compared to the other cell lines, LNCaP cells exhibit a relatively low level of ILK expression, accompanied by a comparatively high level of p-Ser-473-Akt, which is consistent with the notion that a kinase other than ILK may act as the PDK2 in this line. Furthermore, LNCaP cells also possess a high expression level of mTOR, suggesting that mTORC2 might serve as this second PDK2 in this cell line.

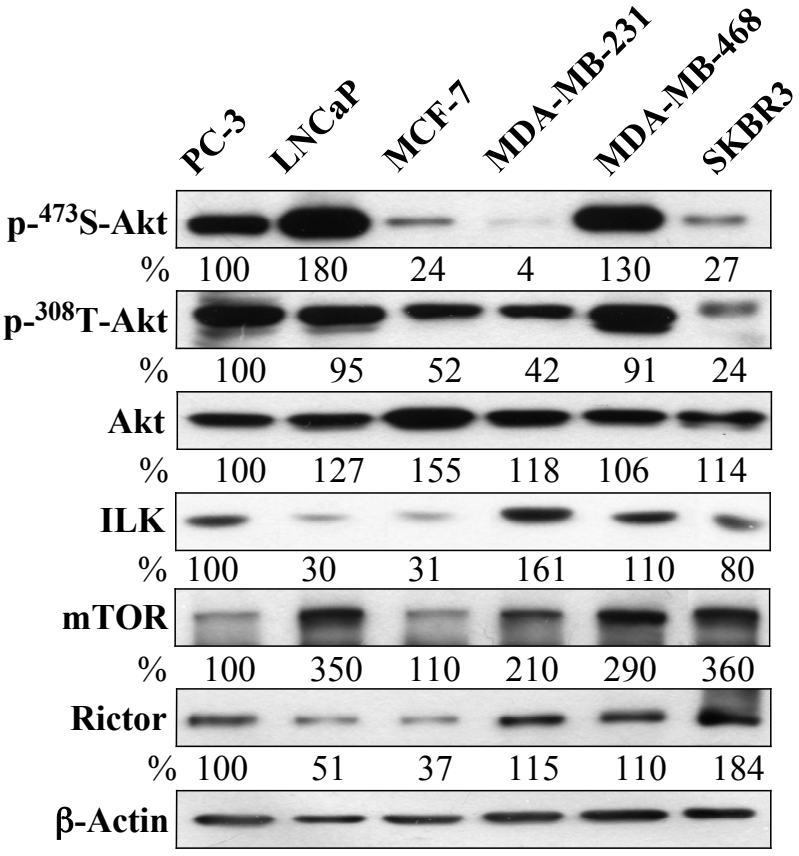

Figure 22. Endogenous expression levels of the ILK, mTORC2 members (mTOR and rictor) and phosphorylated Akt in prostate (PC-3, LNCaP) and breast (MCF7, MDA-MB-231, MDA-MB-468, and SKBR3) cancer cell lines.

Cells were incubated under normal cell culture conditions as described in the Materials and Method section. Using the expression levels in PC-3 cells as reference (100%), the relative expression levels (%) in the other cell lines were quantified and listed below each band.

3.3 Identification of the major PDK2 in LNCaP and PC-3 cells through pharmacological and molecular biological approaches

To investigate the relative roles of ILK and mTORC2 as PDK2s in different cell lines, we used T315 (ILK inhibitor) and a selective mTORC2 inhibitor as pharmacological tools to investigate this issue. The pharmacological effects were then confirmed by using shRNA-mediated knockdown experiments.

3.3.1 Antiproliferative effects of PDK2 inhibitors in prostate and breast cancer cell lines

The pyrido[2,3-*d*]pyrimidine-2,4-diamine, KU-0063794, is a selective dual mTORC1/2 inhibitor (Figure 23) that can inhibit the phosphorylation of p70S6K at Thr-389 and Akt at Ser-473 (Malagu et al., 2009; García-Martínez et al., 2009). The IC_{50} value of KU-0063794 for *in vitro* kinase inhibition is approximtely 10 nM for either mTORC1 or mTORC2 (García-Martínez et al., 2009). First, the antiproliferative activities of T315 and KU-0063794 were assessed in a panel of prostate (PC-3 and LNCaP) and breast (MDA-MB-468 and SKBR3) cancer cell lines using MTT assays. As shown in Figure 24, compared to the consistent low micromolar IC_{50} values of T315 in all

of the cell lines tested, KU-0063794 exhibited markedly greater antiproliferative activity against LNCaP cells (IC_{50}: 0.4 μM) versus the other lines examined, suggesting that mTORC2 plays a major role in the viability in LNCaP cells.

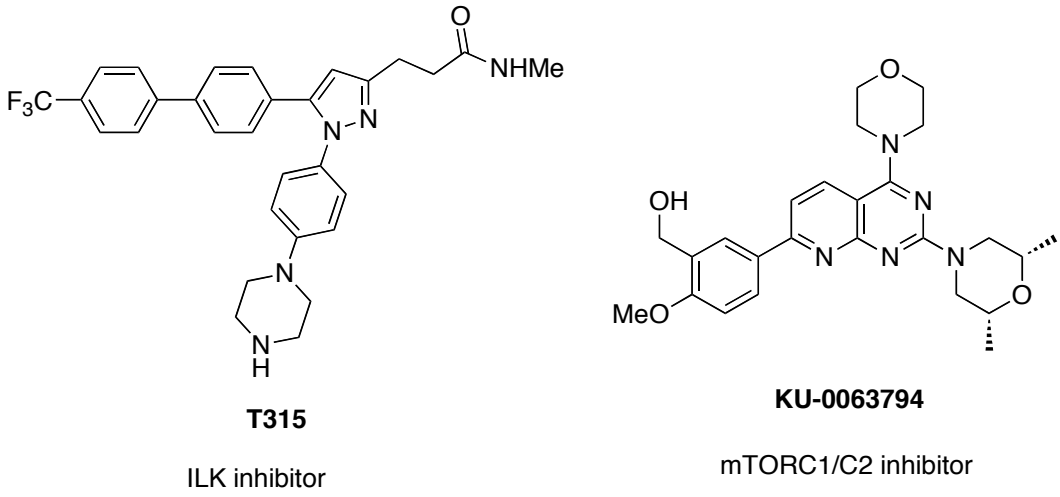

Figure 23. Structure of PDK2 inhibitors: T315 and KU-0063794.

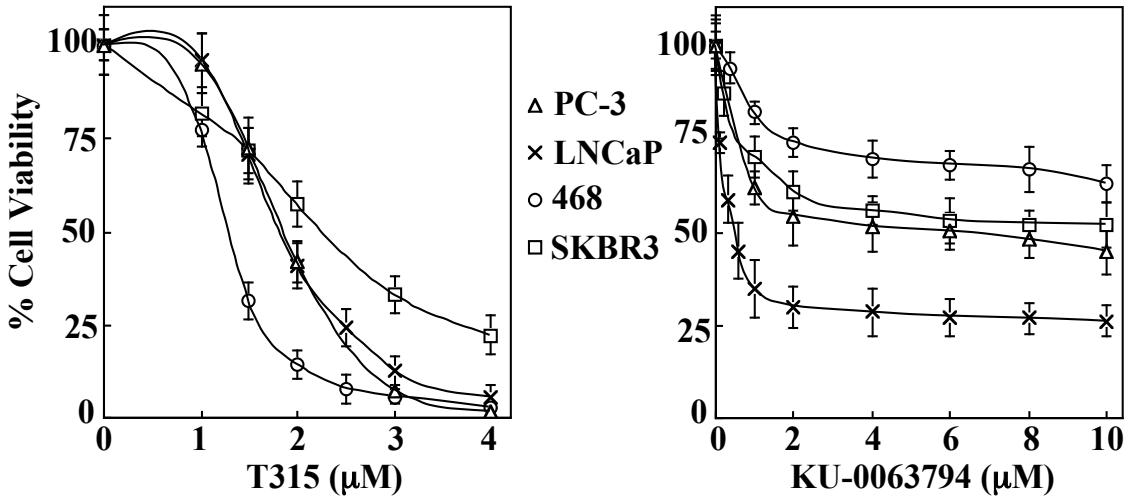

Figure 24. Cell viability assay of T315 versus KU-0063794.

Dose-dependent suppressive effects of T315 (left panel) versus KU-0063794 (right panel) on the viability of PC-3, LNCaP, MDA-MB-468, and SKBR3 cancer cells in 5% FBS-supplemented medium after 24 h treatment. Cell viability was determined by MTT assays. Points, means; bars, SD (n = 6).

3.3.2 Western blot analysis of PDK2 inhibitors in prostate and breast cancer cell lines

Pursuant to the MTT findings described above in section 3.3.1, we compared the ability of T315 and KU-0063794 to regulate the phosphorylation of ILK and mTORC1/C2 downstream targets in the same cell lines (Figure 25). Western blot analyses indicate that in all four cell lines, T315 can reduce the phosphorylation of the ILK substrate, Ser-9-GSK3β, while KU-0063794 caused the dephosphorylation of the mTORC1 substrate, Thr-389-p70S6K. This finding indicates that ILK and mTORC1 are functional in these cell lines in phosphorylating their respective downstream targets. However, with respect to PDK2 activity, KU-0063794 treatment caused the dose-dependent dephosphorylation of p-Ser-473-Akt in LNCaP cells, but no appreciable effect in the other cell lines, while T315 showed the opposite effects; i.e. no effect on p-Ser-473-Akt in LNCaP cells, but clear reductions in the other cell lines. These findings support our hypothesis that mTORC2 is the major PDK2 in LNCaP cells. Furthermore, this data also suggests that each of these PDK2s is the primary regulator of Ser-473-Akt phosphorylation in the respective cell lines. To confirm this premise, we conducted experiments using combination treatments of the two PDK2 inhibitors in PC-3 and LNCaP cells (Figure 26).

Two methods for the combination treatments were used: (1) a constant concentration of T315 (3 μM in LNCaP 2.5 μM in PC-3) in combination with a dose range of KU-0063794 (0~800 nM); and (2) a constant concentration of KU-0063794 (0.4 μM in LNCaP; 1 μM in PC-3) with a dose range of T315 (0~4 μM). In LNCaP cells, method (1) treatment (Figure 26 A, left panel) demonstrated an additive effect of the two inhibitors on p-Ser-473-Akt dephosphorylation. The same phenomenon was also observed in PC-3 cells receiving the method (2) treatment (Figure 26 B, upper right panel). It is noteworthy that there is no dose-dependent dephosphorylation of p-Ser-473-Akt in LNCaP cells under method (2) treatment (Figure 26 A, right panel), and in PC-3 under method (1) treatment (Figure 26 B, lower right panel). This is mostly because the remaining activities of mTORC2 in LNCaP and ILK in PC-3 are still strong enough to compensate the inhibition effect of the other PDK2s.

Together, these data demonstrate that PC-3 and LNCaP cells respond oppositely to the two PDK2 inhibitors at the level of Ser-473-Akt phosphorylation, which supports our hypothesis that mTORC2 serves as the major PDK2 in LNCaP cells.

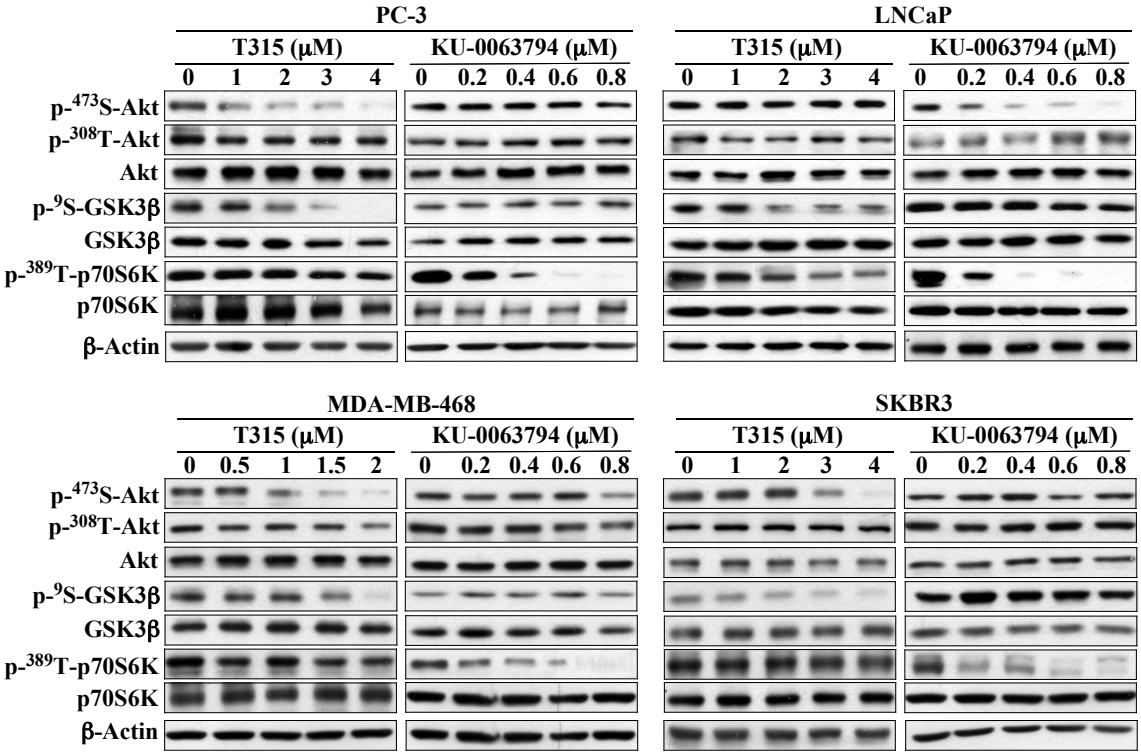

Figure 25. Western blotting analysis of the suppressive effects of T315 and KU-0063794 on ILK and mTORC1/2 pathways in prostate and breast cancer cells.

Prostate (upper panel: PC-3 and LNCaP) and breast (lower panel: MDA-MB-468 and SKBR3) cancer cells. Cells were exposed to the inhibitors at the indicated concentrations for 24 h in 5% FBS-supplemented medium. The immunoblots shown are representative of three independent experiments.

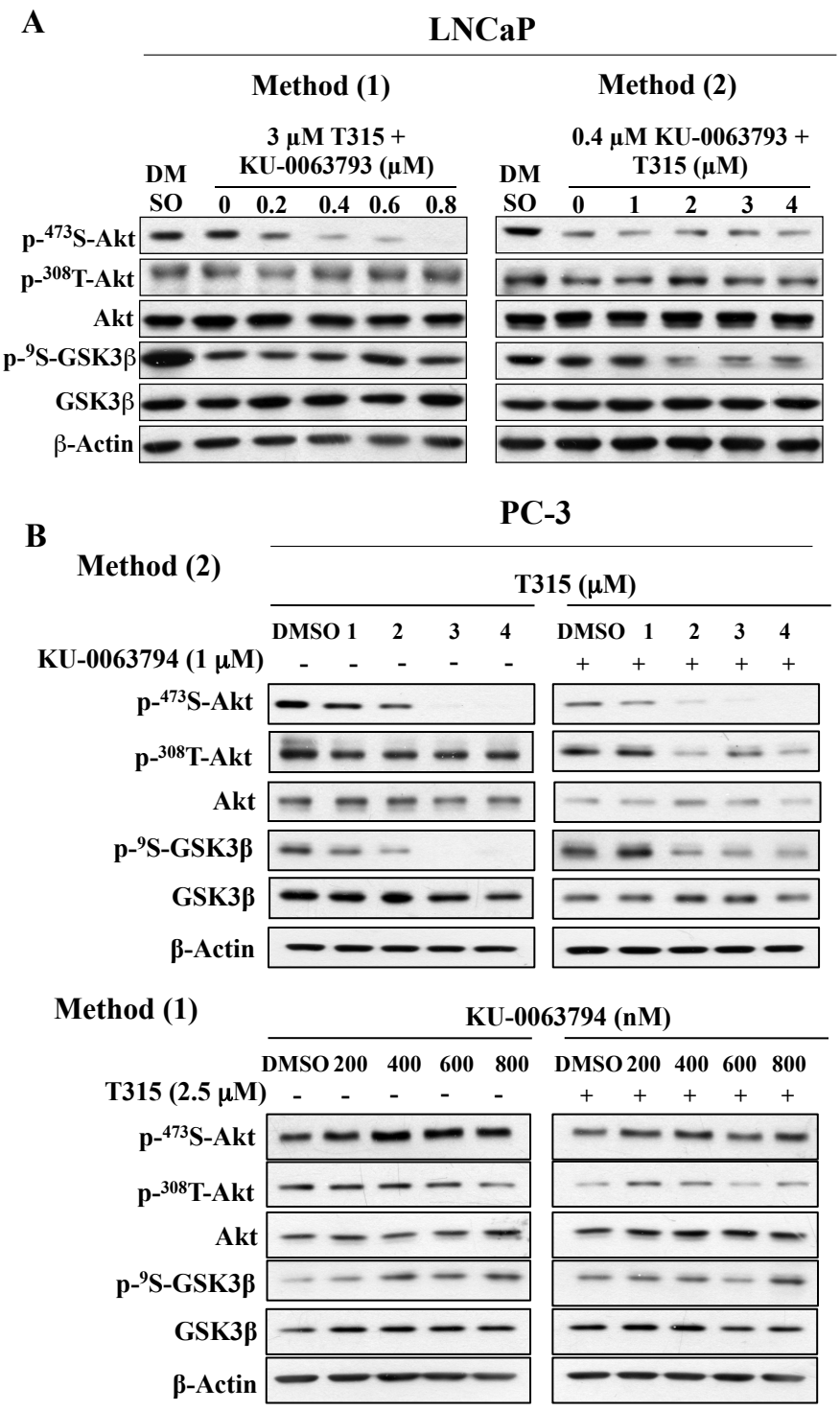

Figure 26. Western blotting analysis of the combination treatment of T315 and KU-0063794 in (A) LNCaP and (B) PC-3 cells.

The combination methods are divided into methods (1) and (2) as indicated. Cells were exposed to the inhibitors at the indicated concentrations for 24 h in 5% FBS-supplemented medium. The immunoblots shown are representative of three independent experiments.

3.3.3 Confirmation of pharmacological inhibitor findings using a molecular biological approach

The roles of ILK and mTORC2 as the major PDK2s in PC-3 and LNCaP cells, respectively, were confirmed by shRNA-mediated knockdowns of ILK, rictor, and mTOR, and co-treatment with the pharmacologic PDK2 inhibitors. The knockdown of rictor or mTOR expression will diminish the activity of mTORC2. Accordingly, as shown in Figure 27A (left and right panels), the phosphorylation levels of Ser-473-Akt and Ser-657-PKCα (another mTORC2 downstream effector) in LNCaP cells were reduced after shRNA-mediated repression of rictor and mTOR. Further dephosphorylation of p-Ser-473-Akt can be achieved by co-treating the shRNA-rictor transfected LNCaP cells with T315. This phenomenon is consistent with the additive effects in our previous studies (Figure 26A left panel). In contrast, no effects on p-Ser-473-Akt levels were observed after shRNA-silencing of ILK alone in LNCaP cells, but significant dephosphorylation occurred after KU-0063794 co-treatment (Figure 27A, middle panel). Equally important, overexpression of CA-ILK in LNCaP cells through transient transfection slightly increased the phosphorylation of Ser-473-Akt. However, after co-treatment of these cells with KU-0063794, which eliminated the contribution of mTORC2 to Ser-473-Akt

phosphorylation, a significant dose-dependent increase of p-Ser-473-Akt was revealed (Figure 28).

By applying the same shRNA approach in PC-3 cells, we found the opposite effects than those observed in LNCaP cells. For instance, the phosphorylation level of Ser-473-Akt was unaffected by shRNA-mediated suppression of rictor, but was decreased after co-treatment with T315 (Figure 27B, left panel). In contrast, the phosphorylation of Ser-473-Akt was clearly reduced by suppression of ILK expression, with a small, if any, additional decrease after KU-0063794 co-treatment (Figure 27B, right panel).

Taken together, the results of these shRNA-mediated knockdown experiments are consistent with those using the pharmacological inhibitors T315 and KU-0063794. These finding indicate that the major PDK2 in LNCaP cells is mTORC2, while that in PC-3 cells is ILK. Moreover, the results of the CA-ILK experiment in LNCaP cells provide evidence that ILK still functions as a minor PDK2 in LNCaP cells, and suggest that the two PDK2s contribute to Ser-473-Akt phosphorylation.

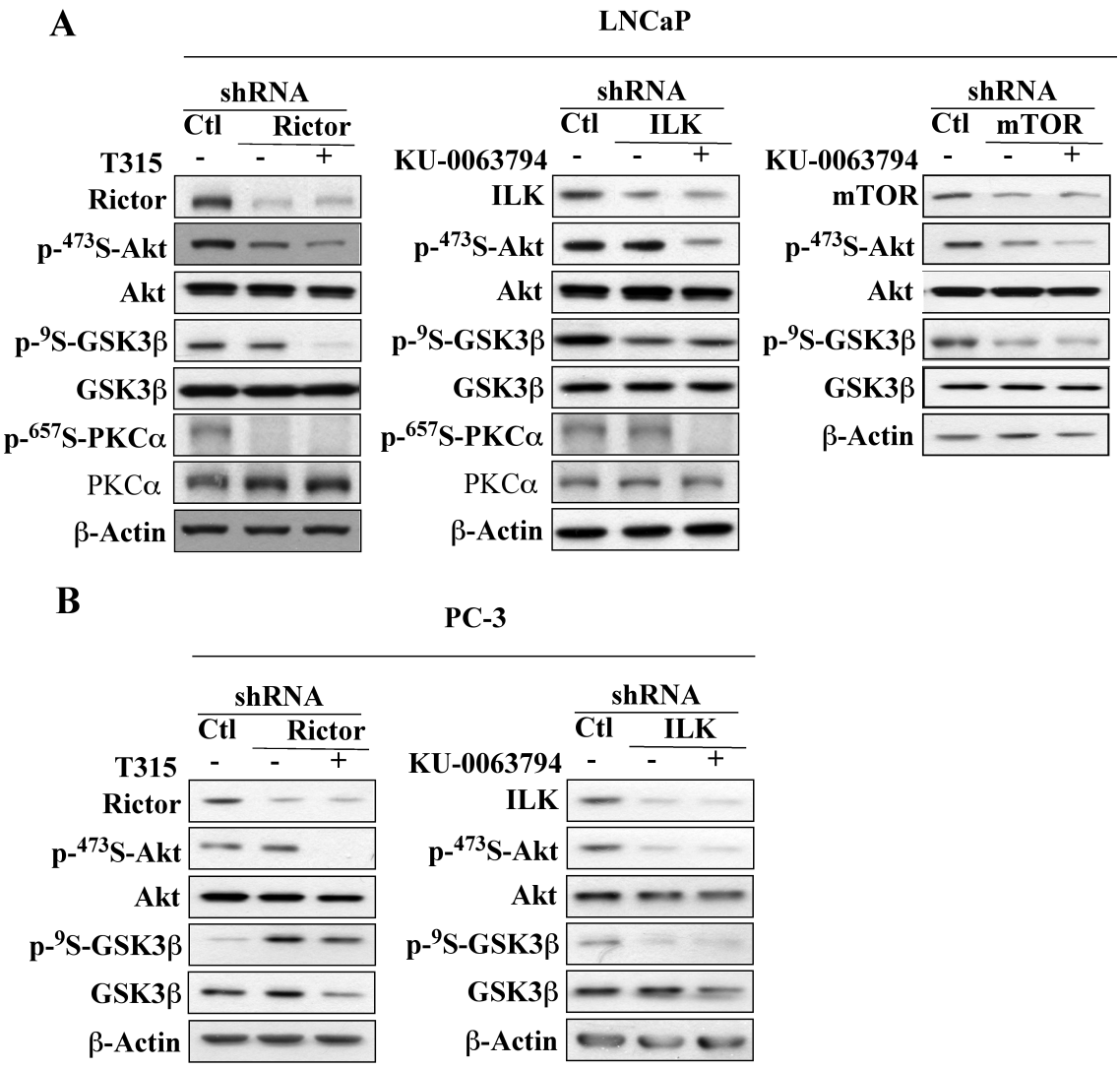

Figure 27. Western blot analysis of p-Ser-473-Akt and p-Ser-9-GSK3β expression after shRNA-mediated knockdown of rictor, ILK, and/or mTOR with or without co-treatment with T315 or KU0063794 in (A) LNCaP and (B) PC-3 cells.

The cells were transfected for 48 h in 10% FBS-supplemented medium, and then exposed to inhibitors (T315, 2.5 μM; KU0063794, 0.4 μM) for 24 h in 5% FBS-supplemented medium. The immunoblots shown are representative of three independent experiments.

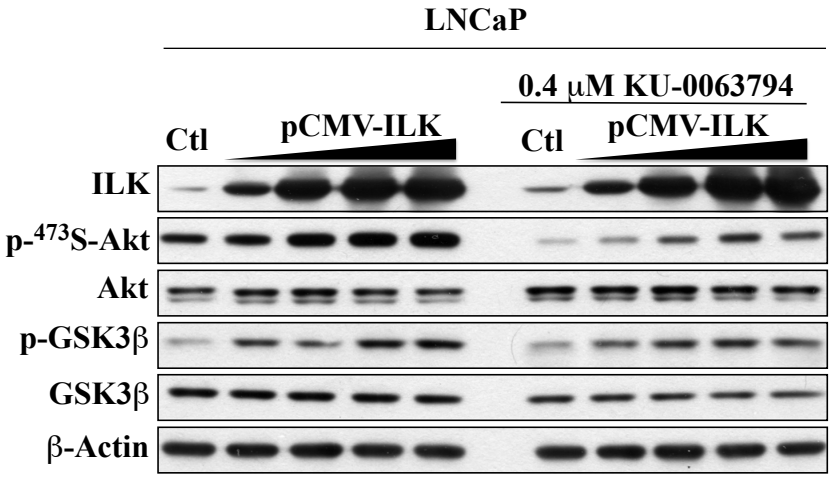

Figure 28. Western blot analysis of p-Ser-473-Akt and p-Ser-9-GSK3β expression in LNCaP cells overexpressing CA-ILK.

The cells were transfected for 24 h in 10% FBS-supplemented medium, and then exposed to KU-0063794 (0.4 μM) for another 24 h in 5% FBS-supplemented medium. The immunoblots shown are representative of three independent experiments.

3.4 Conclusion

Based on our data showing that the ILK inhibitor T315 failed to exhibit PDK2 inhibitory activity in LNCaP cells, as opposed to other cell lines tested, we sought to identify the kinase serving as the major PDK2 in LNCaP cells. We showed that different cancer cell lines exhibit different endogenous levels of two putative PDK2s, ILK and mTORC2. Using pharmacologic and molecular biological approaches, we identified ILK and mTORC2 as the major PDK2s in PC-3 and LNCaP cells, respectively. The understanding of the molecules contributing to PDK2 activity in different cell lines will

provide valuable information for further development of novel PDK2-targeted therapies. The evaluation of the major PDK2 in breast cancer cells is underway.

Chapter 4

Materials and Methods

4.1 Reagents and antibodies

Chemical reagents and organic solvents were purchased from Sigma- Aldrich (St. Louis, MO) unless otherwise mentioned. T315 and other compounds in the focused compound library (Figure 9) were synthesized in the authors' laboratory, of which the identity and purity were confirmed by nuclear magnetic resonance spectroscopy (300 MHz), high-resolution mass spectrometry, and elemental analysis.

The target proteins and commercial sources of antibodies used in the study were as follows: Akt, p-^{473}S-Akt, p-^{308}T-Akt, GSK-3β, p-^{9}S-GSK-3β, MLC, p-^{18}T/^{19}S-MLC, LC3, EGFR, ATG5, GFP, PCKα, ILK, p70S6K, p-^{389}T-p70S6K, S6, p-$^{235/236}$S-S6, ERK1/2, p-$^{202/204}$T-ERK1/2, p38, p-^{180}T/^{182}Y-P38, JNK, p-^{183}T/^{185}Y-JNK, PARP, mTOR, rictor (Cell Signaling Technology, Inc., Beverly, MA), p-^{422}S-SGK1, YB-1 (Abcam, Inc., Cambridge, MA), p-^{657}S-PCKα (Millipore, Billerica, MA), HER2, SGK1 (Santa Cruz Biotechnology, Inc., Santa Cruz, CA), The loading control of western blot analysis was determined by β-actin (MP Biomedicals, Irvine, CA). shRNA for ILK in the pLKO.1 vector was purchased from Sigma (St. Louis, MO). Human ILK full-length cDNA in the pCMV-SPORT6 vector was purchased from Thermo Scientific (Rockford, IL). GFP-ILK-CA

(ILK constitutive active form S343D) was constructed into pEGFP-C1 vector by site-direct mutagenesis PCR. Control siRNA and ATG5 siRNA were purchased from Cell Signaling Technology (Danvers, MA). shRNA for mTOR and rictor in the pLKO.1 vector were purchased from Addgene (Cambridge, MA).

For *in vitro* studies, stock solutions were made in DMSO and diluted in culture medium to a final DMSO concentration of 0.1%. For administration to nude mice, agents were prepared as suspensions in sterile water containing 0.5% methylcellulose and 0.1% Tween 80.

4.2 Cell culture

PC-3, LNCaP prostate cancer cells were purchased from the American Type Culture Collection (Manassas, VA) and cultured in RPMI 1640 medium containing 10% FBS. MDA-MB-231 and MDA-MB-468 breast cancer cells were purchased from the American Type Culture Collection and cultured in DMEM medium containing 10% FBS. SKBR3 and MCF7 breast cancer cells were purchased from the American Type Culture Collection and cultured in DMEM/F12 medium containing 10% FBS. Human prostate normal epithelial cells, PrEC, and mammary normal epithelial cells, MEC, were obtained from Lonza Biologics inc. (Hopkinton, MA) maintained in commercial supplement medium from Lonza. Cells were amplified at 37^{o}C in a humidified incubator with 5% CO_2 and 95% air.

4.3 Cell viability assay

Cell viability was determined using the 3-(4,5-dimethylthiazol-2-yl)-2,5-diphenyltetrazolium bromide) (MTT) assay. Cells were seeded in 96-well plates (5000 cells/well for cancer cells; 8000 cells/well for normal cells) and incubated in 10% FBS-supplemented medium for 24 h and were then treated with individual agents in 5% FBS-supplemented medium for 24 h. Drug-containing medium was then added with 5 x MTT (0.25 mg/mL) followed by incubation at 37 °C for 1.5 h. After removal of medium, the reduced MTT dye was solubilized in 100 μL/well DMSO, and absorbance at 570 nm was measured.

4.4 Immunoblotting

The general procedure for the western blot analysis for protein expression is described briefly as follows. Cells were seeded in 10 cm plates (1 x 10^6 cells/plate) and incubated in 10% FBS-supplemented medium for 24 h and were then treated with individual agents with tested agents at the doses and durations indicated in the text (10 mL/plate). Cells were collected by scraping followed by centrifugation, washed once with cold phosphate-buffered saline (PBS), and then lysed in lysis buffer, consisting of 1% sodium dodecyl sulfate (SDS), 10 mM ethylenediaminetetraacetic acid (EDTA) and 50 mM Tris-HCl (pH 8.1), in the presence of a protease inhibitor cocktail (Sigma-Aldrich, St. Louis, MO). Lysates were sonicated for 10 s to disrupt cellular organelles and genomic DNA, and then centrifuged at 13,2000 x *g* for 15 min. Protein concentrations of

the supernatants were determined using a colorimetric bicinchoninic acid assay (Pierce, Rockford, IL). After addition to each sample of an equivalent volume of 5X SDS-polyacrylamide gel electrophoresis sample loading buffer (300 mM Tris-HCl, pH 6.8; 10% SDS; 5% β-mercaptoethanol; 50% glycerol and 0.05% bromophenol blue), the mixture was incubated in boiling water for 10 min. Equal amounts of protein were resolved in SDS-polyacrylamide gels on a minigel apparatus and then transferred to nitrocellulose membranes. After blocking with Tris-buffered saline containing 0.1% Tween 20 (TBST) and 5% non-fat milk for 40 min, the membrane was washed three times with TBST for a total of 30 min and then incubated with primary antibody at 1:1000 or 1: 500 dilution in TBST at 4°C for 16 h. The membrane was washed again as described above and then incubated with goat anti-rabbit or anti-mouse immunoglobulin G-horseradish peroxidase conjugates (1:5000 for rabbit, 1:3000 for mouse) for 1 h at room temperature. After a final three washes, the proteins were then visualized by enhanced chemiluminescence.

4.5 Transfection and generation of stable sublines.

Plasmids or siRNA were nucleofacted into cancer cells by the Cell Line Nucleofector Kit (Lonza) according to manufacturer's instructions for further experiment after transfection for 48 h. G418 (250 μg/mL) was used to select stable pools of GFP-ILK-CA or GFP in PC-3 cell line. After one-week selection, the survival cells were sorted by GFP signal using flow cytometry facility, FACS aria (BD, Franklin Lakes, NJ).

The expression level was validated by western blot and fluorescent microscope.

4.6 RNA extraction and RT-PCR

The total RNA from PC3, PC-3/CA-ILK, SKBR3, and SKBR3/CA-ILK (1 x 10^6 cells) were isolated by Trizol reagent (Invitrogen Corporation, Carlsbad, CA). Aliquots of 1 μg of total RNA from each sample were reverse-transcribed to cDNA using the iScript cDNA Synthesis Kit (Bio-Rad Laboratories, Hercules, CA). PCR products were resolved in 2% agarose gels by electrophoresis and visualized by ethidium bromide staining. The sequences of primers used for RT-PCR were as follows.

YB-1: forward primer, 5'-AAGTGATGGAGGGTGCTGAC-3'; reverse primer 5'-TTC-TTCATTGCCGTCCTCTC-3'. HER2: forward primer, 5'-TCCTGTGTGGACCTGGA-TGAC-3'; reverse primer, 5'-CCAAAGACCACCCCCAAGA-3'; EGFR: forward primer, 5'-GGACGACGTGGTGGATGCCG-3'; EGFR: reverse primer, 5'- GGCGCC-TGTGGGGTCTGAGC-3'; β-actin: forward primer, 5'- CACGAAACTACCTTCAACT-CCA-3'; reverse primer, 5'- GAAGCATTTGCGGTGGACGAT-3'.

4.7 Radiometric ILK kinase assay

The kinase activity of immunoprecipitated ILK was determined in an in vitro radiometric kinase assay using myelin basic protein (MBP) as substrate and [γ-^{32}P] ATP

as phosphate donor, according to reported procedures with modifications (Hill et al., 2002; Persad et al., 2000).

ILK proteins were extract from PC-3 cell lysate by immumoprecipitation. PC-3 cells (5 x 10^5 /sample) were exposed with EGF (100 nM) for 2 h prior to collection. Cells were lysed in 250 μL of lysis buffer, pH 7.5 containing Tris-HCl (20 mM), NaCl (150 mM), and 1% Triton X-100. After centrifugation, the supernatants were immunoprecipitated with ILK antibody (#3856, Cell signaling Technology, Inc., Beverly, MA) and pull down with 15 μL of Protein A/G PLUS-Agarose (Santa Cruz Biotechnology, Inc., Santa Cruz, CA). Myelin basic protein (MBP, Sigma-Aldrich, MO) was used as substrate for ILK, and [γ-^{32}P] ATP (3000 Ci/mmol, 10mCi/ml; Perkin-Elmer, Waltham, MA) was used as the phosphate donor in the kinase assay. Protein kinase assays were performed in 25 μL kinase reaction buffer (25 mM Tris-HCl (pH 7.5), 5 mM beta-glycerophosphate, 2 mM dithiothreitol (DTT), 0.1 mM Na_3VO_4, 10 mM $MgCl_2$), containing 5 μg of MBP, 2.5 μCi [γ-^{32}P] ATP, with and without 15 μL of A/G plus–ILK. Reactions were incubated at 30°C for 25 min, and stopped by addition of SDS-PAGE sample buffer. Proteins were resolved on 15% SDS-polyacrylamide gels and [γ-^{32}P] MBP was detected by autoradiography. Densitometric analysis was performed to determine the relative intensities in drug-treated samples versus those in the respective DMSO treated controls.

4.8 Cell cycle analysis

After 48h treatment of T315, the suspending and adhesive cells were trypsinized and

pelleted by centrifuge; subsequently the same amount of cells (1 x 10^6) were resuspended in 200 µL ice-cold PBS and fixed with 1 mL 100% ethanol. The fixed cells were pelleted, resuspended in 500 µL PI staining solution (80 µg/mL PI, 100 µg/mL RNase, Triton X-100 0.1 % v/v in PBS) at 37°C for 30 min in dark, and filtered through a cell strainer with 40 µm nylon mesh (BD). The subG1 apoptotic cell populations of DNA content in cell cycle analysis were quantitated by using a BD FACS Calibur flow cytometer. The results were analysis by FlowJo software (Tree Star, Inc., Ashland, OR).

4.9 Annexin V-PI staining

After 48 h treatment of T315, the suspending and adhesive cells were trypsinized and pelleted by centrifuge; subsequently the cells were washed twice with ice-cold PBS and co-stained with annexin V conjugated with FITC and propidium iodide (PI) according to manufacturer's instructions. This double staining assay revealed the cells on early apoptotic stage with Annexin V positive and PI negative signal by using flow cytometer, FACS calibur (BD). The results were analysis by FlowJo software (Tree Star, Inc., Ashland, OR).

4.10 Animal studies

The procedures performed were in accordance with protocols approved by the Institutional Animal Care and Use Committee of The Ohio State University. T315 (25

mg/kg and 50 mg/kg), or vehicle was orally administered to nude mice by gavage once daily for five weeks. Biomarkers associated with ILK inhibition were assessed in lysates of prostate tissues that were snap-frozen at animal sacrifice.

4.11 Statistical analysis

Quantitative data from *in vitro* experiments are presented as mean ± SD. Data from *in vivo* experiments are expressed as mean ± SEM. Differences among group means were analyzed for statistical significance using one-way ANOVA or unpaired Student's t-test. Differences were considered significant at $P < 0.05$. All statistical analyses were performed using SPSS software (SPSS Inc., Chicago, IL, USA). Western blot and RT-PCR analyses were performed in triplicate.

4.12 Molecular docking

The ILK protein kinase domain crystal structure was extracted from PDB bank (PDB ID: 3KMW). The crystal structure was processed by removing the α-parvine structure, water molecules, magnesium ion, and the ATP; followed with adding hydrogens by Molecular Operation Environment 2008.10 (Chemical Computing Group, Montreal, Canada; http://www.chemcomp.com/). Molecular structure of OSU-T315 was generated with Molecular Operation Environment 2008.10 and initially subjected to 1000 steps of Monte Carlo simulation using Merck Molecular Force Field program available in

Spartan 08 (Wavefuction, Inc., Irvine, Ca; http://www.wavefun.com/). The minimum conformation reached by the simulation was then minimized at a density function theory level of B3LYP/6-31G* with Gaussian 03 (Gaussian, Inc., Wallingford, CT; http://www.gaussian.com/). All the fully optimized structures were confirmed by normal-mode analysis; no negative frequencies were found. The atomic Gasteiger charges to the ligand and macromolecule were assigned with AutoDockTools-1.5.4 (The Scripps Research Institute, La Jolla, CA; http://autodock.scripps.edu/) based on the AMBER force field. The docking experiment was conducted with Autodock 4.2 (The Scripps Research Institute, La Jolla, CA) for long tern calculation (population size: 250; number of evaluations: 50,000,000; number of generations: 50,000; number of runs: 100). The results were visualized with Molecular Operation Environment 2008.10.

4.13 Chemistry

4.13.1Chemistry general information

All commercial chemicals and solvents were reagent grade and were used without further purification unless otherwise specified. All reported yields are isolated yields after chromatography or crystallization. Microwave reactions were carried under CEM Discover SP-D microwave digester (CEM, NC). ^{1}H and ^{13}C NMR spectra were recorded on a Bruker AV300 (Bruker Biospin, Germany), Chemical shifts are reported in ppm relative to the residual solvent peak ($CDCl_3$, ^{1}H 7.27, ^{13}C 77.00; TMS: 0.00). Multiplicity was indicated as follows: s (singlet); d (doublet); t (triplet); q (quartet); m (multiplet); dd

(doublet of doublet); bs (broad singlet), and so on. The high resolution mass spectrometric analysis were conducted at The Ohio State University Campus Chemical Instrument Center (CCIC) using on a Micromass Q-Tof II. (Waters, MA). Products were purified by flash column chromatography on silica gel (230-400 mesh). The eluent used for purification were described in parentheses. Elemental analyses were conducted at Atlantic Microlab, Inc (GA.) for checking purity (>95%). Thin-layer chromatography (TLC) was performed on silica gel plates (silica gel 60 F_{254} 0.25 mm), and the components were visualized by observation under UV light (254 nm). Distilled water was polished using ion exchange and filtration.

4.13.2 Synthetic procedures

A general route for the preparation of compounds of the invention is shown in Scheme 1.

4.13.2.1 General procedure for synthesis of **iia-c**: Step a.

The appropriate 4-substituded phenylboronic acid (25.1 mmol, 1 equiv) was added to a mixture of 4-bromoacetophenone (**i**) (5 g, 25.1 mmol, 1 equiv), palladium (II) acetate (125 mg, 2 mol%), powder potassium carbonate (10.4 g, 75.3 mmol, 3 equiv), and tetrabutylammonium bromide (10.5 g, 32.6 mmol, 1.3 equiv). The mixture was flushed with argon, and water (250 mL) was introduced with syringe. Resulting suspension was stirred and heated to 60°C for 2 hours. Then cooled to room temperature, diluted with

water, extracted with ethyl acetate, dried over Na_2SO_4 and concentrated to dryness under vacuum. The products were purified by flash chromatography on silica gel, eluted with 30% EtOAc in hexane to give the product **iia-c** in quantitative yield.

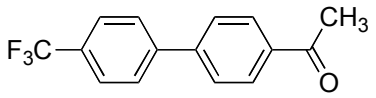

1-(4'-(trifluoromethyl)-[1,1'-biphenyl]-4-yl)ethanone (**iia**)

^{1}H NMR (300 MHz, $CDCl_3$): δ 8.07 (d, *J* = 8.4 Hz, 2H), 7.72 (m, 6H), 2.66 (s, 3H).

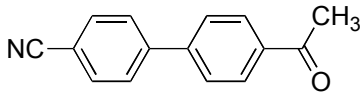

4'-acetyl-[1,1'-biphenyl]-4-carbonitrile (**iib**)

^{1}H NMR (300 MHz, $CDCl_3$): δ 8.08 (d, *J* = 8.1 Hz, 2H), 7.76 (m, 6H), 2.67 (s, 3H).

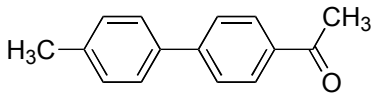

1-(4'-methyl-[1,1'-biphenyl]-4-yl)ethanone (**iic**)

^{1}H NMR (300 MHz, $CDCl_3$): δ 8.03 (d, *J* = 8.1 Hz, 2H), 7.68 (d, *J* = 8.4 Hz, 2H), 7.54 (d, *J* = 7.8 Hz, 2H), 7.29 (d, *J* = 8.4 Hz, 2H), 2.64 (s, 3H), 2.42 (s, 3H).

4.13.2.2 Synthesis of (*Z*)-ethyl 2-hydroxy-4-oxo-4-(4'-(trifluoromethyl)-[1,1'-biphenyl]-4-yl)but-2-enoate **(iii)**: Step b.

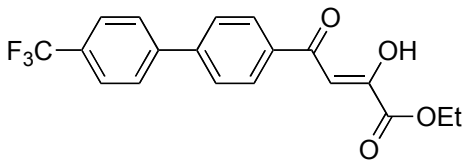

To a suspension of sodium hydride (60% in mineral oil; 6.3 g, 157 mmol, 3 equiv) in 100 mL of anhydrous tetrahydrofurane (THF) was added ethyl oxalate (14.4 g, 99 mmol, 1.5 equiv) under argon. After stirring at RT for 10 minutes, 1-(4'-(trifluoromethyl)-[1,1'-biphenyl]-4-yl)ethanone (**iia**, 13.7 g, 52 mmol, 1 equiv) in 50 mL of tetrahydrofurane solution was added drop wise to the solution. The mixture became clear and dark red within 30 minutes at RT. The mixture was then concentrated under vacuum and suspended in water, neutralized with hydrochloric acid (2N), the mixture became bright yellow suspension. Filter the mixture through vacuum, recrystalized with EtOH to give product **iii**, yellow powder; 18.9 g, quantitative yield. ^{1}H NMR (300 MHz, $CDCl_3$): δ 15.83 (s, 1H), 8.17 (m, 5H), 7.96 (m, 4H), 4.18 (q, J = 4.2 Hz, 2H), 1.31 (t, J = 7.2 Hz, 3H).

4.13.2.3 General procedure for synthesis of **iVa-e**: Step c.

To a solution of substituted arylketone (**iia-e**) (25 mmol, 1 equiv) in 250 mL of dichloromethane was added pre-prepared ethyl 4-(1*H*-benzo[*d*][1,2,3]triazol-1-yl)-4-oxobutanoate (7.4 g, 30 mmol. 1.2 equiv), magnesium bromide ethyl etherate (13 g, 50

mmol, 2 equiv) under argon. After stirring at RT for 10 minutes, *N*,*N*-diisopropylethylamine (DIPEA, 4.8 mL, 50 mmol, 2 equiv) was added drop wise to the solution under argon. After stirring at RT for 16 hours, and washed with 10% HCl aqueous solution (150 mL x 1), followed H_2O (200 mL x 2). The organic phase was dried over sodium sulfate, and concentrated to dryness under vacuum. The crude product was then purified by silica gel chromatography (hexane/EtOAc: 9/1), followed by recrystallization with ethanol to give product (**iVa**, white crystal, 9.7 g, 99 %; **iVb**, white crystal, 5.0 g, 57 %; **iVc**, white crystal, 6.5 g, 77%; **iVd**, white crystal, 6.2 g, 76%; **iVe**, white crystal, 7.0 g, 80%).

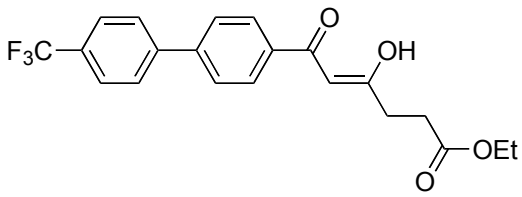

(*Z*)-ethyl 4-hydroxy-6-oxo-6-(4'-(trifluoromethyl)-[1,1'-biphenyl]-4-yl)hex-4-enoate (**iVa**)

^{1}H NMR (300 MHz, $CDCl_3$): δ 15.82 (s, 1H), 7.98 (d, *J* = 8.1 Hz, 2H), 7.74 (m, 4H), 7.68 (d, *J* = 8.1 Hz, 2H), 6.26 (s, 1H), 4.18 (q, *J* = 7.2 Hz, 2H), 2.85 (t, *J* = 7.2 Hz, 2H), 2.72 (t, *J* = 7.2 Hz, 2H), 1.31 (t, *J* = 7.2 Hz, 3H).

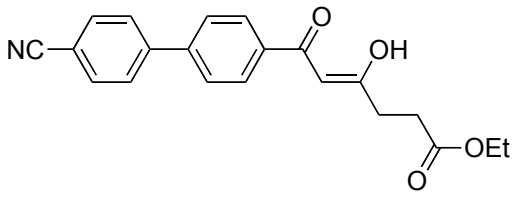

(*Z*)-ethyl 6-(4'-cyano-[1,1'-biphenyl]-4-yl)-4-hydroxy-6-oxohex-4-enoate (**iVb**)

^{1}H NMR (300 MHz, $CDCl_3$): δ 15.78 (s, 1H), 7.82 (d, *J* = 8.4 Hz, 2H), 7.75 (m, 4H), 7.68 (d, *J* = 8.1 Hz, 2H), 6.26 (s, 1H), 4.18 (q, *J* = 7.2 Hz, 2H), 2.85 (t, *J* = 7.2 Hz, 2H), 2.73 (t, *J* = 7.2 Hz, 2H), 1.28 (t, *J* = 7.2 Hz, 3H).

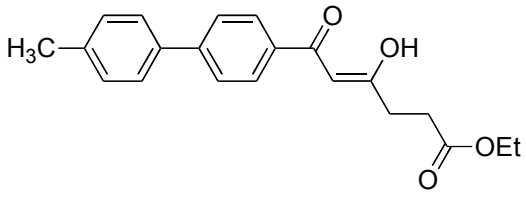

(*Z*)-ethyl 4-hydroxy-6-(4'-methyl-[1,1'-biphenyl]-4-yl)-6-oxohex-4-enoate (**iVc**)

^{1}H NMR (300 MHz, $CDCl_3$): δ 15.87 (s, 1H), 7.93 (d, *J* = 7.8 Hz, 2H), 7.67 (d, *J* = 7.8 Hz, 2H), 7.54 (d, *J* = 7.8 Hz, 2H), 7.28 (d, *J* = 7.8 Hz, 2H), 6.24 (s, 1H), 4.17 (t, *J* = 6.9 Hz, 2H), 2.82 (t, *J* = 7.2 Hz, 2H), 2.73 (t, *J* = 7.2 Hz, 2H), 1.28 (t, *J* = 7.2 Hz, 3H).

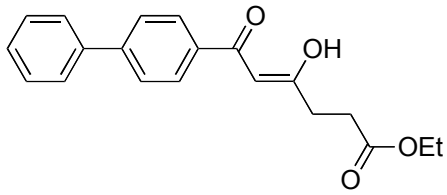

(*Z*)-ethyl 6-([1,1'-biphenyl]-4-yl)-4-hydroxy-6-oxohex-4-enoate (**iVd**)

^{1}H NMR (300 MHz, $CDCl_3$): δ 15.86 (s, 1H), 7.95 (d, *J* = 8.4 Hz, 2H), 7.65 (m, 3H), 7.45 (m, 4H), 6.26 (s, 1H), 4.18 (q, *J* = 6.9 Hz, 2H), 2.83 (t, *J* = 7.2 Hz, 2H), 2.70 (t, *J* = 7.2 Hz, 2H), 1.28 (t, *J* = 7.2 Hz, 3H).

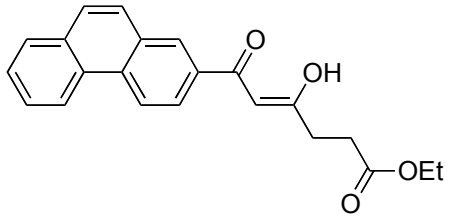

(*Z*)-ethyl 4-hydroxy-6-oxo-6-(phenanthren-2-yl)hex-4-enoate (**iVe**)

^{1}H NMR (300 MHz, $CDCl_3$): δ 15.86 (s, 1H), 8.72 (t, *J* = 6.6 Hz, 2H), 8.45 (s, 1H), 8.09 (d, *J* = 7.2 Hz, 1H), 7.93 (d, *J* = 7.2 Hz, 1H), 7.81 (s, 2H), 7.69 (m, 2H), 6.40 (s, 1H), 4.20 (q, *J* = 7.2 Hz, 2H), 2.88 (t, *J* = 7.2 Hz, 2H), 2.75 (t, *J* = 7.2 Hz, 2H), 1.29 (t, *J* = 7.2 Hz, 3H).

4.13.2.4 General procedures for synthesis of **Va-e** (n = 2): Step d.

To a suspension of appropriate aryldiketone (**iVa-e** 2.5 mmol, 1 equiv) in 10 mL of ethanol was added 4-nitro-phenylhydrazine hydrochloride (570 mg, 3 mmol, 1.2 equiv) and 4-methylbenzenesulfonic acid (430 mg, 2.5 mmol, 1 equiv). The mixture was stirred under microwave at 130°C for 10 min. The mixture became orange solution with yellow crystal suspensions. Concentrate the solution via vacuum, and recrystallized with ethanol to give product (**Va**, yellow crystal, 739 mg, 58 %; **Vb**, yellow powder, 536 mg, 46%; **Vc**, orange powder, 956 mg, 84 %; **Vd**, orange oil, 1026 mg, 93%; **Ve**, orange crystal, 1158 mg, 99%).

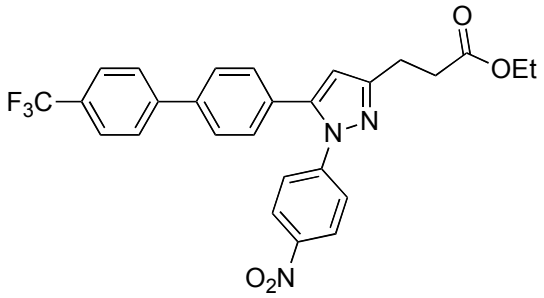

Ethyl 3-(1-(4-nitrophenyl)-5-(4'-(trifluoromethyl)-[1,1'-biphenyl]-4-yl)-1*H*-pyrazol-3-yl)propanoate (**Va**)

^{1}H NMR (300 MHz, $CDCl_3$) δ 8.41 (d, *J* = 8.4 Hz, 2H), 7.97 (d, *J* = 9.3 Hz, 2H), 7.81 (d, *J* = 8.4 Hz, 2H), 7.74 (m, 4H), 7.69 (d, *J* = 8.1 Hz, 2H), 6.69 (s, 1H), 4.18 (q, *J* = 7.2 Hz, 2H), 3.17 (t, *J* = 7.5 Hz, 2H), 2.77 (t, *J* = 7.5 Hz, 2H),1.28 (t, *J* = 7.2 Hz, 3H).

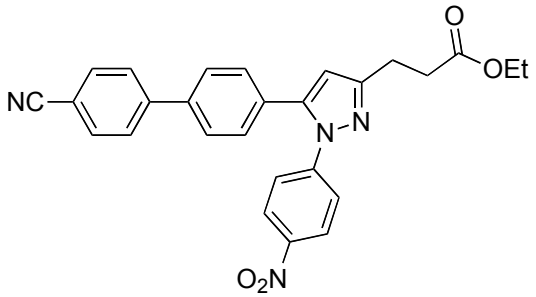

Ethyl 3-(5-(4'-cyano-[1,1'-biphenyl]-4-yl)-1-(4-nitrophenyl)-1*H*-pyrazol-3-yl)propanoate (**Vb**)

^{1}H NMR (300 MHz, $CDCl_3$) δ 8.41 (d, *J* = 9.0 Hz, 2H), 7.97 (d, *J* = 8.1 Hz, 2H), 7.80 (d, *J* = 9.0 Hz, 2H), 7.75 (m, 4H), 7.67 (d, *J* = 8.1 Hz, 2H), 6.68 (s, 1H), 4.17 (q, *J* = 7.2 Hz, 2H), 3.16 (t, *J* = 7.5 Hz, 2H), 2.76 (t, *J* = 7.5 Hz, 2H),1.26 (t, *J* = 7.2 Hz, 3H).

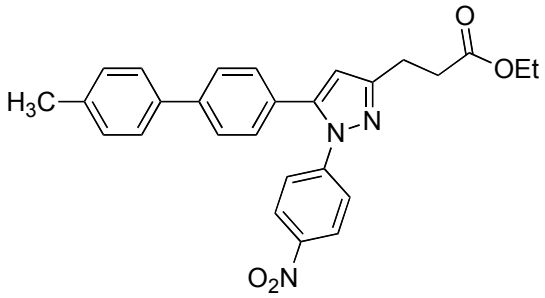

Ethyl 3-(5-(4'-methyl-[1,1'-biphenyl]-4-yl)-1-(4-nitrophenyl)-1*H*-pyrazol-3-yl)propanoate (**Vc**)

^{1}H NMR (300 MHz, $CDCl_3$) δ 8.41 (d, *J* = 9.0 Hz, 2H), 7.92 (d, *J* = 8.4 Hz, 2H), 7.82 (d, *J* = 9.0 Hz, 2H), 7.67 (d, *J* = 8.1 Hz, 2H), 7.56 (m, 4H), 6.67 (s, 1H), 4.18 (q, *J* = 7.2 Hz, 2H), 3.15 (t, *J* = 7.2 Hz, 2H), 2.77 (t, *J* = 7.5 Hz, 2H), 2.43 (s, 3H), 1.27 (t, *J* = 7.2 Hz, 3H).

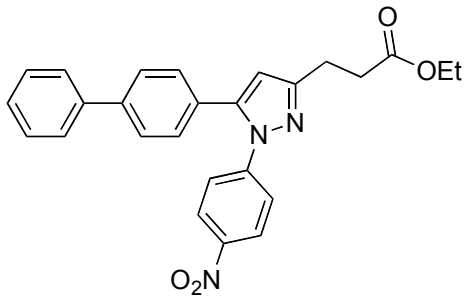

Ethyl 3-(5-([1,1'-biphenyl]-4-yl)-1-(4-nitrophenyl)-1*H*-pyrazol-3-yl)propanoate (**Vd**)

^{1}H NMR (300 MHz, $CDCl_3$) δ 8.41 (d, *J* = 9.0 Hz, 2H), 8.39 (d, *J* = 9.0 Hz, 2H), 7.93 (d, *J* = 8.4 Hz, 2H), 7.62 (m, 5H), 7.31 (m, 3H), 6.67 (s, 1H), 4.19 (q, *J* = 7.2 Hz, 2H), 3.12 (t, *J* = 7.2 Hz, 2H), 2.78 (t, *J* = 7.5 Hz, 2H), 1.27 (t, *J* = 7.2 Hz, 3H).

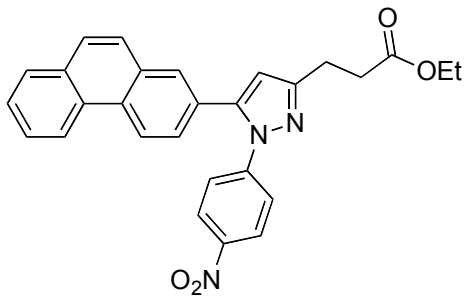

Ethyl 3-(1-(4-nitrophenyl)-5-(phenanthren-2-yl)-1*H*-pyrazol-3-yl)propanoate (**Ve**)

^{1}H NMR (300 MHz, $CDCl_3$) δ 8.73 (m, 2H), 8.38 (m, 2H), 8.14 (m, *2*H), 7.81 (m, 4H), 7.50 (m, 3H), 6.81 (s, 1H), 4.20 (q, *J* = 7.2 Hz, 2H), 3.16 (t, *J* = 7.2 Hz, 2H), 2.83 (t, *J* = 7.2 Hz, 2H), 1.28 (t, *J* = 7.2 Hz, 3H).

4.13.2.5 Synthesis of ethyl 1-(4-nitrophenyl)-5-(4'-(trifluoromethyl)-[1,1'-biphenyl]-4-yl)-1*H*-pyrazole-3-carboxylate (**Vf**) (n = 0)

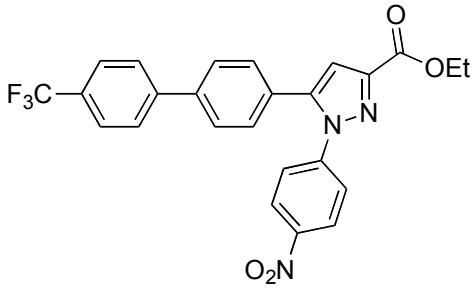

To a suspension of (*Z*)-ethyl 2-hydroxy-4-oxo-4-(4'-(trifluoromethyl)-[1,1'-biphenyl]-4-yl)but-2-enoate (iii) (10 g, 27 mmol) in 200 mL of ethanol was added 4-nitro-phenylhydrazine hydrochloride (5 g, 33 mmol). After stirring at RT for 16 hours,

the mixture became dark brown solution with brown suspension. Concentrate the solution via vacuum, and recrystallized with ethanol to give product (brown powder; 8.2 g, 63%).

^{1}H NMR (300 MHz, $CDCl_3$) δ 8.26 (d, J = 8.7 Hz, 2H), 7.72 (m, 4H), 7.61 (t, J = 8.1 Hz, 4H), 7.35 (d, J = 8.1 Hz, 2H), 7.13 (s, 1H), 4.49 (q, J = 7.2 Hz, 2H), 1.46 (t, J = 7.2 Hz, 3H).

4.13.2.6 General procedure for synthesis of **Via-f"**: Step e.

To a suspension of appropriate **Via-f"** (2 mmol, 1 equiv) in 2 mL of ethanol was added the suitable alkylamine 1M EtOH solution (5 mL, excess equiv). Transfer the mixture solution inside a seal tube, degas and seal the bottle. Heat the bottle to 120°C and stirred for 16 hours. The solution turned into brown solution with yellow suspension. After the heating, remove the solvent under vacuum, and recrystallize with ethanol to give product (all yellow powders; **Via**, 979 mg, 99%; **Via'**, 712 mg, 70%; **Via"**, 679 mg, 65%; **Vib**, 596 mg, 66%; **Vic**, 599 mg, 68%; **Vid**, 426 mg, 50%;**Vie**, 351 mg, 39%; **Vif**, 672 mg, 72%; **Vif'**, 605 mg, 63%; **Vif"**, 544 mg, 55%).

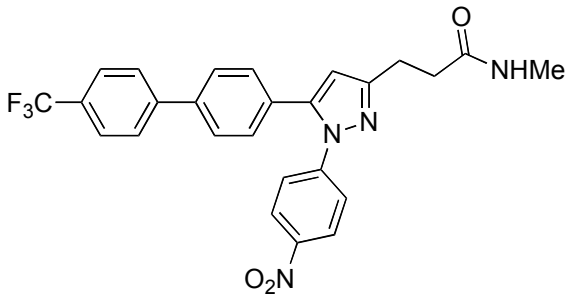

N-methyl-3-(1-(4-nitrophenyl)-5-(4'-(trifluoromethyl)-[1,1'-biphenyl]-4-yl)-1*H*-pyrazol-3-yl)propanamide (**Via**)

^{1}H NMR (300 MHz, $CDCl_3$) δ 8.39 (d, *J* = 8.4 Hz, 2H), 7.96 (d, *J* = 6.9 Hz, 2H), 7.82 (d, *J* = 7.8 Hz, 2H), 7.73 (m, 4H), 7.68 (m, 2H), 6.66 (s, 1H), 5.45 (bs, 1H), 3.21 (t, *J* = 7.2 Hz, 2H), 2.80 (s, 3H), 2.60 (t, *J* = 7.2 Hz, 2H).

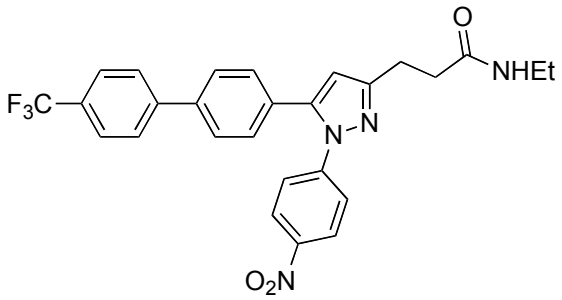

N-ethyl-3-(1-(4-nitrophenyl)-5-(4'-(trifluoromethyl)-[1,1'-biphenyl]-4-yl)-1*H*-pyrazol-3-yl)propanamide (**Via'**)

^{1}H NMR (300 MHz, CD_3OD) δ 8.25 (d, *J* = 8.4 Hz, 2H), 7.83 (d, *J* = 8.1 Hz, 2H), 7.73 (m, 4H), 7.53 (d, *J* = 9.3 Hz, 2H), 7.38 (d, *J* = 8.4 Hz, 2H), 6.56 (s, 1H), 3.22 (t, *J* = 7.2 Hz, 2H), 3.04 (t, *J* = 7.5 Hz, 2H), 2.62 (t, *J* = 7.5 Hz, 2H), 1.09 (t, *J* = 7.5 Hz, 3H).

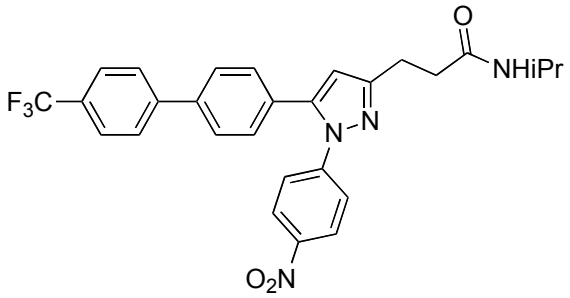

N-isopropyl-3-(1-(4-nitrophenyl)-5-(4'-(trifluoromethyl)-[1,1'-biphenyl]-4-yl)-1*H*-pyrazol-3-yl)propanamide (**Via"**)

^{1}H NMR (300 MHz, CD_3OD) δ 8.43 (d, *J* = 8.2 Hz, 2H), 7.98 (d, *J* = 8.2 Hz, 2H), 7.75 (m, 4H), 7.53 (d, *J* = 9.1 Hz, 2H), 7.37 (d, *J* = 8.2 Hz, 2H), 6.58 (s, 1H), 3.95, (m, 1H), 2.88 (t, *J* = 7.5 Hz, 2H), 2.43 (t, *J* = 7.5 Hz, 2H), 1.09 (d, *J* = 7.2 Hz, 3H).

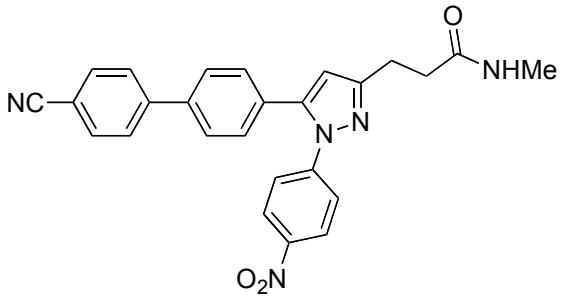

3-(5-(4'-cyano-[1,1'-biphenyl]-4-yl)-1-(4-nitrophenyl)-1*H*-pyrazol-3-yl)-*N*-methylpropanamide (**Vib**)

^{1}H NMR (300 MHz, $CDCl_3$) δ 8.39 (d, *J* = 8.7 Hz, 2H), 7.96 (d, *J* = 8.1 Hz, 2H), 7.82 (d, *J* = 9.0 Hz, 2H), 7.74 (m, 4H), 7.67 (d, *J* = 7.8 Hz, 2H), 6.66 (s, 1H), 5.49 (bs, 1H), 3.20 (t, *J* = 7.8 Hz, 2H), 2.84 (d, *J* = 4.8 Hz, 3H), 2.59 (t, *J* = 7.8 Hz, 2H).

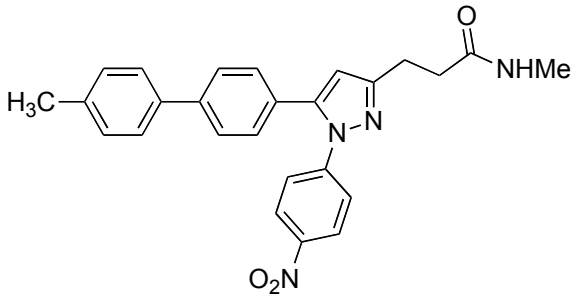

N-methyl-3-(5-(4'-methyl-[1,1'-biphenyl]-4-yl)-1-(4-nitrophenyl)-1*H*-pyrazol-3-yl)propanamide (**Vic**)

^{1}H NMR (300 MHz, $CDCl_3$) δ 8.39 (d, *J* = 9.0 Hz, 2H), 7.90 (d, *J* = 8.1 Hz, 2H), 7.82 (d, *J* = 9.0 Hz, 2H), 7.65 (d, *J* = 8.1 Hz, 2H), 7.55 (d, *J* = 8.1 Hz, 2H), 7.29 (m, 2H), 6.63 (s, 1H), 5.49 (bs, 1H), 3.20 (t, *J* = 7.8 Hz, 2H), 2.84 (d, *J* = 4.8 Hz, 3H), 2.59 (t, *J* = 7.8 Hz, 2H), 2.42 (s, 3H).

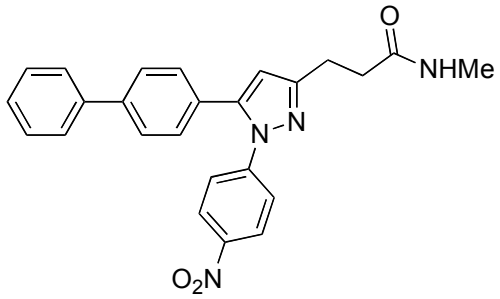

3-(5-([1,1'-biphenyl]-4-yl)-1-(4-nitrophenyl)-1*H*-pyrazol-3-yl)-*N*-methylpropanamide (**Vid**)

^{1}H NMR (300 MHz, $CDCl_3$) δ 8.38 (d, *J* = 8.7 Hz, 2H), 7.92 (d, *J* = 8.4 Hz, 2H), 7.81 (d, *J* = 9.0 Hz, 2H), 7.66 (m, 4H), 7.46 (m, 2H), 7.38 (m, 1H), 6.64 (s, 1H), 5.52 (bs, 1H), 3.19 (t, *J* = 7.8 Hz, 2H), 2.83 (d, *J* = 4.8 Hz, 3H), 2.58 (t, *J* = 7.5 Hz, 2H).

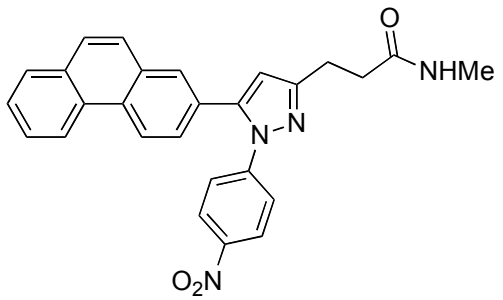

N-methyl-3-(1-(4-nitrophenyl)-5-(phenanthren-2-yl)-1*H*-pyrazol-3-yl)propanamide (**Vie**)

^{1}H NMR (300 MHz, $CDCl_3$) δ 8.72 (t, *J* = 9.3 Hz, 2H), 8.40 (d, *J* = 8.7 Hz, 2H), 8.35 (s, 1H), 8.15 (m, 1H), 7.91 (d, *J* = 7.8 Hz, 1H), 7.85 (d, *J* = 8.7 Hz, 2H), 7.79 (m, 2H), 7.65 (m, 3H), 6.78 (s, 1H), 5.52 (bs, 1H), 3.22 (t, *J* = 7.8 Hz, 2H), 2.84 (d, *J* = 4.8 Hz, 3H), 2.61 (t, *J* = 7.8 Hz, 2H).

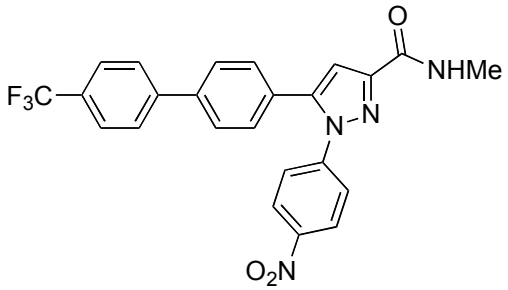

N-methyl-1-(4-nitrophenyl)-5-(4'-(trifluoromethyl)-[1,1'-biphenyl]-4-yl)-1*H*-pyrazole-3-carboxamide (**Vif**)

^{1}H NMR (300 MHz, $CDCl_3$) δ 8.27 (d, *J* = 8.7 Hz, 2H), 7.72 (s, 4H), 7.53 (d, *J* = 7.5 Hz, 2H), 7.55 (d, *J* = 7.8 Hz, 2H), 7.35 (d, *J* = 7.8 Hz, 2H), 7.14 (s, 1H), 6.99 (bs, 1H), 3.06 (d, *J* = 5.1 Hz, 3H).

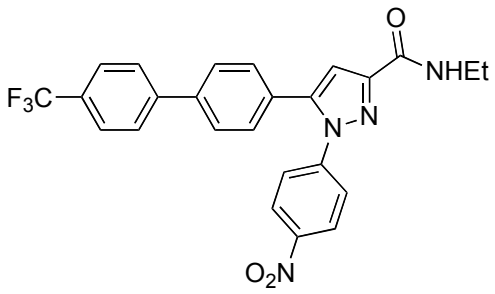

N-ethyl-1-(4-nitrophenyl)-5-(4'-(trifluoromethyl)-[1,1'-biphenyl]-4-yl)-1*H*-pyrazole-3-carboxamide (**Vif'**)

^{1}H NMR (300 MHz, $CDCl_3$) δ 8.27 (d, *J* = 8.7 Hz, 2H), 7.72 (s, 4H), 7.62 (d, *J* = 8.4 Hz, 2H), 7.56 (d, *J* = 9.0 Hz, 2H), 7.35 (d, *J* = 8.1 Hz, 2H), 7.14 (s, 1H), 6.97 (bs, 1H), 3.54 (q, *J* = 6.0 Hz, 2H), 1.30 (t, *J* = 7.2 Hz, 3H).

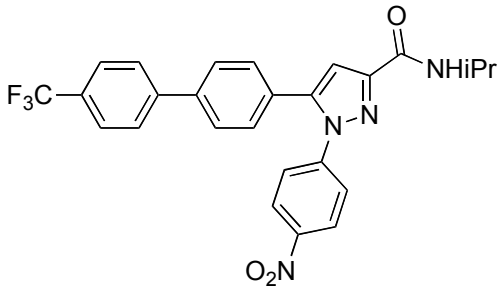

N-isopropyl-1-(4-nitrophenyl)-5-(4'-(trifluoromethyl)-[1,1'-biphenyl]-4-yl)-1*H*-pyrazole-3-carboxamide (**Vif"**)

^{1}H NMR (300 MHz, $CDCl_3$) δ 8.30 (d, *J* = 8.7 Hz, 2H), 7.72 (s, 4H), 7.63 (d, *J* = 6.6 Hz, 2H), 7.56 (d, *J* = 6.9 Hz, 2H), 7.35 (d, *J* = 8.7 Hz, 2H), 7.34 (s, 1H), 6.85 (bs, 1H), 3.38 (m, 1H), 1.30 (d, *J* = 7.8 Hz, 6H).

4.13.2.7 General procedure for synthesis of **Viia-f"**: Step f.

To a solution of compound **Via-f"** (0.5 mmol, 1 equiv) in 10 mL of MeOH/EtOAc (1/3) was added palladium on activated charcoal (Pd/C; 15 mg), stirred under $H_{2(g)}$ at 70 psi for 12 hours, filtered the solution through Celite filter pad to remove the catalyst, and concentrated to dryness under vacuum. The crude product was then purified by silica gel chromatography ($MeOH/CH_2Cl_2/NH_4OH$: 1/99/0.1), followed by recrystallization with CH_2Cl_2 to give product (all white crystals; **Viia-f**, 85~99%.)

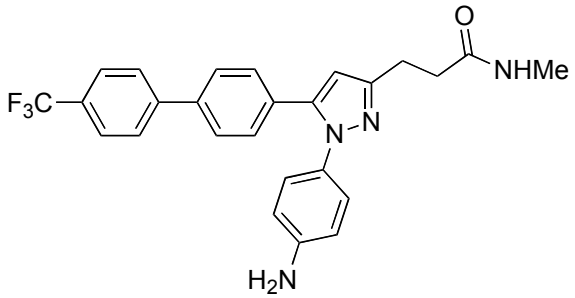

3-(1-(4-aminophenyl)-5-(4'-(trifluoromethyl)-[1,1'-biphenyl]-4-yl)-1*H*-pyrazol-3-yl)-*N*-methylpropanamide (**Viia**)

^{1}H NMR (300 MHz, CD_3OD) δ 7.90 (d, J = 8.1 Hz, 2H), 7.85 (d, J = 8.1 Hz, 2H), 7.73 (m, 4H), 7.39 (d, J = 8.4 Hz, 2H), 7.08 (d, J = 8.4 Hz, 2H), 6.70 (s, 1H), 2.95 (t, J = 7.8 Hz, 2H), 2.69 (s, 3H), 2.53 (t, J = 7.5 Hz, 2H).

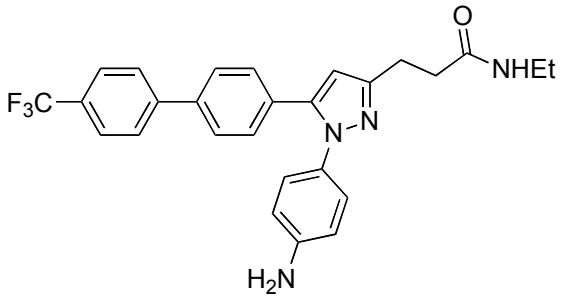

3-(1-(4-aminophenyl)-5-(4'-(trifluoromethyl)-[1,1'-biphenyl]-4-yl)-1*H*-pyrazol-3-yl)-*N*-ethylpropanamide (**Viia'**)

^{1}H NMR (300 MHz, CD_3OD) δ 7.88 (d, *J* = 8.1 Hz, 2H), 7.82 (d, *J* = 8.1 Hz, 2H), 7.71 (m, 4H), 7.26 (d, *J* = 8.4 Hz, 2H), 6.90 (d, *J* = 8.4 Hz, 2H), 6.65 (s, 1H), 2.85 (t, *J* = 7.2 Hz, 2H), 3.04 (t, *J* = 7.5 Hz, 2H), 2.46 (t, *J* = 7.5 Hz, 2H), 1.09 (t, *J* = 7.5 Hz, 3H).

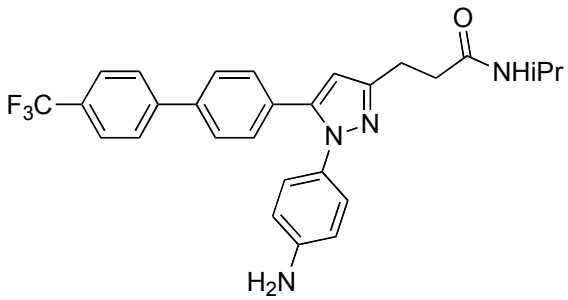

3-(1-(4-aminophenyl)-5-(4'-(trifluoromethyl)-[1,1'-biphenyl]-4-yl)-1*H*-pyrazol-3-yl)-*N*-isopropylpropanamide (**Viia"**)

^{1}H NMR (300 MHz, CD_3OD) δ 7.87 (d, *J* = 8.1 Hz, 2H), 7.80 (d, *J* = 8.1 Hz, 2H), 7.70 (m, 4H), 7.18 (d, *J* = 8.4 Hz, 2H), 6.80 (d, *J* = 8.4 Hz, 2H), 6.61 (s, 1H), 3.94 (m, 1H), 2.89 (t, *J* = 7.5 Hz, 2H), 2.46 (t, *J* = 7.5 Hz, 2H), 1.08 (d, *J* = 6.6 Hz, 6H).

6.85 (bs, 1H), 3.38 (m, 1H), 1.30 (d, *J* = 7.8 Hz, 6H).

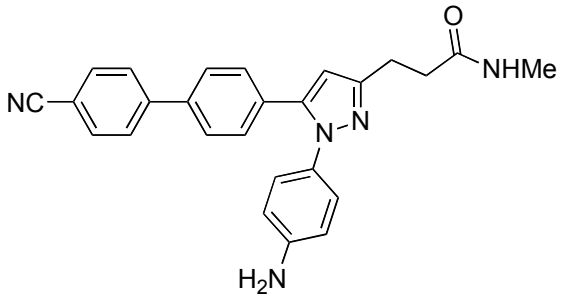

3-(1-(4-aminophenyl)-5-(4'-cyano-[1,1'-biphenyl]-4-yl)-1*H*-pyrazol-3-yl)-*N*-methylpropanamide (**Viib**)

^{1}H NMR (300 MHz, $CDCl_3$) δ 7.89 (d, *J* = 6.6 Hz, 2H), 7.68 (m, 4H), 7.58 (d, *J* = 7.5 Hz, 2H), 7.20 (d, *J* = 8.4 Hz, 2H), 6.71 (d, *J* = 8.1 Hz, 2H), 6.50 (s, 1H), 5.82 (bs, 1H), 2.96 (t, *J* = 7.8 Hz, 2H), 2.74 (d, *J* = 4.2 Hz, 3H), 2.43 (t, *J* = 7.5 Hz, 2H).

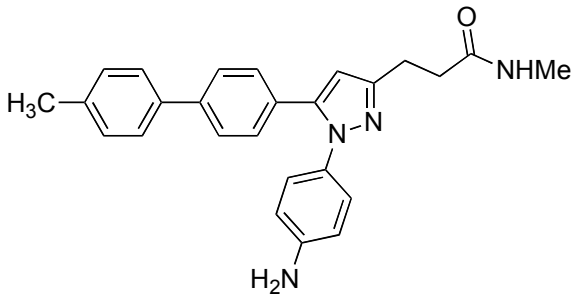

3-(1-(4-aminophenyl)-5-(4'-methyl-[1,1'-biphenyl]-4-yl)-1H-pyrazol-3-yl)-N-methylpropanamide (**Viic**)

^{1}H NMR (300 MHz, $CDCl_3$) δ 7.89 (d, *J* = 7.8 Hz, 2H), 7.62 (d, *J* = 8.4 Hz, 2H), 7.54 (d, *J* = 8.1 Hz, 2H), 7.24 (d, *J* = 2.1 Hz, 2H), 6.75 (d, *J* = 8.7 Hz, 2H), 6.51 (s, 1H), 5.44 (bs, 1H), 3.01 (t, *J* = 7.5 Hz, 2H), 2.79 (d, *J* = 4.8 Hz, 3H), 2.45 (t, *J* = 8.1 Hz, 2H), 2.40 (s, 3H).

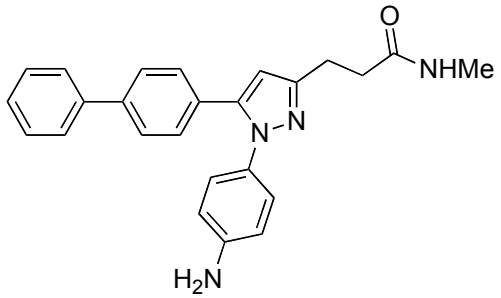

3-(5-([1,1'-biphenyl]-4-yl)-1-(4-aminophenyl)-1*H*-pyrazol-3-yl)-*N*-methylpropanamide (**Viid**)

^{1}H NMR (300 MHz, $CDCl_3$) δ 7.88 (d, *J* = 7.8 Hz, 2H), 7.62 (d, *J* = 7.8 Hz, 4H), 7.39 (m, 3H), 7.16 (d, *J* = 6.6 Hz, 2H), 6.66 (m, 2H), 6.47 (s, 1H), 6.07 (bs, 1H), 3.89 (s, 2H), 2.92 (t, *J* = 6.6 Hz, 2H), 2.68 (s, 3H), 2.37 (t, *J* = 7.2 Hz, 2H).

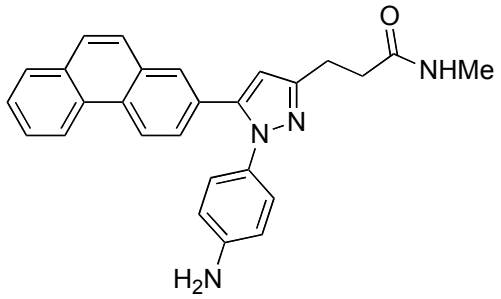

3-(1-(4-aminophenyl)-5-(phenanthren-2-yl)-1H-pyrazol-3-yl)-N-methylpropanamide (**Viie**)

^{1}H NMR (300 MHz, $CDCl_3$) δ 8.70 (d, *J* = 8.4 Hz, 2H), 8.35 (s, 1H), 8.15 (d, *J* = 8.4 Hz, 1H), 7.89 (d, *J* = 7.5 Hz, 1H), 7.74 (m, 2H), 7.62 (m, 2H), 6.66 (m, 2H), 7.30 (s, 1H), 6.77 (d, *J* = 8.4 Hz, 2H), 6.66 (s, 1H), 5.45 (bs, 1H), 3.85 (s, 3H), 3.04 (t, *J* = 7.5 Hz, 2H), 2.80 (d, *J* = 4.2 Hz, 3H), 2.45 (t, *J* = 7.5 Hz, 2H).

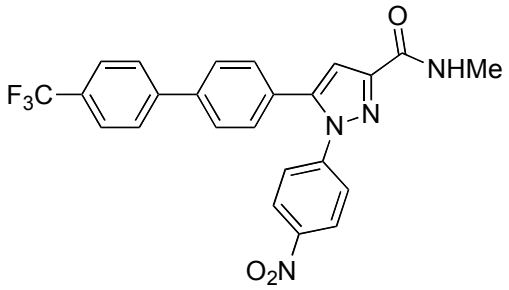

N-methyl-1-(4-nitrophenyl)-5-(4'-(trifluoromethyl)-[1,1'-biphenyl]-4-yl)-1*H*-pyrazole-3-carboxamide (**Viif**)

^{1}H NMR (300 MHz, $CDCl_3$) δ 7.71 (m, 4H), 7.54 (d, *J* = 8.1 Hz, 2H), 7.34 (d, *J* = 6.6 Hz, 2H), 7.12 (m, 3H), 7.00 (m, 1H), 6.67 (d, *J* = 6.6 Hz, 2H), 3.02 (d, *J* = 5.1 Hz, 3H).

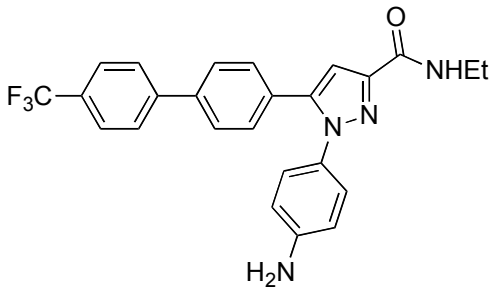

1-(4-aminophenyl)-*N*-ethyl-5-(4'-(trifluoromethyl)-[1,1'-biphenyl]-4-yl)-1*H*-pyrazole-3-carboxamide (**Viif'**)

^{1}H NMR (300 MHz, $CDCl_3$) δ 7.69 (m, 2H), 7.55 (d, *J* = 8.1 Hz, 2H), 7.34 (m, 2H), 7.13 (d, *J* = 6.6 Hz, 2H), 7.09 (s, 1H), 7.01 (m, 2H), 6.67 (d, *J* = 10.2 Hz, 2H), 3.84 (m, 1H), 3.52 (m, 2H), 1.26 (t, *J* = 7.2 Hz, 3H).

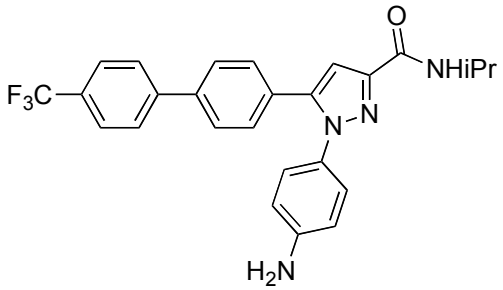

1-(4-aminophenyl)-*N*-isopropyl-5-(4'-(trifluoromethyl)-[1,1'-biphenyl]-4-yl)-1*H*-pyrazole-3-carboxamide (**Viif"**)

^{1}H NMR (300 MHz, $CDCl_3$) δ 7.68 (m, 2H), 7.57 (d, *J* = 8.1 Hz, 2H), 7.30 (m, 2H), 7.10 (m, 3H), 6.98 (m, 2H), 6.67 (d, *J* = 7.0 Hz, 2H), 3.38 (m, 1H), 1.30 (d, *J* = 7.8 Hz, 6H).

4.13.2.8 General procedure for synthesis of **15**-**20**: Step g.

To a solution of **Viia**, **a'a"**, **f**, **f'**, **f"** (0.1 mmol) in 15 mL anhydrous tetrahydrofurane was added β-Ala-Boc (111 mg, 0.59 mmol, 3 equiv) and 1-ethyl-3-(3-dimethylaminopropyl)carbodiimide (EDC, 248 mg, 1.6 mmol, 8 equiv), stir at RT for 16 hours, and concentrated to dryness under vacuum. The residue was suspended in water, and the product was extracted by dichloromethane. The organic phase was dried over sodium sulfate, and concentrated to dryness under vacuum to give Boc-Ala-intermediate. The intermediate was dissolved in 10 mL of hydrochloride methanol solution (3N, 41 mL), stirred at RT for 2 hours, and concentrated to dryness under vacuum. The crude product was purified by silica gel chromatography to give product (white powder **15**, 30

mg, 60 %; **16**, 26 mg, 50 %; **17**, 21 mg, 39 %; **18**, 29 mg, 55 %; **19**, 27 mg, 49 %; **20**, 20 mg, 35 %.)

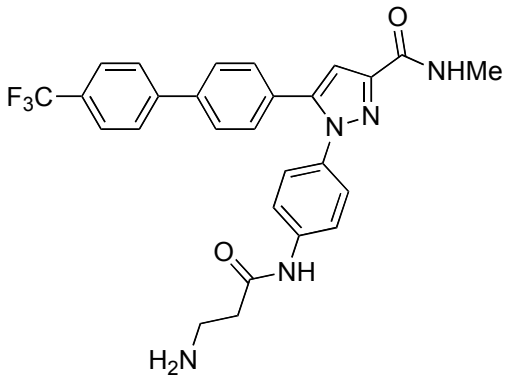

1-(4-(3-aminopropanamido)phenyl)-*N*-methyl-5-(4'-(trifluoromethyl)-[1,1'-biphenyl]-4-yl)-1*H*-pyrazole-3-carboxamide (**15**)

^{1}H NMR (300 MHz, $CDCl_3$): δ 7.80 (d, J = 8.0 Hz, 2H), 7.68 (m, 6H), 7.33 (m, 4H), 7.02 (s, 1H), 3.26 (d, J = 5.7 Hz, 2H), 2.93 (s, 3H), 2.84 (t, J = 5.6 Hz, 2H).

$C_{27}H_{24}F_3N_5O_2$: HRMS ($M+H^+$): calculated mass 508.1960; measured mass, 508.1953.

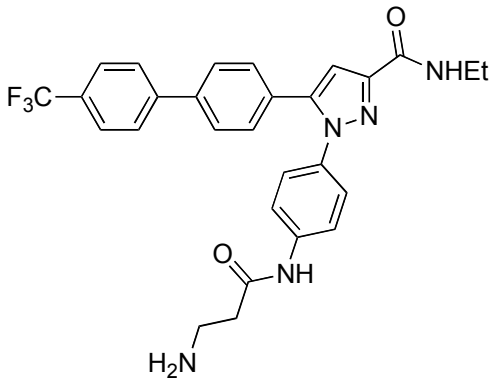

1-(4-(3-aminopropanamido)phenyl)-*N*-ethyl-5-(4'-(trifluoromethyl)-[1,1'-biphenyl]-4-yl)-1*H*-pyrazole-3-carboxamide (**16**)

^{1}H NMR (300 MHz, $CDCl_3$): δ 7.81 (d, J = 8.2 Hz, 2H), 7.69 (m, 6H), 7.41-7.29 (m, 4H), 7.04 (s, 1H), 3.43 (dd, J = 14.1, 7.0 Hz, 2H), 3.23 (m, 2H), 2.82 (t, J = 6.0 Hz, 2H), 1.23 (t, J = 7.1 Hz, 3H).

$C_{28}H_{26}F_3N_5O_2$: HRMS ($M+H^+$): calculated mass, 522.2117; measured mass, 522.2112.

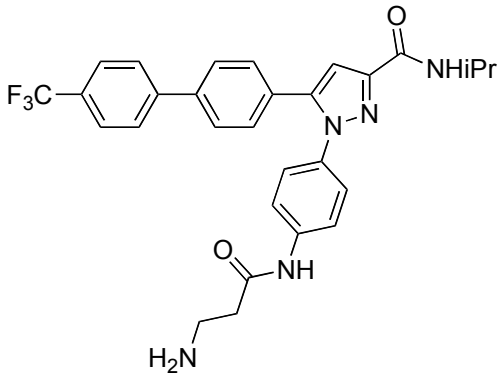

1-(4-(3-aminopropanamido)phenyl)-*N*-isopropyl-5-(4'-(trifluoromethyl)-[1,1'-biphenyl]-4-yl)-1*H*-pyrazole-3-carboxamide (**17**)

^{1}H NMR (300 MHz, $CDCl_3$): δ 7.81 (d, J = 8.2 Hz, 2H), 7.69 (m, 6H), 7.41-7.29 (m, 4H), 7.04 (s, 1H), 4.20 (m, 1H), 3.06 (m, 2H), 2.75 (t, J = 5.8 Hz, 2H), 1.18 (d, J = 6.3 Hz, 6H).

$C_{29}H_{28}F_3N_5O_2$: HRMS ($M+H^+$): calculated mass, 536.2273; measured mass, 536.2269

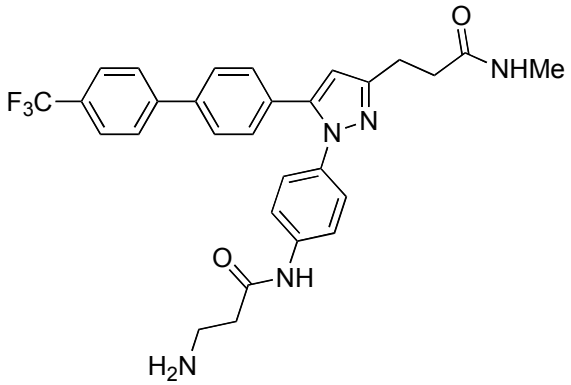

3-amino-*N*-(4-(3-(3-(methylamino)-3-oxopropyl)-5-(4'-(trifluoromethyl)-[1,1'-biphenyl]-4-yl)-1*H*-pyrazol-1-yl)phenyl)propanamide (**18**)

^{1}H NMR (300 MHz, $CDCl_3$): δ 7.86 (m, 4H), 7.73 (m, 4H), 7.19 (d, *J* = 8.5 Hz, 2H), 6.82 (d, *J* = 8.3 Hz, 2H), 6.66 (s, 1H), 3.48 (m, 2H), 3.30 (m, 2H), 3.98 (m, 2H), 2.69 (s, 3H), 2.51 (dd, *J* = 10.0, 5.6 Hz, 2H).

$C_{29}H_{28}F_3N_5O_2$: HRMS ($M+H^+$): calculated mass, 536.2273; measured mass, 536.2269.

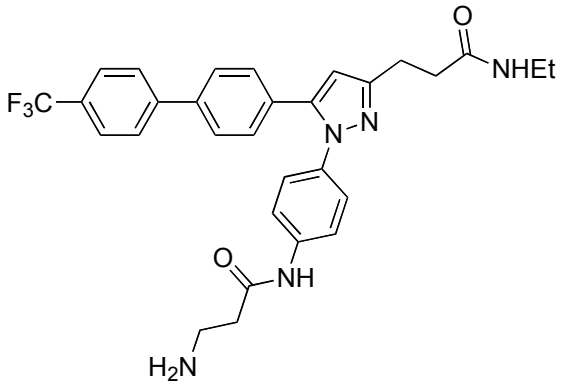

3-amino-*N*-(4-(3-(3-(ethylamino)-3-oxopropyl)-5-(4'-(trifluoromethyl)-[1,1'-biphenyl]-4-yl)-1*H*-pyrazol-1-yl)phenyl)propanamide (**19**)

^{1}H NMR (300 MHz, $CDCl_3$): δ 7.92 (d, *J* = 8.4 Hz, 2H), 7.84 (t, *J* = 7.1 Hz, 4H), 7.74 (d, *J* = 8.3 Hz, 4H), 7.50 (d, *J* = 8.5 Hz, 2H), 6.74 (s, 1H), 3.30 (m, 2H), 3.18 (m, 2H), 2.97 (t, *J* = 7.3 Hz, 2H), 2.88 (t, *J* = 6.3 Hz, 2H), 2.54 (t, *J* = 7.4 Hz, 2H), 1.08 (t, *J* = 7.3 Hz, 3H).

$C_{30}H_{30}F_3N_5O_2$: HRMS ($M+H^+$): calculated mass, 550.2430; measured mass, 550.2429.

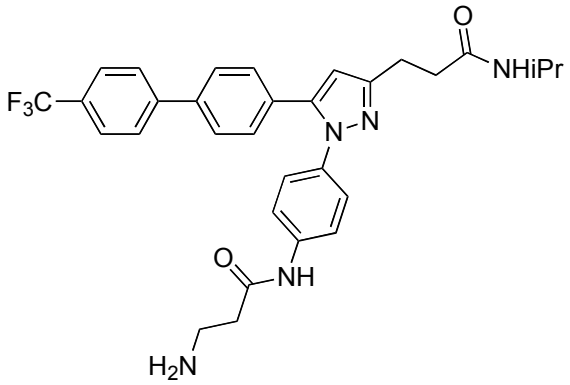

3-amino-*N*-(4-(3-(3-(isopropylamino)-3-oxopropyl)-5-(4'-(trifluoromethyl)-[1,1'-biphenyl]-4-yl)-1*H*-pyrazol-1-yl)phenyl)propanamide (**20**)

^{1}H NMR (300 MHz, $CDCl_3$): δ 7.95 (d, *J* = 8.5 Hz, 2H), 7.87 (t, *J* = 7.4 Hz, 4H), 7.77 (d, *J* = 8.1 Hz, 4H), 7.53 (d, *J* = 8.7 Hz, 2H), 6.77 (s, 1H), 4.95 (m, 1H), 2.99 (m, 2H), 2.91 (m, 2H), 2.56 (m, 2H), 1.12 (d, *J* = 6.6 Hz, 6H).

$C_{31}H_{32}F_3N_5O_2$: HRMS ($M+H^+$): calculated mass, 564.2586; measured mass, 564.2579.

4.13.2.9 General procedure for synthesis of **5**, **14**, **21**-**23**, **54**-**55**: Step h.

To a suspension of compound **Viib**, **e**, **f'**, **a**, **a'**, **c**, **d** (0.3 mmol, 1 equiv) in 10 mL of xylene was added bis(2-chloroethyl)amine hydrochloride (62 mg, 0.36 mmol, 1.2 equiv) and heated to 170°C. After stirring for 20 hours, the solution became brown sticky mixture. Remove the solvent via vacuum, and the crude product was purified by silica gel chromatography ($MeOH/CH_2Cl_2/NH_4OH$: 2/98/0.1), followed by recrystallization with ethyl acetate to give product (all white powders; **5**, 78 mg, 53 %; **14**, 53 mg, 36 %; **21**, 81.1 mg, 52%; **22**, 80.0 mg, 50 %; **23**, 77.2 mg, 47%; **54**, 45 mg, 31 %; **55**, 45 mg, 32 %).

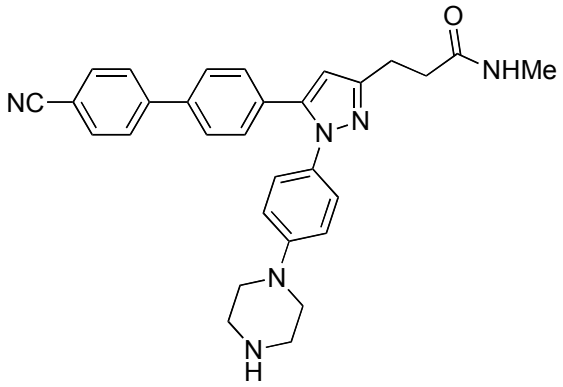

3-(5-(4'-cyano-[1,1'-biphenyl]-4-yl)-1-(4-(piperazin-1-yl)phenyl)-1*H*-pyrazol-3-yl)-*N*-methylpropanamide (**5**)

^{1}H NMR (300 MHz, $CDCl_3$): δ 7.95 (d, *J* = 8.4 Hz, 2H), 7.73 (m, 4H), 7.63 (d, *J* = 8.4 Hz, 2H), 7.37 (d, *J* = 8.7 Hz, 2H), 7.00 (d, *J* = 8.8 Hz, 2H), 6.55 (s, 1H), 5.45 (bs, 1H), 3.27-3.18 (m, 4H), 3.07 (dd, *J* = 3.9, 1.9 Hz, 4H), 3.02 (d, *J* = 8.2 Hz, 2H), 2.80 (d, *J* = 4.7 Hz, 3H), 2.47 (t, *J* = 7.5 Hz, 2H).

$C_{30}H_{30}N_6O$: HRMS ($M+H^+$): calculated mass, 491.2559; measured mass, 491.2546.

Anal. Calcd: C 73.45, H 6.16, N 17.13. Found: C 71.47, H 6.24, N 16.13.

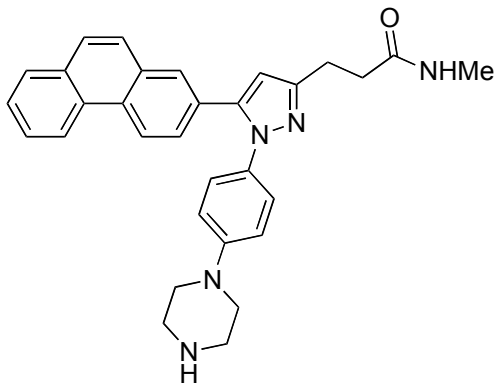

N-methyl-3-(5-(phenanthren-2-yl)-1-(4-(piperazin-1-yl)phenyl)-1*H*-pyrazol-3-yl)propanamide (**14**)

^{1}H NMR (300 MHz, $CDCl_3$): δ 8.71 (dd, *J* = 4.8, 3.7 Hz, 2H), 8.35 (m, 1H), 8.16 (dd, *J* = 8.4, 0.8 Hz, 1H), 7.89 (d, *J* = 7.7 Hz, 1H), 7.76 (q, *J* = 8.7 Hz, 2H), 7.63 (m, 2H), 7.39 (d, *J* = 8.6 Hz, 2H), 7.00 (d, *J* = 8.6 Hz, 2H), 6.67 (s, 1H), 5.49 (bs, 1H), 3.21 (m, 4H), 3.05 (m, 6H), 2.80 (d, *J* = 4.6 Hz, 3H), 2.49 (t, *J* = 7.5 Hz, 2H).

$C_{31}H_{31}N_5O$: HRMS ($M+H^+$): calculated mass, 490.2607; measured mass, 490.2625.

Anal. Calcd: C 76.05, H 6.38, N 14.30. Found: C 72.30, H 6.23, N 13.27.

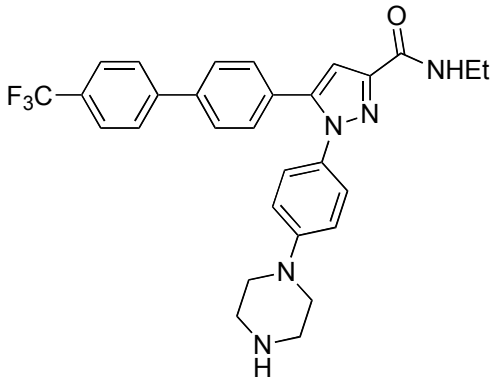

N-ethyl-1-(4-(piperazin-1-yl)phenyl)-5-(4'-(trifluoromethyl)-[1,1'-biphenyl]-4-yl)-1*H*-pyrazole-3-carboxamide (**21**)

^{1}H NMR (300 MHz, $CDCl_3$): δ 7.69 (s, 4H), 7.55 (d, J = 7.8 Hz, 2H), 7.35 (d, J = 7.9 Hz, 2H), 7.23 (d, J = 8.4 Hz, 2H), 7.10 (s, 1H), 7.00 (t, J = 5.4 Hz, 1H), 6.92 (d, J = 8.6 Hz, 1H), 3.51 (m, 2H), 3.20 (m, 4H), 3.05 (m, 4H), 1.26 (t, J = 7.1 Hz, 3H).

$C_{29}H_{28}F_3N_5O$: HRMS ($M+H^+$): calculated mass, 520.2324; measured mass, 520.2312.

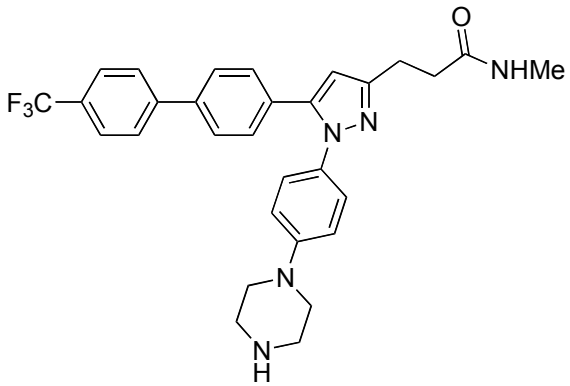

N-methyl-3-(1-(4-(piperazin-1-yl)phenyl)-5-(4'-(trifluoromethyl)-[1,1'-biphenyl]-4-yl)-1*H*-pyrazol-3-yl)propanamide (**22**) T315

^{1}H NMR (300 MHz, $CDCl_3$): δ 7.93 (d, J = 8.3 Hz, 2H), 7.71 (q, J = 8.6 Hz, 4H), 7.64 (d,

J = 8.3 Hz, 2H), 7.35 (d, J = 8.8 Hz, 2H), 6.98 (d, J = 8.9 Hz, 2H), 6.54 (s, 1H), 5.54 (bs, 1H), 3.21 (dd, J = 6.2, 3.6 Hz, 4H), 3.06 (m, 4H), 3.01 (d, J = 8.0 Hz, 2H), 2.78 (d, J = 4.8 Hz, 3H), 2.45 (dd, J = 8.0, 7.4 Hz, 2H).

$C_{30}H_{30}F_3N_5O$: HRMS ($M+H^+$): calculated mass, 534.2480; measured mass, 534.2467.

Anal. Calcd: C 67.53,H5.67, F 10.68,N13.13. Found: C 67.17, H 5.61, F 10.36, N 12.95.

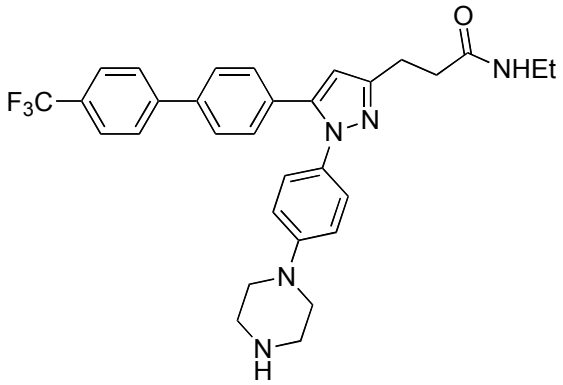

N-ethyl-3-(1-(4-(piperazin-1-yl)phenyl)-5-(4'-(trifluoromethyl)-[1,1'-biphenyl]-4-yl)-1*H*-pyrazol-3-yl)propanamide (**23**)

^{1}H NMR (300 MHz, $CDCl_3$): δ 7.93 (d, J = 8.3 Hz, 2H), 7.71 (q, J = 8.6 Hz, 4H), 7.63 (d, J = 8.3 Hz, 2H), 7.35 (d, J = 8.8 Hz, 2H), 6.98 (d, J = 8.9 Hz, 2H), 6.54 (s, 1H), 5.53 (bs, 1H), 3.28 (m, 2H), 3.20 (m, 4H), 3.03 (m, 6H), 2.44 (t, J = 7.7 Hz, 2H), 1.10 (t, J = 7.3 Hz, 3H).

$C_{31}H_{32}F_3N_5O$: HRMS ($M+H^+$): calculated mass 548.2637; measured mass, 548.2623.

Anal. Calcd: C 67.99, H 5.89, F 10.41, N 12.79. Found: C 67.67, H 5.83, F 10.16, N 12.63.

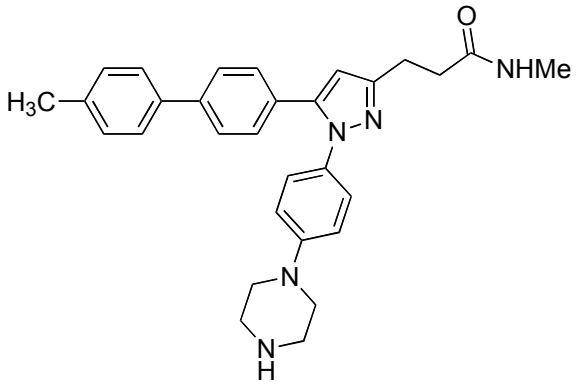

N-methyl-3-(5-(4'-methyl-[1,1'-biphenyl]-4-yl)-1-(4-(piperazin-1-yl)phenyl)-1*H*-pyrazol-3-yl)propanamide (**54**)

^{1}H NMR (300 MHz, $CDCl_3$): δ 7.89 (d, *J* = 8.3 Hz, 2H), 7.62 (d, *J* = 8.3 Hz, 2H), 7.54 (d, *J* = 7.9 Hz, 2H), 7.36 (d, *J* = 8.9 Hz, 2H), 7.24 (m, 2H), 6.99 (d, *J* = 8.8 Hz, 2H), 6.52 (s, 1H), 5.46 (s, 1H), 3.22 (m, 4H), 3.07 (dd, *J* = 8.6, 4.4 Hz, 4H), 3.01 (d, *J* = 8.3 Hz, 2H), 2.79 (d, *J* = 4.8 Hz, 3H), 2.46 (m, 2H), 2.40 (s, 3H).

$C_{30}H_{33}N_5O$: HRMS ($M+H^+$): calculated mass 480.2763; measured mass, 480.2765.

Anal. Calcd: C 75.13, H 6.94, N 14.60. Found: C 74.16, H 7.00, N 14.46.

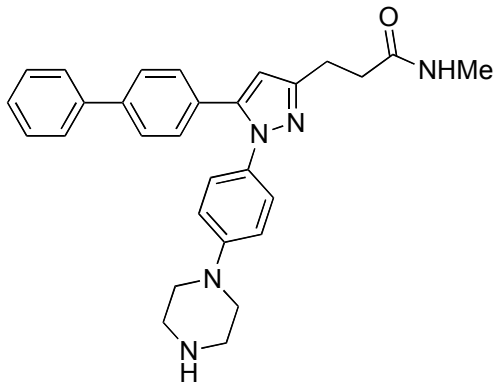

3-(5-([1,1'-biphenyl]-4-yl)-1-(4-(piperazin-1-yl)phenyl)-1*H*-pyrazol-3-yl)-*N*-methylpropanamide (**55**)

^{1}H NMR (300 MHz, $CDCl_3$): δ 7.91 (d, *J* = 8.3 Hz, 2H), 7.64 (d, *J* = 7.5 Hz, 4H), 7.45 (t, *J* = 7.4 Hz, 2H), 7.36 (d, *J* = 8.3 Hz, 3H), 6.99 (d, *J* = 8.6 Hz, 2H), 6.53 (s, 1H), 5.48 (s, 1H), 3.23 (m, 4H), 3.08 (m, 4H), 3.01 (d, *J* = 8.2 Hz, 2H), 2.79 (d, *J* = 4.7 Hz, 3H), 2.46 (t, *J* = 7.6 Hz, 2H).

$C_{29}H_{31}N_5O$: HRMS ($M+H^+$): calculated mass 466.2607; measured mass, 466.2602.

Anal. Calcd: C 74.84, H 6.71, N 15.04. Found: C 74.83, H 6.89, N 13.76.

4.13.2.10 Synthesis of *N*-methyl-3-(1-(4-morpholinophenyl)-5-(4'-(trifluoromethyl)-[1,1'-biphenyl]-4-yl)-1*H*-pyrazol-3-yl)propanamide (**53**): Step i.

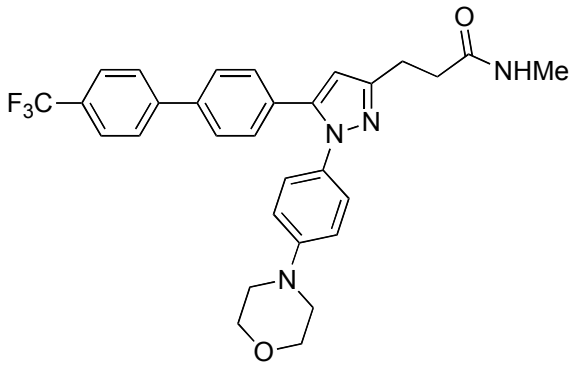

To a suspension of **Viib** (60 mg, 0.13 mmol, 1 equiv) in 10 mL of xylene was added 1-iodo-2-(2-iodoethoxy)ethane (77 mg, 0.39 mmol, 3 equiv) and heated to 170°C. After stirring for 20 hours, the solution became brown sticky mixture. Remove the

solvent via vacuum, and the crude product was purified by silica gel chromatography ($MeOH/CH_2Cl_2/NH_4OH$: 1/99/0.1), followed by recrystallization with ethyl acetate to give product (white powder, **53**, 20 mg, 29 %). ^1H NMR (300 MHz, $CDCl_3$): δ 7.94 (d, *J* = 8.1 Hz, 2H), 7.72 (q, *J* = 8.7 Hz, 4H), 7.64 (d, *J* = 8.1 Hz, 2H), 7.38 (d, *J* = 8.4 Hz, 2H), 6.98 (d, *J* = 8.7 Hz, 2H), 6.54 (s, 1H), 5.49 (bs, 1H), 3.90 (m, 4H), 3.22 (m, 4H), 3.03 (m, 2H), 2.78 (d, *J* = 4.8 Hz), 2.47 (t, *J* = 7.5 Hz, 2H). $C_{30}H_{29}F_3N_4O_2$: HRMS ($M+Na^+$): calculated mass 557.2140; measured mass, 557.2144.

Bibliography

Ahmed, N., Riley, C., Oliva, K., Stutt, E., Rice, G. E., and Quinn, M. A. (2003). Integrin-linked kinase expression increases with ovarian tumour grade and is sustained by peritoneal tumour fluid. *The Journal of Pathology*. *201*, 229–237.

Alessi, D. R., James, S. R., Downes, C. P., Holmes, A. B., Gaffney, P. R., Reese, C. B., and Cohen, P. (1997). Characterization of a 3-phosphoinositide-dependent protein kinase which phosphorylates and activates protein kinase Balpha. *Current biology*. *7*, 261–269.

Arico, S., Pattingre, S., Bauvy, C., Gane, P., Barbat, A., Codogno, P., and Ogier-Denis, E. (2002). Celecoxib induces apoptosis by inhibiting 3-phosphoinositide-dependent protein kinase-1 activity in the human colon cancer HT-29 cell line. *The Journal of Biological Chemistry*. *277*, 27613–27621.

Bhagwat, S. V., Gokhale, P. C., Crew, A. P., Cooke, A., Yao, Y., Mantis, C., Kahler, J., Workman, J., Bittner, M., Dudkin, L., et al. (2011). Preclinical characterization of OSI-027, a potent and selective inhibitor of mTORC1 and mTORC2: distinct from rapamycin. *Molecular Cancer Therapeutics*. *10*, 1394–1406.

Bravou, V., Klironomos, G., Papadaki, E., Taraviras, S., and Varakis, J. (2006). ILK over-expression in human colon cancer progression correlates with activation of beta-catenin, down-regulation of E-cadherin and activation of the Akt-FKHR pathway. *The Journal of Pathology*. *208*, 91–99.

Cary, L. A., and Guan, J. L. (1999). Focal adhesion kinase in integrin-mediated signaling. *Frontiers in Bioscience*. *4*, D102–D113.

Casagrande, F. (1998). G1 phase arrest by the phosphatidylinositol 3-kinase inhibitor LY 294002 is correlated to up-regulation of p27Kip1 and inhibition of G1 CDKs in choroidal melanoma cells. *FEBS Letters*. *422*, 385–390.

Chan, J., Ko, F. C., Yeung, Y. S., Ng, I. O., and Yam, J. W. (2011). Integrin-linked kinase overexpression and its oncogenic role in promoting tumorigenicity of hepatocellular carcinoma. *PLoS One*. *6*, e16984.

Chang, S. M., Wen, P., Cloughesy, T., Greenberg, H., Schiff, D., Conrad, C., Fink, K., Robins, H. I., De Angelis, L., Raizer, J., et al. (2005). Phase II study of CCI-779 in patients with recurrent glioblastoma multiforme. *Investigational New Drugs*. *23*, 357–361.

Chresta, C. M., Davies, B. R., Hickson, I., Harding, T., Cosulich, S., Critchlow, S. E., Vincent, J. P., Ellston, R., Jones, D., Sini, P., et al. (2010). AZD8055 is a potent, selective, and orally bioavailable ATP-competitive mammalian target of rapamycin kinase inhibitor with in vitro and in vivo antitumor activity. *Cancer Research*. *70*, 288–298.

Codogno, P., and Meijer, A. J. (2005). Autophagy and signaling: their role in cell survival and cell death. *Cell Death & Differentiation*. *12 Suppl 2*, 1509–1518.

Cybulski, N., and Hall, M. N. (2009). TOR complex 2: a signaling pathway of its own.

Trends in Biochemical Sciences. *34*, 620–627.

Delcommenne, M., Tan, C., Gray, V., Rue, L., Woodgett, J., and Dedhar, S. (1998). Phosphoinositide-3-OH kinase-dependent regulation of glycogen synthase kinase 3 and protein kinase B/AKT by the integrin-linked kinase. *Proceedings of the National Academy of Sciences of the United States of America*. *95*, 11211–11216.

Deng, J. T., Van Lierop, J. E., Sutherland, C., and Walsh, M. P. (2001). Ca^{2+}-independent smooth muscle contraction, a novel function for integrin-linked kinase. *The Journal of Biological Chemistry*. *276*, 16365–16373.

Deng, J. T., Sutherland, C., Brautigan, D. L., Eto, M., and Walsh, M. P. (2002). Phosphorylation of the myosin phosphatase inhibitors, CPI-17 and PHI-1, by integrin-linked kinase. *Biochemical Journal*. *367*, 517–524.

Dong, L. Q., and Liu, F. (2005). PDK2: the missing piece in the receptor tyrosine kinase signaling pathway puzzle. *American journal of physiology - Endocrinology and Metabolism*. *289*, E187–E196.

Douros, J., and Suffness, M. (1981). New antitumor substances of natural origin. *Cancer Treatment Reviews*. *8*, 63–87.

Eke, I., Leonhardt, F., Storch, K., Hehlgans, S., and Cordes, N. (2009). The small molecule inhibitor QLT0267 Radiosensitizes squamous cell carcinoma cells of the head and neck. *PloS One*. *4*, e6434.

Eng, C. P., Sehgal, S. N., and Vézina, C. (1984). Activity of rapamycin (AY-22,989)

against transplanted tumors. *The Journal of Antibiotics*. *37*, 1231–1237.

Esfandiarei, M., Yazdi, S. A., Gray, V., Dedhar, S., and van Breemen, C. (2010). Integrin-linked kinase functions as a downstream signal of platelet-derived growth factor to regulate actin polymerization and vascular smooth muscle cell migration. *BMC Cell Biology*. *11*, 16.

Fingar, D. C., Salama, S., Tsou, C., Harlow, E., and Blenis, J. (2002). Mammalian cell size is controlled by mTOR and its downstream targets S6K1 and 4EBP1/eIF4E. *Genes & Development*. *16*, 1472–1487.

Fresno Vara, J. A., Casado, E., de Castro, J., Cejas, P., Belda-Iniesta, C., and González-Barón, M. (2004). PI3K/Akt signalling pathway and cancer. *Cancer Treatment Reviews*. *30*, 193–204.

Fukuda, K., Gupta, S., Chen, K., Wu, C., and Qin, J. (2009). The pseudoactive site of ILK is essential for its binding to alpha-Parvin and localization to focal adhesions. *Molecular Cell*. *36*, 819–830.

García-Martínez, J. M., Moran, J., Clarke, R. G., Gray, A., Cosulich, S. C., Chresta, C. M., and Alessi, D. R. (2009). Ku-0063794 is a specific inhibitor of the mammalian target of rapamycin (mTOR). *The Biochemical Journal*. *421*, 29–42.

Graff, J. R., Deddens, J. A., Konicek, B. W., Colligan, B. M., Hurst, B. M., Carter, H. W., and Carter, J. H. (2001). Integrin-linked kinase expression increases with prostate tumor grade. *Clinical Cancer Research*. *7*, 1987–1991.

Hannigan, G. E., Leung-Hagesteijn, C., Fitz-Gibbon, L., Coppolino, M. G., Radeva, G., Filmus, J., Bell, J. C., and Dedhar, S. (1996). Regulation of cell adhesion and anchorage-dependent growth by a new beta 1-integrin-linked protein kinase. *Nature*. *379*, 91–96.

Hannigan, G., Troussard, A. a, and Dedhar, S. (2005). Integrin-linked kinase: a cancer therapeutic target unique among its ILK. *Nature Reviews Cancer*. *5*, 51–63.

Herbst, R. S. (2002). ZD1839: targeting the epidermal growth factor receptor in cancer therapy. *Expert Opinion on Investigational Drugs*. *11*, 837–849.

Hidalgo, M., Siu, L., and Nemunaitis, J. (2001). Phase I and pharmacologic study of OSI-774, an epidermal growth factor receptor tyrosine kinase inhibitor, in patients with advanced solid malignancies. *Journal of Clinical Oncology*. *19*, 3267–3279.

Hill, M. M., Feng, J., and Hemmings, B. A. (2002). Identification of a plasma membrane raft-associated PKB Ser-473 kinase activity that is distinct from ILK and PDK1. *Current Biology*. *12*, 1251–1255.

Hu, L., Zaloudek, C., Mills, G. B., Gray, J., and Jaffe, R. B. (2000). In vivo and in vitro ovarian carcinoma growth inhibition by a phosphatidylinositol 3-kinase inhibitor (LY294002). *Clinical Cancer Research*. *6*, 880–886.

Huang, S., and Houghton, P. J. (2003). Targeting mTOR signaling for cancer therapy. *Current Opinion in Pharmacology*. *3*, 371–377.

Huang, Y., Li, J., Zhang, Y., and Wu, C. (2000). The roles of integrin-linked kinase in the

regulation of myogenic differentiation. *The Journal of Cell Biology*. *150*, 861–872.

Hudis, C. A. (2007). Trastuzumab--mechanism of action and use in clinical practice. *The New England Journal of Medicine*. *357*, 39–51.

Ishii, T., Satoh, E., and Nishimura, M. (2001). Integrin-linked kinase controls neurite outgrowth in N1E-115 neuroblastoma cells. *The Journal of Biological Chemistry*. *276*, 42994–43003.

Ito, R., Oue, N., Zhu, X., Yoshida, K., Nakayama, H., Yokozaki, H., and Yasui, W. (2003). Expression of integrin-linked kinase is closely correlated with invasion and metastasis of gastric carcinoma. *Virchows Arch*. *442*, 118–123.

Kalra, J., Sutherland, B. W., Stratford, A. L., Dragowska, W., Gelmon, K. A., Dedhar, S., Dunn, S. E., and Bally, M. B. (2010). Suppression of Her2/neu expression through ILK inhibition is regulated by a pathway involving TWIST and YB-1. *Oncogene*. *29*, 6343–6356.

Kalra, J., Warburton, C., Fang, K., Edwards, L., Daynard, T., Waterhouse, D., Dragowska, W., Sutherland, B. W., Dedhar, S., Gelmon, K., et al. (2009). QLT0267, a small molecule inhibitor targeting integrin-linked kinase (ILK), and docetaxel can combine to produce synergistic interactions linked to enhanced cytotoxicity, reductions in P-AKT levels, altered F-actin architecture and improved treatment outc. *Breast Cancer Research*. *11*, R25.

Kaneko, Y., Kitazato, K., and Basaki, Y. (2004). Integrin-linked kinase regulates vascular

morphogenesis induced by vascular endothelial growth factor. *Journal of Cell Science*. *117*, 407–415.

Kim, S. H., Um, J. H., Dong-Won, B., Kwon, B. H., Kim, D. W., Chung, B. S., and Kang, C. D. (2000). Potentiation of chemosensitivity in multidrug-resistant human leukemia CEM cells by inhibition of DNA-dependent protein kinase using wortmannin. *Leukemia Research*. *24*, 917–925.

Lee, S.-L., Hsu, E.-C., Chou, C.-C., Chuang, H.-C., Bai, L.-Y., Kulp, S. K., and Chen, C.-S. (2011). Identification and characterization of a novel integrin-linked kinase inhibitor. *Journal of Medicinal Chemistry*. *54*, 6364–6374.

Legate, K. R., Montanez, E., Kudlacek, O., and Fassler, R. (2006). ILK, PINCH and parvin: the tIPP of integrin signalling. *Nature Reviews Molecular Cell Biology*. *7*, 20–31.

Leung-Hagesteijn, C., Hu, M. C., Mahendra, A. S., Hartwig, S., Klamut, H. J., Rosenblum, N. D., and Hannigan, G. E. (2005a). Integrin-linked kinase mediates bone morphogenetic protein 7-dependent renal epithelial cell morphogenesis. *Molecular and Cellular Biology*. *25*, 3648–3657.

Leung-Hagesteijn, C., Hu, M. C., Mahendra, A. S., Hartwig, S., Klamut, H. J., Rosenblum, N. D., and Hannigan, G. E. (2005b). Integrin-linked kinase mediates bone morphogenetic protein 7-dependent renal epithelial cell morphogenesis. *Molecular and Cellular Biology*. *25*, 3648–3657.

Lim, D., Fang, F., Zhou, G., and Coltart, D. M. (2007). Direct carbon-carbon bond formation via soft enolization: a facile and efficient synthesis of 1,3-diketones. *Organic Letters*. *9*, 4139–4142.

MacDonald, M. L., Lamerdin, J., Owens, S., Keon, B. H., Bilter, G. K., Shang, Z., Huang, Z., Yu, H., Dias, J., Minami, T., et al. (2006). Identifying off-target effects and hidden phenotypes of drugs in human cells. *Nature Chemical Biology*. *2*, 329–337.

Malagu, K., Duggan, H., Menear, K., Hummersone, M., Gomez, S., Bailey, C., Edwards, P., Drzewiecki, J., Leroux, F., Quesada, M. J., et al. (2009). The discovery and optimisation of pyrido[2,3-d]pyrimidine-2,4-diamines as potent and selective inhibitors of mTOR kinase. *Bioorganic & Medicinal Chemistry Letters*. *19*, 5950–5953.

Manning, B. D., and Cantley, L. C. (2007). AKT/PKB signaling: navigating downstream. *Cell*. *129*, 1261–1274.

Margolin, K., Longmate, J., Baratta, T., Synold, T., Christensen, S., Weber, J., Gajewski, T., Quirt, I., and Doroshow, J. H. (2005). CCI-779 in metastatic melanoma: a phase II trial of the California Cancer Consortium. *Cancer*. *104*, 1045–1048.

Muthukkumar, S., Ramesh, T. M., and Bondada, S. (1995). Rapamycin, a potent immunosuppressive drug, causes programmed cell death in B lymphoma cells. *Transplantation*. *60*, 264–270.

Oloumi, A., McPhee, T., and Dedhar, S. (2004). Regulation of E-cadherin expression and

beta-catenin/Tcf transcriptional activity by the integrin-linked kinase. *Biochimica et Biophysica Acta*. *1691*, 1–15.

Persad, S., Attwell, S., Gray, V., Delcommenne, M., Troussard, a, Sanghera, J., and Dedhar, S. (2000). Inhibition of integrin-linked kinase (ILK) suppresses activation of protein kinase B/Akt and induces cell cycle arrest and apoptosis of PTEN-mutant prostate cancer cells. *Proceedings of the National Academy of Sciences of the United States of America*. *97*, 3207–3212.

Persad, S., Attwell, S., Gray, V., Mawji, N., Deng, J. T., Leung, D., Yan, J., Sanghera, J., Walsh, M. P., and Dedhar, S. (2001). Regulation of protein kinase B/Akt-serine 473 phosphorylation by integrin-linked kinase: critical roles for kinase activity and amino acids arginine 211 and serine 343. *The Journal Biological Chemistry*. *276*, 27462–27469.

Porchia, L., Guerra, M., Wang, Y.-C., Zhang, Y., Espinosa, A. V., Shinohara, M., Kulp, Samuel, K., Kirschner, L. S., Saji, M., Chen, C.-S., and Ringel, M. D. (2007). 2-amino-N-{4-[5-(2-phenanthrenyl)-3-(trifluoromethyl)-1H-pyrazol-1-yl]-phenyl} acetamide (OSU-03012), a celecoxib derivative, directly targets p21-activated kinase. *Molecular Pharmacology*. *72*, 1124-1131.

Pontier, S. M., Huck, L., White, D. E., Rayment, J., Sanguin-Gendreau, V., Hennessy, B., Zuo, D., St-Arnaud, R., Mills, G. B., Dedhar, S., et al. (2010). Integrin-linked kinase has a critical role in ErbB2 mammary tumor progression: implications for human breast cancer. *Oncogene*. *29*, 3374–3385.

Powis, G., Bonjouklian, R., Berggren, M. M., Gallegos, A., Abraham, R., Ashendel, C., Zalkow, L., Matter, W. F., Dodge, J., Grindey, G., et al. (1994). Wortmannin , a potent and selective inhibitor of wortmannin, a potent and selective inhibitor of phosphatidylinositol-3-kinase. *Cancer Research*. *54* ,2419–2423.

Ross, J. S., Schenkein, D. P., Pietrusko, R., Rolfe, M., Linette, G. P., Stec, J., Stagliano, N. E., Ginsburg, G. S., Symmans, W. F., Pusztai, L., et al. (2004). Targeted therapies for cancer 2004. *American Journal of Clinical Pathology*. *122*, 598–609.

Sarkaria, J. N., Tibbetts, R. S., Busby, E. C., Kennedy, A. P., Hill, D. E., and Abraham, R. T. (1998). Inhibition of phosphoinositide 3-kinase related kinases by the radiosensitizing agent wortmannin. *Cancer Research*. *58*, 4375–4382.

Sato, S., Fujita, N., and Tsuruo, T. (2002). Interference with PDK1-Akt survival signaling pathway by UCN-01 (7-hydroxystaurosporine). *Oncogene*. *21*, 1727–1738.

Sawai, H., Okada, Y., Funahashi, H., Matsuo, Y., Takahashi, H., Takeyama, H., and Manabe, T. (2006). Integrin-linked kinase activity is associated with interleukin-1 alpha-induced progressive behavior of pancreatic cancer and poor patient survival. *Oncogene*. *25*, 3237–3246.

Schaeffer, D. F., Assi, K., Chan, K., Buczkowski, A. K., Chung, S. W., Scudamore, C. H., Weiss, A., Salh, B., and Owen, D. A. (2010). Tumor expression of integrin-linked kinase (ILK) correlates with the expression of the E-cadherin repressor snail: an immunohistochemical study in ductal pancreatic adenocarcinoma. *Virchows Arch*. *456*, 261–268.

Stratford, A. L., Habibi, G., Astanehe, A., Jiang, H., Hu, K., Park, E., Shadeo, A., Buys, T. P., Lam, W., Pugh, T., et al. (2007). Epidermal growth factor receptor (EGFR) is transcriptionally induced by the Y-box binding protein-1 (YB-1) and can be inhibited with Iressa in basal-like breast cancer, providing a potential target for therapy. *Breast Cancer Research*. *9*, R61.

Su, J. L., Chiou, J., Tang, C. H., Zhao, M., Tsai, C. H., Chen, P. S., Chang, Y. W., Chien, M. H., Peng, C. Y., Hsiao, M., et al. (2010). CYR61 regulates BMP-2-dependent osteoblast differentiation through the αvβ3 integrin/integrin-linked kinase/ERK pathway. *The Journal of Biological Chemistry*. *285*, 31325–31336.

Tabe, Y., Jin, L., Tsutsumi-Ishii, Y., Xu, Y., McQueen, T., Priebe, W., Mills, G. B., Ohsaka, A., Nagaoka, I., Andreeff, M., et al. (2007). Activation of integrin-linked kinase is a critical prosurvival pathway induced in leukemic cells by bone marrow-derived stromal cells. *Cancer Research*. *67*, 684–694.

Tan, C., Cruet-Hennequart, S., Troussard, A., Fazli, L., Costello, P., Sutton, K., Wheeler, J., Gleave, M., Sanghera, J., and Dedhar, S. (2004). Regulation of tumor angiogenesis by integrin-linked kinase (ILK). *Cancer Cell*. *5*, 79–90.

Troussard, A. A., Mawji, N. M., Ong, C., Mui, A., St -Arnaud, R., and Dedhar, S. (2003). Conditional knock-out of integrin-linked kinase demonstrates an essential role in protein kinase B/Akt activation. *The Journal of Biological Chemistry*. *278*, 22374–22378.

Troussard, A. A., McDonald, P. C., Wederell, E. D., Mawji, N. M., Filipenko, N. R.,

Gelmon, K. A., Kucab, J. E., Dunn, S. E., Emerman, J. T., Bally, M. B., et al. (2006). Preferential dependence of breast cancer cells versus normal cells on integrin-linked kinase for protein kinase B/Akt activation and cell survival. *Cancer Research*. *66*, 393–403.

Tsuruo, T., Naito, M., Tomida, A., Fujita, N., Mashima, T., Sakamoto, H., and Haga, N. (2003). Molecular targeting therapy of cancer: drug resistance, apoptosis and survival signal. *Cancer Science*. *94*, 15–21.

Tu, Y., Huang, Y., Zhang, Y., Hua, Y., and Wu, C. (2001). A new focal adhesion protein that interacts with integrin-linked kinase and regulates cell adhesion and spreading. *The Journal of Cell Biology*. *153*, 585–598.

Vilar, E., Perez-Garcia, J., and Tabernero, J. (2011). Pushing the envelope in the mTOR pathway: the second generation of inhibitors. *Molecular Cancer Therapeutics*. *10*, 395–403.

Vivanco, I., and Sawyers, C. L. (2002). The phosphatidylinositol 3-kinase Akt pathway in human cancer. *Nature Reviews Cancer*. *2*, 489–501.

White, D. E., Cardiff, R. D., Dedhar, S., and Muller, W. J. (2001). Mammary epithelial-specific expression of the integrin-linked kinase (ILK) results in the induction of mammary gland hyperplasias and tumors in transgenic mice. *Oncogene*. *20*, 7064–7072.

Wickstrom, S. A., Lange, A., Montanez, E., and Fassler, R. (2010). The

ILK/PINCH/parvin complex: the kinase is dead, long live the pseudokinase! *The EMBO Journal*. *29*, 281–291.

Wu, C., and Dedhar, S. (2001). Integrin-linked kinase (ILK) and its interactors: a new paradigm for the coupling of extracellular matrix to actin cytoskeleton and signaling complexes. *The Journal of Cell Biology*. *155*, 505–510.

Yamaji, S., Suzuki, A., Sugiyama, Y., Koide, Y.-i., Yoshida, M., Kanamori, H., Mohri, H., Ohno, S., and Ishigatsubo, Y. (2001). A novel integrin-linked kinase-binding protein, affixin, is involved in the early stage of vell-substrate interaction. *The Journal of Cell Biology*. *153*, 1251–1264.

Zhu, J., Huang, J.-W., Tseng, P.-H., Yang, Y.-T., Fowble, J., Shiau, C.-W., Shaw, Y.-J., Kulp, S. K., and Chen, C.-S. (2004). From the cyclooxygenase-2 inhibitor celecoxib to a novel class of 3-phosphoinositide-dependent protein kinase-1 inhibitors. *Cancer Research*. *64*, 4309–4318.